EXPERIMENTAL INVESTIGATION OF DME ASSISTED GASOLINE CAI COMBUSTION WITH RE-BREATHING VALVE STRATEGY

A thesis submitted for the degree of Doctor of Philosophy

by

Kangwoo Seo

School of Engineering and Design

Brunel University

November 2015

Abstract

Controlled auto-ignition (CAI), also known as HCCI combustion in a gasoline engine has been extensively researched due to their potential of improved engine efficiency and low NOx emission. However, the combustion timing and the phasing of conventional CAI combustion depend on the in-cylinder condition, such as temperature and combustible mixture strength and thus cannot be directly controlled.

In this study, direct DME (Dimethyl Ether) injection was adopted to increase the ignitability of premixed gasoline/air charge and to trigger the auto ignition of premixed charge. Re-breathing valve strategies were used to obtain hot internal EGR to eliminate a need of intake heating. Firstly, the pilot valve opening event, including its opening and closing timing, valve lift and dwell duration between the main valve event, was analysed by the WAVE simulation. Based on the analysis a re-breathing cam lobe was manufactured and installed on a Ricardo E6 engine to achieve the intake rebreathing and exhaust rebreathing operations. The intake re-breathing was realised by the pilot intake valve opening during the exhaust stroke and the exhaust re-breathing was achieved by the secondary exhaust valve opening during the intake stroke. Effects of the pilot intake valve open timing, 2nd DME injection timing, split DME injection ratio, air/fuel ratio and compression ratio were examined during the intake rebreathing operation. Then the performance and emission characteristics of DME assisted gasoline CAI combustion were examined during the exhaust re-breathing operation. Finally, results of the intake and exhaust re-rebreathing operations were compared to the conventional SI operation.

The experimental study found that both the intake and the exhaust re-breathing operations provided enough heat to initiate DME assisted gasoline CAI combustion. The direct DME injection enabled to control the start of combustion and phasing. The quantity of the first DME injection showed greater effect than its timing, whereas the injection timing of 2nd DME injection had more dominant effect than its quantity. The exhaust re-breathing strategy provided stratified and hotter internal EGR that does not impact negatively on the volumetric efficiency because exhaust gas was re-breathed from the exhaust port during the intake stroke. High

load of both CAI and SI baseline operations were limited by knocking combustion and their low load were limited by incomplete combustion. Exhaust re-breathing operation extended substantially the operational range of the DME assisted gasoline CAI combustion. Extremely low NOx emissions were obtained by DME/gasoline CAI operations. Most importantly, the exhaust rebreathing method produced dramatically improved overall efficiency of 43% compared to 28% of SI operation at a typical part-load operation of 4.0-5.0bar IMEP. It was also found that slightly improved efficiency and the extended operation range could be obtained by 33%:67% split DME injection ratio at higher load, while 67%:33% split DME injection ratio at lower load.

Acknowledgements

Nomenclature

Abbreviations

BDC	Bottom Dead Centre
CA 10	10% of mass fraction burnt
CA 50	50% of mass fraction burnt
CA 90	90% of mass fraction burnt
CAI	Controlled Auto-Ignition
CARB	California Air Resources Board
CI	Compression Ignition
CNC	Computer Numerical Control
CNG	Compressed Natural Gas
CO	Carbon Monoxide
CO_2	Carbon Dioxide
COV	Coefficient of Variation
DAQ	Data Acquisition system
DI	Direct Injection
DISI	Direct Injection Spark Ignition
DME	Dimethyl Ether
DTBP	Di-tert butyl peroxide cetane improver
E10	10 % ethanol and 90% gasoline
E85	85% ethanol and 15% gasoline
EE	Extended Expansion
EGR	Exhaust gas Recirculation
EIVC	Extreme Early Valve Closing
EPA	Environmental Protection Agency
EVC	Exhaust Valve Close
EVO	Exhaust Valve Opening
FID	Flame Ionization Detector
FFP	Formaldehyde Formation Potential

FTP	Federal Test Procedure
GDI	Gasoline Direct Injection
HCCI	Homogeneous Charge Compression Ignition
HRR	Heat Release Rate
IBDC	Inlet Bottom Dead Centre
IMEP	Indicated Mean Effect Pressure
IVO	Intake Valve Opening
LHV	Latent Heat of Vaporization
LEV	Low Emission Vehicle
LIVC	Late Intake Valve closing
LPG	Liquefied Petroleum
LTC	Low Temperature Combustion
MAP	Manifold Absolute Pressure
MBT	Minimum Advanced for the Best Torque
MFB	Mass Fraction Burnt
MPRR	Maximum Pressure Rise Rate
NDIR	Non-Dispersive Infrared
NEDC	New European Driving Cycle
NVO	Negative Valve Overlap
PCCI	Premixed Charge Compression Ignition
PFI	Port Fuel Injection
PLIEF	Planar Laser Induced Exciplex Fluorescence
PLM	Professional Lambda Meter
PM	Particulate Matter
PMT	Photomultiplier
PPCI	Partially Pre-mixed Charge Compression Ignition
PVO	Positive Valve Overlap
RCCI	Reactivity Controlled Compression Ignition
RON	Research Octane Number

SI   Spark Ignition

SOC   Start of Combustion

TDC   Top Dead Centre

ULEV   Ultra-Low Emission Vehicle

VVT   Variable Valve Timing

WOT   Wide Open Throttle

Symbols

θ	a crank angle
γ	specific heat ratio (C_p/C_v)
η_b	brake efficiency
η_c	combustion efficiency
η_g	gross efficiency
η_{ge}	gas exchange efficiency
η_m	mechanical efficiency
η_n	net indicated efficiency
η_t	thermal efficiency
C	the calibration factor of the system (bar/v)
C_6H_6	benzene
C_3H_6	propene
C_2H_4	ethane
CH_4	methane
E	the charge amplifier output (v)
E_b	the bias voltage with zero pressure
E_{IBDC}	the charge amplifier output at IBDC where the absolute pressure is determined
HC	hydrocarbons
LHV_{DME}	lower heating values of DME (28.882 MJ/kg)
$LHV_{gasoline}$	lower heating values of gasoline (43.448 MJ/kg)
LHV	lower heating values of CO (10.1 MJ/kg) and HC (44 MJ/kg)
$\dot{m}_{air}$	air flowrate (g/min)
MW_{DME}	molecular weight of DME = 46 g/mol
m_D	mass of DME in one cycle
MFB_i	mass fraction burnt at a crank angle
MFB_{total}	mass fraction burnt from start to end
$\dot{m}_{gasoline}$	gasoline flowrate (g/min)
m_g	mass of gasoline in one cycle
$MW_{gasoline}$	molecular weight of gasoline = 144 g/mol
MW_{air}	molecular weight of air = 28.97 g/mol
MW_{DME}	molecular weight of DME = 46 g/mol
N	the pressure rise due to combustion becoming zero
n	the slope of the PV diagram during compression
N_2O	nitrous oxide
NO	nitric oxide
NO_2	nitrogen dioxide
NOx	nitric oxide and nitrogen dioxide
O_3	ozone
ΔP	total the cylinder pressure rise

ΔP^*_c	the pressure rise due to combustion (including volume effect)
P_i	pressure at a crank angle
P_{i+1}	pressure increment to its next value
P_{IBDC}	intake manifold absolute pressure
P_{max}	maximum cylinder pressure
ΔP_v	the pressure rise due to volume
Q	heat release rate
r_v	the compression ratio
R	the ratio of connecting rod length to crank radius
V_c	the clearance volume
V_i	volume at a crank angle
V_{i+1}	volume increment to its next value
χ	mass fraction burnt
x_i	mass fractions of CO and HC

Contents

Abstract

Acknowledgements

Nomenclature

Published paper:

List of Figures

List of Tables

Chapter 1   INTRODUCTION

1.1   BACKGROUND

Mobility and transport of people and goods are essential to the economic and social progress [1]. As population and economy grow, it is accompanied with an increased number of vehicles and thereby transport related air pollution. Until recently, CO, uHCs, NOx and PM were only the transport emissions that have been regulated to minimise the air pollution. However, CO_2 emission has been added to the regulation due to their greenhouse effect and the climate change issues.

Various technologies have been developed to improve the emission and efficiency of internal combustion engines, such as exhaust gas recirculation (EGR), variable valve timing, direct injection (DI) system and boosting. Engine downsizing has been aggressively adopted in spark ignition engines to minimise fuel consumption by means of direct injection and boosting. Meanwhile, compression ignition engines have achieved great reduction of NOx and PM emission by using direct injection and EGR, as well as sophisticated exhaust aftertrement systems. Despite all the efforts, transport emission is going to remain as a dominant source to the air pollution due to the increasing number of vehicles.

CAI (Controlled Auto-ignition) or HCCI (Homogeneous Charge Compression Ignition) is achieved by compressing premixed charge that initiates multiple auto-ignition. CAI has been considered to be a replacement of SI or CI engine due to its potential for improved emission and efficiency. Fuel consumption of gasoline CAI combustion is comparable to CI engine and its NOx emission is dramatically reduced to eliminate the requirement of after-treatment. However there are several challenges of CAI combustion. Since the CAI engine operates at wide open throttle with the premixed charge, there is not a direct method to control the start of combustion timing, and its operation range is very limited. Numerous researches have been carried out to overcome the drawback of CAI engines by employing intake charge heating, increasing compression ratio, more ignitable fuel, and variable valve timing to trap the residual gas to provide favourable condition for CAI combustion.

In this thesis, direct DME injection with intake and exhaust re-breathing valve strategies have been employed to control gasoline CAI combustion. The intake re-breathing strategy opens the intake valve during the exhaust stroke to premix exhaust gas in the intake port, while the exhaust re-breathing strategy opens the exhaust valve during the intake stroke to directly introduce exhaust gas into cylinder. Direct DME injection has been used to increase the ignitability of premixed gasoline/air mixture and initiate CAI combustion by means of split DME (Di-methyl ether) injections. DME is characterised with its high cetane number of 55 and can be produced from various feedstocks. The gaseous DME injection produces little soot emission. The re-breathing valve strategy is employed to provide sufficient EGR level.

1.2 OBJECTIVES

The objectives of this study are:

- to determine the effect of direct DME injection strategies on gasoline CAI combustion with intake and exhaust re-breathing valve strategies

- to investigate the effect of intake and exhaust re-breathing on DME assisted gasoline CAI combustion and emissions;

- to investigate the effect of compression ratio on DME assisted gasoline on DME assisted gasoline CAI combustion and emissions;

- To evaluate the potential benefits of DME assisted gasoline CAI combustion operations over the conventional SI combustion.

1.3 OUTLINE OF THE THESIS

Following the brief introduction of Chapter 1, Chapter 2 presents a review of the literature relating to the DME assisted gasoline CAI combustion. Firstly, a review of emission legislations and of the current and future laws regarding CO_2 emission is described. Then advanced gasoline engine technologies and alternative fuels to achieve low emission and high efficiency are presented and their advantages and

disadvantages discussed. Finally fundamentals of the CAI combustion and previous research on CAI combustion engines are reviewed.

Chapter 3 describes the experimental test facilities, the data acquisition and processing system used for combustion and emission analysis. Details are presented of the research engine and its modification, the DME supply and injection system, DME fuel flow measurement system.

Chapter 4 presents the design of a re-breathing cam lobe and the engine operation procedure. The 1-D engine simulation (Ricardo WAVE) of the rebreathing operation is presented and the effects of re-breathing cam lob design analysed. At the end of this chapter, preparation of the research engine and emission analysers and the test procedure are presented.

Chapter 5 presents experimental studies of DME assisted gasoline CAI combustion with the intake re-breathing strategy. Firstly the optimum intake re-breathing valve timings is determined for the rest of experiments. Then the 2nd DME injection timing and the split DME injection ratio are investigated. The effect of the compression ratio and the relative air/fuel ratio are varied to determine the operation range map and their effects on performance, emissions and efficiencies are studied in details.

Chapter 6 reports the experimental study of DME assisted gasoline CAI combustion with the exhaust re-breathing strategy. The exhaust re-breathing operation range is determined by varying the compression ratio and the relative air/fuel ratio, and their effects are discussed in detail. At the end of this chapter, DME assisted gasoline CAI combustion engine operations with the re-breathing strategies are compared to the SI baseline.

Chapter 7 summarises the conclusions from the results obtained in Chapter 5 and 6. The recommendations for the future work are suggested.

Chapter 2   LITERATURE REVIEW

2.1 INTRODUCTION

Vehicle exhausted emissions are an important contributor to air pollution, and likely to remain a significant contributor in the coming decades [2]. After the event of photochemical smog in 1952, the first emission standard was introduced in 1966 to control HC, CO and NOx emission in California [3]. More recently, CO_2 emission standard has been introduced to minimise their greenhouse effect.

The exhaust pollutants are HC (hydrocarbons), NOx (nitric oxide and nitrogen dioxide), CO (carbon monoxide), PM (particulate matter). HC and NOx emissions are dominant factors for photochemical smog. CO emission and PM directly affect the human health. CO emission reduces the oxygen carrying capacity of the blood and limits the availability of oxygen to the body, can cause brain damage [4]. Inhalation of PM can cause variety of problem, including heart or lung disease. Smaller size PM (fine particles less than 2.5 micrometres in diameter) has a higher potential for causing health problem, because fine particles can reach to lung and it might get into the blood stream [5]. CO_2 is a product of complete combustion of hydrocarbon, and does not directly harm human health, but CO_2 contributes to greenhouse gas that can cause global warming.

Numerous researches have been carried out to reduce the emission from transportation. A three-way catalyst leads to great reduction in total traffic emission over the last few decades [6]. In addition, the advanced technology leads to improvement of the engine efficiency. CAI (Controlled auto-ignition) combustion has been considered to be a future combustion technology due to its dramatic reduction in NOx emission. In addition a gasoline CAI engine has potential to match the fuel consumption of a diesel CI engine. However extending the operation range, controlling the start of auto-ignition and the combustion phasing of CAI combustion are challenges for their adoption in production engines.

In this chapter, automotive emissions standardsand the mechanism of emission formation will be discussed first. This will be followed by an overview of advanced gasoline engine technologies that have contributed to reducing the emission as well as improving the engine efficiency. The main subject of CAI combustion will

be discussed in detail. Firstly principle and combustion characteristics of CAI combustion will be presented and its low and high load boundary limits discussed. This will be followed by a review on various approaches to overcome the downside of CAI combustion.

2.2 INTERNAL COMBUSTION ENGINE EMISSIONS

2.2.1 Emission standard trends

There are two emission standards in the United States, and a state can follow either the federal legislation by Environmental Protection Agency (EPA) or the Californian legislation set by California Air Resources Board (CARB), as shown in Table 2-1. Vehicle manufactures are required to certify their vehicle to one of the emission bins, in order to sell their vehicles in a state. The vehicles are tested by using FTP-75 (Federal Test Procedure) driving cycle, which includes cold start, stabilised, hot start phases. Emissions from each phase are separately collected in a Teflon bag, and analysed in g/mile. Since 2004, the emission standards were structured into various certification levels of different stringency, called certification bins or LEV (Low Emission Vehicle) or ULEV (Ultra Low Emission Vehicle) that defends the NOx emission level. California emission standards are stricter than federal standard for NOx emission due to the smog history, but both standards are going to be identical after 2017.

Table 2-1 US emission standards for light duty vehicle, FTP 75, g/mile (NMHC: non-methane hydrocarbons) [7] [8] [9] [10].

Legislation	Category (g/mile)					
Federal Tier 1 (1994)	THC	CO	NMHC	NOx		PM
				CI	SI	
Passenger cars	0.41	3.4	0.25	1.0	0.4	-
Federal Tier 2 (2004)	HCHO	CO	NMHC	NOx		PM
Bin8	0.015	3.4	0.1	0.14		-
Bin7	0.015	3.4	0.075	0.11		-
Bin6	0.015	3.4	0.075	0.08		-
Bin5	0.015	3.4	0.075	0.05		-
Federal Tier 3 (2017)	HCHO	CO	NMHC + NOx			PM
Bin 160	0.004	4.2	0.16			0.03
Bin 125	0.004	2.1	0.125			0.03
Bin 70	0.004	1.7	0.07			0.03

Federal Tier 3 (2017)	HCHO	CO	NMHC + NOx		PM
Bin 50	0.004	1.7	0.05		0.03
Bin 30	0.004	1.0	0.03		0.03
Bin 20	0.004	1.0	0.02		0.03
California emission stands	Category (g/mile)				
LEV 1 (1998)	HCHO	CO	NMHC	NOx	PM
Tier 1	-	3.4	0.25	0.4	0.08
TLEV	0.015	3.4	0.125	0.4	-
LEV 2 (2004)	HCHO	CO	NMHC	NOx	PM
LEV	0.075	3.4	0.075	0.2	-
ULEV	0.008	1.7	0.040	0.2	-
LEV 3 (2015)	HCHO	CO	NMHC + NOx		PM
LEV 160	0.004	4.2	0.16		0.03
ULEV 125	0.004	2.1	0.125		0.03
ULEV 70	0.004	1.7	0.07		0.03
ULEV 50	0.004	1.7	0.05		0.03
SULEV 30	0.004	1.0	0.03		0.03
SULEV 20	0.004	1.0	0.02		0.03

Table 2-2: EU Emission standards for passenger cars (> 2,500kg), PN (particle number) [11]

Legislation		Category (g/km)					
Diesel engine		CO	HC	HC+NOx	NOx	PM	PN (#/km)
Euro 1 (1992)		2.72	-	0.97	-	0.14	
Euro 2 (1996)	IDI	1.0	-	0.7	-	0.08	
	DI	1.0	-	0.9	-	0.10	
Euro 3 (2000)		0.64	-	0.56	0.50	0.05	
Euro 4 (2005)		0.50	-	0.30	0.25	0.025	
Euro 5a (2009)		0.50	-	0.23	0.18	0.005	
Euro 5b (2011)		0.50	-	0.23	0.18	0.005	6.0×10^{11}
Euro 6 (2014)		0.50	-	0.17	0.08	0.005	6.0×10^{11}
Gasoline engine		CO	HC	HC+NOx	NOx	PM	PN (#/km)
Euro 1 (1992)		2.72		0.97			
Euro 2 (1996)		2.2		0.5			
Euro 3 (2000)		2.3	0.20		0.15		
Euro 4 (2005)		1.0	0.10		0.08		
Euro 5 (2009)		1.0	0.10		0.06	0.005 (DI)	
Euro 6 (2014)		1.0	0.10		0.06	0.005 (DI)	6.0×10^{11}(DI)

Table 2-2 shows EU emission standards. The test procedure is similar to US test as the emission is collected in a Teflon bag and analysed in g/km, but US exhaust emissions standards cannot directly compare to the European emission due to different driving cycle. Vehicles were used to test over ECE 15 driving cycle that allows 40s to warm-up the engine until Euro 2, but NEDC (New European Driving Cycle) that applied from Euro 3, eliminated the 40s engine warm-up period. Euro 5 has a separate regulation for DI (direct injection) gasoline engine and also introduces a particle number emission limit in addition to the mass based PM limit.

In addition to emission standards, both US and EU have introduced CO_2 emission standards in order to reduce greenhouse gases and improve fuel economy. EU CO_2 emission standard has been set to 130g/km for 2015 and 95g/km for 2020 [12] while US CO_2 emission standard has been set 212g/mi for 2017 and 143g/mi for 2025 [13], and if vehicle emits exceed CO_2, a manufacture will be charged for penalty payments of up to EUR 95 per gram and per vehicle. Similar CO2 emission legislations have also been introduced or considered in many other countries, such as Japan, China and Korea.

2.2.2 Carbon Monoxide (CO)

Carbon monoxide emission is highly dependent on the air/fuel ratio. The level of CO is increased with decreased air/fuel ratio [14], thus CO emission from SI engines tend to be higher than CI engines, which operate at fuel lean mixture. CO emission is formed in the flame zone by one of the principal reaction step in the hydrocarbon combustion mechanism as:

$$RH \rightarrow R \rightarrow RO_2 \rightarrow RCHO \rightarrow RCO \rightarrow CO$$

Where R is the hydrocarbon radical. The formed CO is then oxidised into carbon dioxide (CO_2) in the flame zone by [15]:

$$CO + OH = CO_2 + H$$
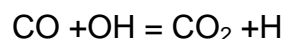
CO_2 formation is slower then CO formation, and CO oxidation process is continued during the expansion stroke. Thus, the early opening of exhaust valve during the expansion stroke can lead to increase CO emission by eliminating CO oxidation process [16].

2.2.3 Unburned hydrocarbon (HC)

Engine exhaust HC emission contains various species of organic gases, such as methane (CH_4), ethane (C_2H_4), propene (C_3H_6), benzene (C_6H_6) and etc. The composition of the unburnt hydrocarbon emissions from an engine depends on the fuel, the air/fuel ratio, the age of the catalyst and its temperature. The total hydrocarbon concentration is expressed in parts per million and only the total quantity is considered [16]. Although all the hydrocarbon compounds are not fully considered, the hydrocarbons are divided into the simplest scale, which are methane and non-methane hydrocarbon. This is because methane hydrocarbon is a non-reactive, while non-methane hydrocarbon is a reactive from the standpoint of photochemical smog.

HC emission is a product of incomplete combustion caused by several reasons. In a direct injection gasoline engine, Zhao, et al [17] found that injector position and injection strategy affected HC emission due to the oil film on the surface of cylinder and the piston crown. Daniel [18] determined that HC emission originate from the flame quench layer where the flame is extinguished by cold boundary. Crevices between the piston and cylinder wall was found to produce most HC emission in a port fuel injection gasoline engine because flame cannot reach to the premixed fuel/air mixture in the small area [19].

2.2.4 NOx

NOx indicates the mixture of nitric oxide (NO) and nitrogen dioxide (NO_2). The reason to use NOx is because NO reacts readily with oxygen in the atmosphere to produce nitrogen dioxide [20].

NO formation is manly occurred by temperature (above 1800K) and when there is sufficient time, because NO formation is very slow compare to the combustion speed. This NO formation caused by temperature is known as the thermal mechanism that based on the extended Zeldovich mechanism [15]:

$$O + N2 \leftrightarrow NO + N$$

$$N + O2 \leftrightarrow NO + O$$

$$N + OH \leftrightarrow NO + H$$
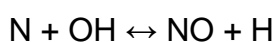
The assumption of thermal mechanism is only valid when NO formation is made in the hot combustion gases, in which it can be taken that all the other species are in equilibrium apart from the NO. When NO is considered to form in the flame, and this mechanism is called prompt mechanism [16]:

$$CH + N_2 \rightarrow HCN + N$$
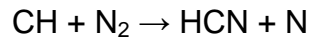
The prompt mechanism is only dominant when the combustion temperature is low, and when there is fuel-bound nitrogen.

The nitrous oxide (N_2O) can also be produced when the combustion temperature is low in the lean-premixed mixture ($\lambda > 1.6$):

$$N_2 + O + M \rightarrow N_2O + M$$
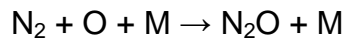
It has to notice that NOx emission manly depends on temperature, thus the thermal mechanism is the dominant mechanism to increase NOx emission.

2.3 ADVANCED GASOLINE ENGINE TECHNOLOGIES

2.3.1 Direct injection system

Direct injection spark ignition (DISI) engine provides higher fuel economy than Port fuel injection (PFI) system [21]. The benefit can be achieved by means of operating at lean mixture at part load, the increased volumetric efficiency due to charge cooling effect and operating at a higher compression ratio [22]. DISI engine utilises the injection timing to form the mixture to be homogeneous charge at high load by injecting during the intake stroke, while injection is made during the compression stroke to achieve stratified mixture for part load. At full power, the fuel is injected during the intake stroke, the volumetric efficiency is increased by the charge cooling effect. At low speed full load, when fuel injection takes place during the compression stroke, the charge temperature is reduced by fuel evaporation. This lowers charge temperature and enable the engine to operate at higher compression ratio, without incurring knocking combustion.

2.3.2 Atkinson/Miller cycle

Atkinson cycle has a longer expansion stroke than the compression stroke. The advantage of having a higher expansion ratio and shorter compression ratio is the increased expansion work and lower charge temperature to avoid knocking

combustion, leading to improved fuel consumption. Atkinson cycle can be achieved by geometrically arranging unequal compression and expansion stokes. However due to the difficult of designing the engine, Atkinson cycle is typically achieved by adjusting intake and exhaust valves timing. This is why Atkinson cycle is also referred as EIVC (Early Intake Valve Closing), LIVC (Late Intake valve closing) and EE (Extended expansion) [23].Toyota Prius Hybird is powered by an Atkinson cycle engine together with electric motor to improve emissions and fuel consumption.

Miller cycle also employs the LIVC or EIVC valve strategy, but this is distinguished by having air boosting to increase effective compression ratio. Miler cycle utilise air boosting to achieve two-stages compression stoke [24]. The increased intake pressure from boosting compresses the charge in a cylinder and the charge is further compressed by the piston after the intake valve fully close. The application of Miller cycle is normally applied with other technologies, such as variable valve timing (VVT), turbo charging and gasoline direct injection (GDI) in order to achieve higher net indicated efficiency.

2.3.3 Engine Downsizing and down speeding

The engine downsizing technology has been shown to be effective in reducing the pumping loss by moving the engine operation points to higher load region with wider open throttle. Engine downsizing refers to having a smaller capacity of boosted engine that produces similar power output of a larger naturally aspirated engine. In a downsized engine, the lack of displacement is compensated by the increased charge density from boosting. The increased charge density enables an engine to operate higher load region to improve the fuel consumption by reducing the mechanical loss and the pumping loss. The boosting system is crucial to engine downsizing. In order to maintain the power and torque output, turbocharging and/or super charging have been used to increase the charge air density. A turbocharger is driven by an exhaust gas turbine by the exhaust energy. While a supercharger is driven from electrical motor or the engine crank by means of an electromagnetic clutch and is typically a positive displacement compressor such as root blower, sliding vane compressor and screw compressor [15].

The challenge of turbocharging is to minimise turbo-lag (a delay in response to change in load) that occurs due to the inertia of the rotor, and is to increase exhaust temperature with minimum back pressure for higher efficiency [14]. Supercharger provides improved flow characteristics and the transient response due to direct drive, but fuel consumption is increased as well as increased thermal loading [14]. Twin charging and wastegate boost pressure regulation are used to provide sufficient boosting pressure from a very low to high engine speed with minimum transient delay. Various combinations of a turbocharger and a supercharger can be used, such as a small turbocharger with a large turbo charger or a large turbocharger with a small supercharger in series or parallel [25]. A wastegate is used to bypass a turbocharger turbine when it is not required, thus a smaller diameter turbine can be used to improve the transient response [26].

In recent years, downsized engines have been produced by many vehicle manufactures. Volkswagen replaced 2.0 litre FSI engine with 1.4 R4 16v TSI engine that produces 125kW by the use of a twincharger system, and achieved 5% less fuel consumption with 14% of the increased power output, while BMW replaced 3.0 litre naturally aspirated six cylinder gasoline engine with 2.0 litre turbocharged four cylinder gasoline engine that can produce 180kW of power output and achieved 15% reduction in fuel consumption [27]. Ford's EcoBoost engine is one of the most successful downsized engines in the market. The Ecoboost engine can produce over 25 bar of a peak BMEP and achieve 20% less fuel consumption with 15% reduced CO_2 emission [28]. In the last several years, more aggressive downsized engines are continuously developed to improve the fuel consumption. Mahle powertrain demonstrated a 1.2 litre downsized engine with 50% downsizing factor, resulting in a potential of 30% fuel consumption and CO_2 emission reduction. The Ultraboost engine project demonstrated that a 2.0litre engine could replace a naturally-aspirated 5.0 litre V8 engine with potential 35% reduction in fuel consumption [29].

Although downsizing has shown to be an effective way to meet upcoming CO_2 emission standard in the short term, it would be difficult to achieve further reduction of CO_2 emission [30]. Since the charge density has been dramatically increased by boosting, the compression ratio has to be reduced, and spark timing has to be retarded to avoid knocking combustion at high load. Increasing

downsizing factor requires higher BMEP at low engine speeds to maintain acceptable performance and transient response. Engine geometry becomes more complex to withstand the increased peak in-cylinder pressure, and its bore size and cylinder number need to be re-optimised.

2.3.4 Alternative fuels

Alternative fuels are made from materials other than petroleum, and main scope of alternative fuel is to improve air quality as well as reducing CO_2 [31]. There are various alternative fuels such as compressed natural gas, liquefied petroleum gas, methanol, ethanol and dimethyl ether. Alternative fuel can be used as a main fuel or mixed with petroleum based fuel for instance petrol and methane, or petrol and ethanol.

2.3.4.1 Compressed natural gas

Compressed natural gas (CNG) has a low carbon-to-hydrogen ratio, thus the emission of PM, CO_2, NOx are reduced with a very low photochemical smog potential. However since CNG is mainly composed of methane (CH_4), it results in relatively high emissions of methane, which is a strong greenhouse gas.

2.3.4.2 Liquefied petroleum gas

Liquefied petroleum gas (LPG) is a mixture of light hydrocarbons (propane and butane). LPG has a higher octane rating (104) than gasoline (95), and performance and drivability is equivalent to the gasoline fuelled vehicle. The emission of NOx, HC and CO can be reduced by optimization. However, LPG contains less energy than gasoline, and it is difficult to start in cold condition.

2.3.4.3 Ethanol

Ethanol is an alcohol fuel that can be fermented and distilled from biomass and crops. Ethanol is blended with gasoline to be used in a vehicle, such as E10 (10 % ethanol and 90% gasoline) and E85 (85% ethanol and 15% gasoline). E10 fuelled vehicle tend to show great reduction of HC emission with slight reduction of PM, CO, benzene and NOx emission, however E85 results in higher emission of unburned ethanol, because the conversion rate of the three-way catalyst for unburned ethanol is low [2].

2.3.4.4 Methanol

Methanol is an alcohol fuel that can be blend with gasoline, diesel and dimethyl ether. Methanol blended fuels help to reduce CO_2 and HC, and are less expensive than ethanol blended fuel. However Methanol is highly corrosive and toxic and has lower energy density than ethanol.

2.3.4.5 Dimethyl ether

The properties of Dimethyl ether (DME) are shown in Table 2-3. DME can be produced from a variety of feedstocks, including natural gas, coal and biomass. DME has a high cetane number (>55) and the ignition delay is shorter than other alternative fuels. DME has been used in compression ignition engines and the levels of emissions are comparable to those of the lean-burn heavy duty engine using LPG, CNG and gasoline engines equipped with three-way catalyst. DME is non-toxic and its combustion is smokeless without emissions of benzene due to the absence of carbon-carbon bonds [32].

Table 2-3: DME properties

DME					
Chemical structure	Critical temperature	Critical Pressure	Critical density	Auto - ignition temperature	Boiling point at 1 atm
CH_3-O-CH_3	400 K	5.37 MPa	259 kg/m^3	508 K	248.1 K

2.4 CAI COMBUSTION ENGINE

2.4.1 Introduction

Conventional engines compromises the engine efficiency for reduction of NOx emission. In a spark ignition engine, the stoichiometric air/fuel ratio is used for a three-way catalyst, while the compression ignition engine utilises EGR (exhaust gas recirculation) and after-treatment (SCR, DENOx) to reduce NOx emission. CAI combustion can achieve extremely low NOx emission that could match to gasoline engine equipped with three-way catalyst, and has high potential for improving fuel consumption at part load.

There are various ways to achieve CAI combustion and different names are given to such combustion. CAI combustion is achieved by compressing the premixed charge to auto-ignite, and thus is also called HCCI (homogeneous charge

compression ignition) combustion. HCCI combustion is achieved by low reactive fuel such as gasoline and LPG. With high reactive fuels such as diesel and DME CAI combustion is achieved by multiple injections by means of direct injection. Pilot injections (up to 35% of total fuel) are made during the compression stroke to premix with air and followed by main injection. This is known as PPCI (partially pre-mixed charge compression ignition) or (PCCI premixed charge compression ignition). RCCI (reactivity controlled compression ignition), utilises both high reactive and low reactive fuels to control the ignitability of premixed charge, thus the start of combustion (SOC) and combustion phasing can be set to optimised timing.

The CAI combustion relies on auto-ignition chemistry which is dependent on the in-cylinder thermal and mixture distributions and their time histories. Hence there is no direct control over the SOC in a pure CAI combustion operation and the combustion phasing. Since CAI combustion temperature is low, CAI engine emits relatively high CO and HC emission. In addition, its operating range can be limited. In this section the general characteristics of CAI gasoline engine and previous research on CAI combustion engines will be presented and discussed.

2.4.2 Principle and characteristics of CAI combustion

CAI Combustion characteristic is distinguished from diffusion combustion in a CI engine, and flame propagation in a SI engine. CAI combustion is caused by controlled auto-ignition of a premixed air/fuel mixture and involves the simultaneous reactive envelopment of the entire air/fuel mixture. The flame front does not exist and the heat release rate of CAI combustion is strongly coupled with local air/fuel ratio and pressure, thus CAI combustion is more closely described by ideal constant volume cycle. Figure 2-1 shows the heat release characteristics of SI and CAI combustions.

In the SI engine, combustion occurs through a flame propagation process and the change in state of the unburned and burned gas are separated by a flame front or a thin reaction zone. The heat release only occurs in the reaction zone, therefore the cumulative heat released in the flame is the sum of the heat released by a certain mass,dm_i in the reaction zone and it can be expressed as

$$Q = \int_0^N q \cdot dm_i$$

Where q is the heating value per unit mass of a fuel and air mixture, N is the number of reaction zones [33].
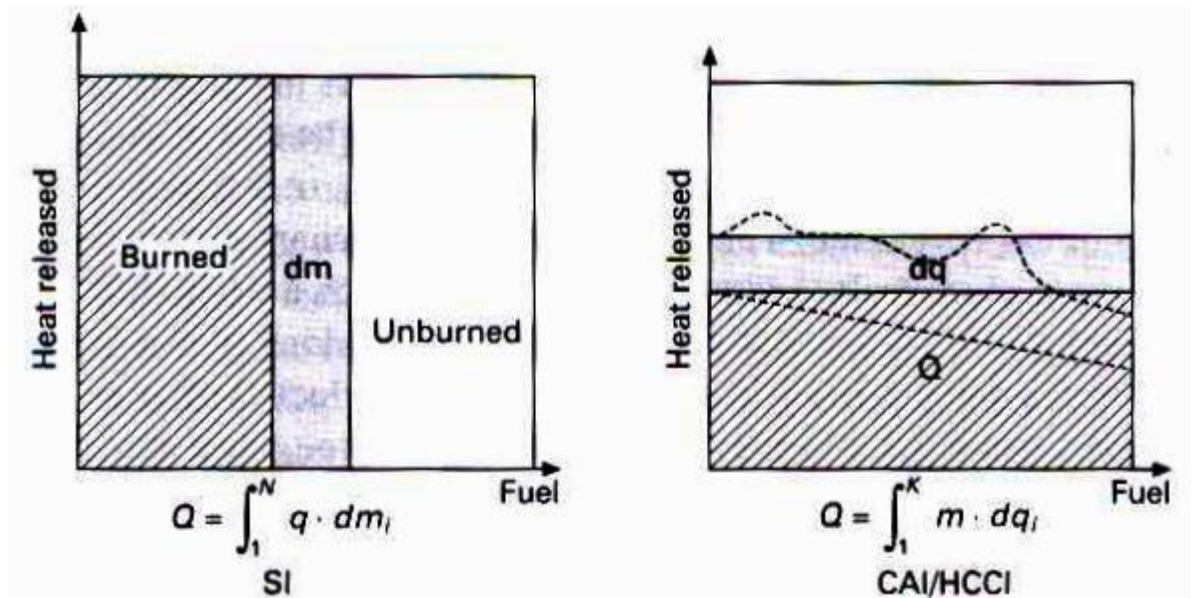
Figure 2-1: Heat release characteristics of SI and CAI combustion [33]

As the initiation of CAI combustion always occurs at multiple sites in the entire premixed air/fuel mixture, the cumulative heat release of CAI combustion is the sum of the heat released from each combustion reaction, dp_i of the complete mixture in the cylinder, m . This equation is described as

$$Q = \int_1^K m \cdot dq_i$$

Where K is the total number of heat release reactions, and q_i is the heat released from the ith heat release reaction involving per unit mass of fuel and air mixture. Theoretically heat release of CAI combustion is more uniformly than its SI combustion. Because in SI combustion, only a finite duration is available to the mixture for releasing the entire heating value in the reaction zone. However in practice, CAI combustion requires large amount of charge dilution to control runaway rates of the heat releasing reactions. This causes inhomogeneous mixture composition and temperature distribution, and resulting in a non-uniform heat release pattern as the heat release rate is partially increased in the less

diluted mixture and high temperature region, shown by the dashed lines in Figure 2-1.

2.4.3 CAI operating region

Extending the operation range is the biggest challenge in CAI research as the operating range affects the improvement in vehicle fuel economy over drive cycles using CAI [33]. Figure 2-2 shows relationship between the average charge temperature at the beginning of compression and quantity of fresh charge and residual gas.
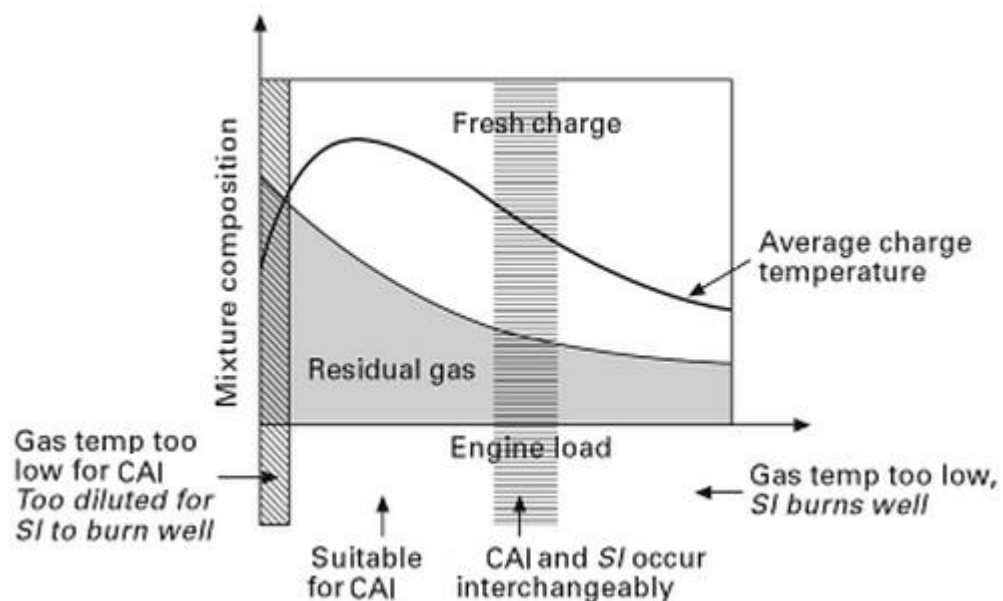
Figure 2-2: CAI and SI combustion regions according to engine conditions [33], [34]

At very low load condition, the heat release per cycle is too low to obtain sufficient temperature from internal EGR for auto-ignition at the end of compression stroke. This causes partial burn or misfire at very low load and combustion becomes unstable that results in increased cycle to cycle variation and CO and HC emissions. As the load increases, the charge temperature initially increases and sufficient internal EGR moderates the heat release rate to achieve stable combustion. However as the load further increases, the larger amount of fresh charge replaces the residual gas, thus the average charge temperature is decreased. Moreover, the SOC timing is progressively advanced and the runaway heat release rate is also increased due to the increased amount of fuel and the decreased internal EGR rate. In this condition, 50% of mass fraction burnt (CA 50)

occurs before TDC and makes unacceptable noise, casing violent combustion with increased NOx emission [34].

In the Last decade, extensive researches have been carried out by many researchers to extend the operation rage of CAI combustion. High load can be extended by minimizing the charge temperature and phasing the combustion as late as possible [33]. Sjöberg and Dec [35] found that combustion phasing can be retarded by lowering the intake temperature and coolant temperature, and increasing the in-cylinder air swirl. However overly retarded combustion leaded to unstable combustion with increased emissions, and high air swirl decreased IMEP. Wildman [36] and Scaringe [37] also found similar results. They studied extending high load boundary by controlling intake temperature and internal EGR rate on gasoline CAI combustion, and showed that manipulating both parameters delayed combustion phasing, however misfire was occurred as the combustion is further delayed. They also found that the maximum net IMEP can be obtained at the point where just before the misfire limit.

Intake boosting is also reported to extend the high load boundary of CAI combustion. Yang et al. [38] carried out an experiment on a single cylinder four stroke gasoline engine with intake heating, boosting and EGR. He achieved the enlargement of high load region from 2.5 bar IMEP to 8 bar IMEP by increasing boosting inlet pressure from 0.5 bar to 1 bar without increasing NOx and CO emission. The boosting resulted in decreasing combustion and thermal efficiency, but they were improved by adding EGR. Dec and Yang [39] also achieved extending high load boundary from 5 bar IMEP to 16 bar IMEP by intake boosting with EGR. They increased IMEP by firstly increasing the fuelling rate until the knocking boundary and then increased EGR rate until it reaches to misfire limit, by repeating these procedures. The combination of internal and external EGR has also reported to extend high load boundary. Cairns et al. [40] achieved an increase in engine load of 20-65% by introducing cooled EGR (external EGR). The EGR reduced heat release rate and the effect was greater at lower engine speed, however excessive EGR rate caused unstable combustion.

In a direct injection SI engine, the injection timing can be used to extend CAI operation range [33]. Li [41] tested the effects of injection timing on mixture and

CAI combustion by using a single-cylinder GDI engine with negative valve overlap (NVO). Planar laser induced exciplex fluorescence (PLIEF) technique was used to analyse the liquid and vapour phase of fuel spray. Late injection timing (late in compression stroke) leaded to stratified charge, and caused slow and unstable combustion with higher HC and CO but lower NOx and noise, whereas homogeneous charge was obtained by early injection (during intake stroke) and combustion speed decreased HC and CO emission, but NOx emission and noise were increased. The result shows that the Low load boundary can be significantly expended by negative valve overlap and early injection approaches.

As the low load limit of CAI combustion occurs by low temperature to initiate auto ignition, various strategies that keeps the in-cylinder temperature as high as possible can extend low load boundary. Discharging spark aids to extend low load boundary [42]. The assist of spark discharge shortens the low temperature chemical reaction process and advances the auto-ignition timing, and improves fuel consumption and cycle to cycle variation. Milovanovic et al. [43] demonstrated extending both the high and the low boundary by controlling coolant temperature. Increasing the coolant temperature from 90 ^{0}C to 125 ^{0}C extended the low limit by 28%, while decreasing it from 90 ^{0}C to 65 ^{0}C extended upper limit by 14%. Increasing the compression ratio and intake temperature helped extending low limits of CAI boundary, but narrowed its upper limits [33], [38].

2.4.4 Emissions

CAI combustion is the low temperature combustion (LTC) that minimises NOx emission with relatively high CO and uHC emission. The emissions of CAI combustion depends on the air/fuel ratio unless large amount of EGR is present in a cylinder as the emissions have strong relation to maximum gas temperature [33].

The low combustion temperature is even lower as the relative air/fuel ratio is increased, decreasing the heat release rate and combustion temperature. As a result, less complete oxidation of uHC and CO can occur. As the relative air/fuel ratio reduces, uHC and CO emission are reduced by the increased combustion temperature, and the lowest level of these emissions are obtained close to upper limits. Compared to SI operation under same conditions, CAI combustion emits higher uHC emission in its operation range. However CAI combustion emits less

CO emission close to the upper limit although higher CO emission are measured at the rest of operation region. These are considered as the major drawback of CAI combustion.

As expected, the maximum NOx emission is obtained at the upper limit of CAI combustion. Because low EGR rate and high lambda lead to high heat release rate, and result in increased combustion temperature. Moreover, the lowest combustion efficiency at this condition also contributes to the highest specific emission of NOx as the specific emission is the result of relative difference between fuel consumption and power output. Compared to SI operation near the knocking boundary, CAI combustion still shows around 94% reduction in specific NOx emission, and the reduction percentage increases as load decrease [33]. This is the main benefit of CAI combustion.

Zhao et al. [44] achieved CAI combustion on a production type 4-stroke 4 cylinder gasoline engine with only the modification of camshaft to trap residual gas. The results showed the great reduction in fuel consumption, CO and NOx emission, and NOx emission was reduced by more than 93% across the while CAI range. However the improvements were moderated by comparing a SI engine and a CAI/SI hybrid engine on the NEDC driving cycle vehicle due to the limited operation range. Oakley et al. [45] studied CAI combustion by using a single cylinder research engine. Over 97% reduction of NOx emission was achieved, and found that the small amount of EGR to the intake charge leads to the dramatic reduction of HC emission though improvement in combustion efficiency.

Christensen, et al. [46] tested CAI combustion with isooctane, ethanol and natural gas. Their emission results showed similar trend to its gasoline fuel trend as maximum level of NOx emission was observed at the knocking boundary, with the opposite trend of CO and HC emissions. They found out that with natural gas the EGR did not help to reduce the NOx emission, but with ethanol and isooctane, NOx emission was reduced by having an additional EGR rate. Onishi, et al. [47] demonstrated reducing CO and HC emission by simply using oxidation catalyst.

2.4.5 Efficiencies

Unthrottled operation of the CAI gasoline engine by using both the EGR and the lean mixture allows the engine to operate at a higher engine efficiency and better

fuel economy than SI combustion [33]. Borgqvist et al. [48] compared throttled and unthrottled SI with HCCI combustion. Unthrottled SI engine showed around 6% improvement of the net indicated efficiency from throttled SI engine, and the relative improvement from SI engine to CAI engine further increased to 20%. They pointed out that the improved net indicated efficiency is due to the increased thermodynamic and combustion efficiency.

Hyvönen et al. [49] showed the effects of engine displacements on CAI combustion by testing on a five cylinder $1.6dm^3$ VCR engine, a four-cylinder $2.0dm^3$ engine, and a six-cylinder $11.7dm^3$ truck engine. They found that the indicated efficiency was similar regardless engine design, but the brake efficiency varied between engines. The truck engine showed the highest brake efficiency due to higher combustion and mechanical efficiency. Dec et al. [50] studied the effects of E10 on boosted CAI engine, and found that CAI combustion with E10 provided higher thermal efficiency than CAI combustion with gasoline due to less EGR requirement. The increased thermal efficiency was about 5% and corresponding improvement of fuel consumption was about 11%. The study also pointed out that thermal efficiency can be increased by adjusting the parameters to lower intake temperature, less CA 50 retard and less EGR.

2.4.6 Exhaust gas recirculation

The requirements of a certain quantities of charge dilution and high intake charge temperatures for CAI combustion can be satisfied by the use of recycling the burnt gas.

Zhao et al. [51] divided the effects of EGR on CAI combustion into four. (1) The charge heating effect is defined as the increased intake temperature due to the heating effect of the hot burnt gas, and is the dominant factor for the advanced AI timing, (2) The dilution effect indicates the reduction of air/oxygen due to the present of burnt gas, and is mainly responsible for the extended combustion duration. (3) The heat capacity effect describes the increased heat capacity of cylinder charge due to the high specific heat capacity value of carbon dioxide (CO_2) and water vapour (H_2O) in burnt gas. Its main effect is the reduction of peak combustion temperature. (4) The chemical effect is named for the effects of chemical products present in the bunt gas on the chemical reaction leading to auto

ignition and subsequent combustion, and it can accelerate the autoignition process.

EGR can be used for extending both low limit and upper limit of CAI combustion. The charge heating effect of internal EGR or trapped residual gas can be used to extend the low load limit. External EGR (cooled EGR) can be used for extending upper limit of CAI combustion. Dec et al. [52] achieved IMEP from 4.5 bar to 4.75 bar by increasing EGR rate and fuelling rate. Although the fuelling rate was increased, a small reduction in maximum rate of the pressure rise extended the knocking boundary. Lotus engineering [53] demonstrated CAI combustion with a fully variable valve train. The analysis showed that the amount of internal EGR controls the start of auto ignition timing, thus CAI combustion can be controlled.

2.4.7 Approaches to CAI operation in gasoline engines

2.4.7.1 Direct Intake charge heating

Using an intake heating is the most common way to increase inlet temperature in order to have favourable auto-ignition condition. Yang et al. [38] achieved CAI combustion by the controlling intake temperature from 120 ^{0}C to 220 ^{0}C by means of intake heater. Higher intake temperature allowed leaner air/fuel mixture, but narrowed the upper limit of CAI combustion. Persson et al. [54] investigated the effects of intake temperature on CAI combustion using negative valve overlap. They found that large amount of internal EGR and spark assisted reduces the impact of the intake temperature, and needed lower intake heating to initiate auto ignition. At high load, internal EGR cannot provide sufficient heat energy due to the limited amount, but a small increase of the inlet temperature found to minimise cycle to cycle variation.

2.4.7.2 Higher compression ratio

As the auto-ignition of CAI combustion depends on the in-cylinder condition at the end of the compression stroke, compression ratio plays important role in CAI engine. The effects of increasing compression ratio leads to similar result of increasing intake temperature. Higher compression ratio extends the lower limit boundary, but narrowed high load limit [33]. Haraldsson et al. [55] carried out an experiment on a multi cylinder engine with variable compression ratio, and determined the trade-off between the intake temperature and compression ratio. Higher compression ratio reduced the requirement of inlet preheating, and

21

increased brake thermal efficiency with decreased NOx emission. However increasing the compression ratio increased CO emission due to shortened reaction time. Variable compression ratio also showed the faster response charge temperature variation than intake charge heating.

2.4.7.3 More ignitable fuels

Rather than controlling the in-cylinder condition for auto-ignition of premixed charge, adjusting the ignitability of fuel is another option to achieve CAI combustion. Christensen et al. [56] investigated CAI combustion in a single cylinder engine by means of variable compression ratio, intake air heating, and dual port injection system that enabled a change of octane rating between 0 and 100. The study concluded that n-heptane (0 RON) and iso-octane (100 RON) required a CR of 11:1 and 21.5:1 respectively. But interestingly gasoline (98 RON) required higher CR (22.5:1) than its iso-octane (100 RON). Increasing CR did not improve the indicated efficiency due to the decrease in combustion efficiency.

Aroonsrisopn et al. [57] carried out a series of engine experiments to analyse the effect of intake temperature, engine speed and fuel composition on the CAI operating range of a single cylinder research engine. Four different fuels were used. One of the fuels was a blend of primary reference fuels and had a research octane number of 70, while rest of the three fuels had a research octane number of 91.8 with different chemical composition. They showed that the same research octane number fuels with different composition resulted in different CAI operating ranges, thus the octane number cannot be used as the indicator of the fuels CAI combustion characteristics, consistent with the findings by Christense etl al. [56].

Bessonette et al. [58] investigated fuel effects on HCCI engine operating range and emissions in a Caterpillar 3401E single cylinder oil test engine. Test fuels were developed in the gasoline and diesel boiling range covering a broad range of ignition quality, fuel chemistry, and volatility. Their experiments demonstrated that the fuel ignitability was the dominant factor for operating load range and a reduction in fuel ignitability increased the maximum load and the operating range. Fuel volatility and fuel chemistry did not show significant effect on the achievable minimum/maximum loads or operating range. No significant emission differences were observed regardless of the fuels tested.

22

Milpied et al. [59] defined four major fuel properties that affect to CAI combustion and determined the effects of them. Four major fuel properties were research octane number (RON), Latent Heat of Vaporization (LHV), Formaldehyde Formation Potential (FFP) and EGR sensitivity. The analysis showed that high RON of low auto ignition properties, and high LHV of large cooling effect are favourable for high load enlargement, whereas high FFP of high fuel ignitability, and low RON number are favourable for low load enlargement. EGR sensitivity was linked to fuel reactivity and its relation with fuel temperature.

Diesel fuelled CAI combustion is often called as PPCI combustion. The advantages of PPCI combustion are the dramatic reduction of NOx and PM emission. However there is disadvantage of increased fuel consumption. Lechner et al. [60] achieved PPCI combustion by using diesel, and the results were compared to diesel CI engine. The compression showed that PCCI combustion reduced NOx emission by 82% and PM by 39%, but the fuel consumption was increased by 4.5%. As CAI combustion can be achieved by various fuels, blended fuel can be used to achieve CAI combustion. Zhang et al. [61] pre-blended gasoline and diesel at 50:50 ratio in volume to achieve CAI combustion and the results were compared to diesel CI engine. The analysis showed that over 90% reduction in PM and NOx, but net indicated efficiency was reduced by1.5% with a slightly increased noise level.

In-cylinder fuel blending by using both direct injection of high reactive fuel and port fuel of low reactive fuel are named RCCI (Reactive Controlled Compression Ignition) combustion by Wisconsin University. Various combinations of high reactive and low reactive (main fuel) fuelled RCCI combustions were demonstrated by using a heavy duty 2.44L single cylinder engine with an intake heating [62]. The results showed that the thermal efficiency can be increased by controlling the dual fuel ratio to optimise combustion phasing. Gasoline-diesel dual fuel operation showed 59% of gross thermal efficiency, and its gasoline-gasoline + DTBP (di-tert butyl peroxide cetane improver) was 57%, and followed by 56% of thermal efficiency from ethanol (E85)-diesel operation. Although similar value of the thermal efficiency was obtained by the different combination of dual fuel, the required test condition such as dual fuel ratio air/fuel ratio and intake temperature was significantly different due to the temperature, local and global reactivity and

chemistry different. In addition, additional boost is required to operate the lean mixture, which could have negative impact on the overall engine efficiency.

Kim et al. [63] carried out DME-gasoline dual fuel CAI combustion by modifying a CI engine. The DME injection pressure was varied from 300 bar to 600 bar while the gasoline was injected by PFI injection system. DME injection mass was varied from 10 % to 100% with 10% to 50% gasoline injection mass. Their results showed that the auto-ignition timing depends on the DME injection timing rather than the DME/gasoline ratio, and increasing DME injection pressure shortened the ignition delay with increased thermal efficiency and NOx emission. Zhang et al. [64] also achieved CAI combustion by using DME-gasoline combination. The experiment was carried out by using a single cylinder research engine with GDI and gasoline PFI injection system. The analysis showed that injection strategy vary the combustion type, for example gasoline with early single injection leaded to pure CAI combustion, gasoline with split DME injection leaded to hybrid combustion, which develop from flame propagation to CAI combustion and late single injection caused flame propagation. By controlling the combustion mode, the enlargement of high and low operation range was achieved, ultralow NOx emission was achieved over the operation range.

2.4.7.4 Valve strategy (internal EGR control)
Various valve strategies have been used to obtain internal EGR or residual gas in a CAI engine. Compared to the external EGR that is obtained by an external loop, internal EGR contains the heat energy to initiate the CAI combustion without intake heating [33].

Zhang et al. [65] demonstrated CAI combustion without intake heating by using VVT to realise NVO. In order to measure in-cylinder residual gas, they employed fast response NDIR analyser to measure cycle by cycle trapped residual gas. They measured CO_2 centration in the cylinder in order to determine the amount of residual gas, and the value was compared to the EGR that calculated by pressure measure at EVC and exhaust temperature. The calculated EGR rate was consistently 5% higher than measured EGR over test range. They stated that the optimum valve timing should produce the highest indicated thermal efficiency and optimised combustion phasing with the minimum EGR during re-compression to minimise the pumping loss.

Zhang et al. [64] also achieved CAI combustion without an intake heater by employing PVO with exhaust back pressure control. With fixed intake and exhaust valve timing, controlling the exhaust back pressure enabled to vary EGR rate, however the pumping loss was increased with increasing the EGR. The difference between the gross and net indicated efficiency was only 2% with minimum EGR, but the difference was increased to 38% with the maximum EGR.

Re-breathing valve strategy that has either pilot intake valve event or post exhaust valve event can be used to trap a large amount of internal EGR. Duffour et al. [66] studied the effects of exhaust re-breathing on CAI combustion by controlling the profile of post exhaust valve opening by means of VVA. They showed that the post EVC timing affected the effective compression ratio, and earlier post EVC timing leaded to advancing auto-ignition timing due to the increased in-cylinder pressure and temperature. Early EVO increased the amount of EGR and decreased the combustion speed. Kawasaki et al. [67] achieved CNG CAI combustion by using the intake and the exhaust re-breathing strategy with controlling the exhaust valve throttle to control the amount of internal EGR. The exhaust re-breathing provides higher thermal efficiency than the intake re-breathing due to the increased combustion temperature.

2.5 SUMMARY

This chapter has presented emission standards and described the formation of CO, HC and NOx emissions. Engine downsizing technology that used for the latest production gasoline engines is discussed. CAI combustion has been described in detail. The CAI engine emits extreme low NOx emission due to low combustion temperature, and has higher potential to improve fuel consumption. However CAI combustion operation range is limited. The knocking combustion limits high load operation, while the misfire and partially combustion limits low load. Moreover, the auto-ignition timing and the combustion phasing are difficult to control due to the unattended ignition system.

Previous research works showed that the operation rage of CAI combustion can be extended by:

- Intake heating

- Coolant temperature control

- Variable compression ratio

- Air Boosting

- Spark assistant

- Variable valve timing

- In-cylinder fuel blending (RCCI or dual fuel strategy)

Increasing the temperature of intake heating and coolant were found to extend high load, but response time was too slow to control the auto-ignition timing. In-cylinder fuel blending was the most practical strategy to control auto ignition timing as the auto-ignition timing was directly related to the injection timing of high reactive fuel. Furthermore when multiple injections are used for high reactive fuel, a pilot injection can be used to control the ignitability of a premixed mixture, thereby the combustion phasing can be controlled. DME showed beneficial characteristic to be used for high reactive fuel. DME has a higher cetane number than diesel fuel and less emission than diesel. The intake or exhaust rebreathing methods have shown to be effective to obtaining internal EGR. Therefore, research was planned and carried out on the combined use of DME/Gasoline to control the fuel reactivity and internal EGR by intake or exhaust rebreathing to regulate the charge temperature and dilution ratio.

Chapter 3 EXPERIMENT FACILITY

3.1 INTRODUCTION

A single cylinder Ricardo E6 variable compression engine has been modified for DME assisted gasoline CAI combustion experiments. The single camshaft was modified to provide variable intake/exhaust valve timings and valve lift. A direct DME injection system was designed, installed and optimised for accurate DME injection. A port fuel injection system was employed to inject gasoline into the intake port. A DAQ (Data acquisition) system was set up to record in-cylinder pressure for the subsequent combustion and heat release analysis. The engine's exhaust emissions were measured and used to determine the specific emissions. In order to quantity the in-cylinder residual gas concentration, a fast-sampling system was adopted to the engine. In this chapter the engine setup and all the measurement systems will be presented and described in details.

3.2 RICARDO E6 VARIABLE COMPRESSION RATIO ENGINE

A gasoline version of Ricardo E6 is a single-cylinder four-stroke 2 valve engine with a bore of 76.2 mm and a stroke of 111.1mm and speed range of the engine is 1,000 – 3,000 RPM. The compression ratio can be varied between 4.5 and 20. The combustion chamber is cylindrical shape, and flat surface of the cylinder head and piston form the ends. There are two M14 holes at the opposite sides of the combustion chamber between the valves, in which an in-cylinder pressure transducer and a direct DME injector can be fitted.

Figure 3-1 shows the setup of the E6 engine and the key components to achieve variable compression ratio. E6 engine consists of a cylinder block that travels in vertical motion, and liner that made of hardened cast iron is fixed on a floor. The upper part of the cylinder block that contains water jacket guides its sliding motion, and the lower part of the block is screwed to a nut, which has worm teeth on its outer surface. Rotation of a handle spins the nut that raises and lowers the cylinder block relative to the crankshaft. A clamp bolt can be tighten to lock the handle so that the cylinder block can be fixed at a desired position. The position of the cylinder block is measured by means of a manometer, which reading is used

to read off a corresponding compression ratio from a calibration curve that supplied with the E6 engine. Total cylinder movement distance is 24.5 mm that covers the range of compression ratio from 4.5 to 20.
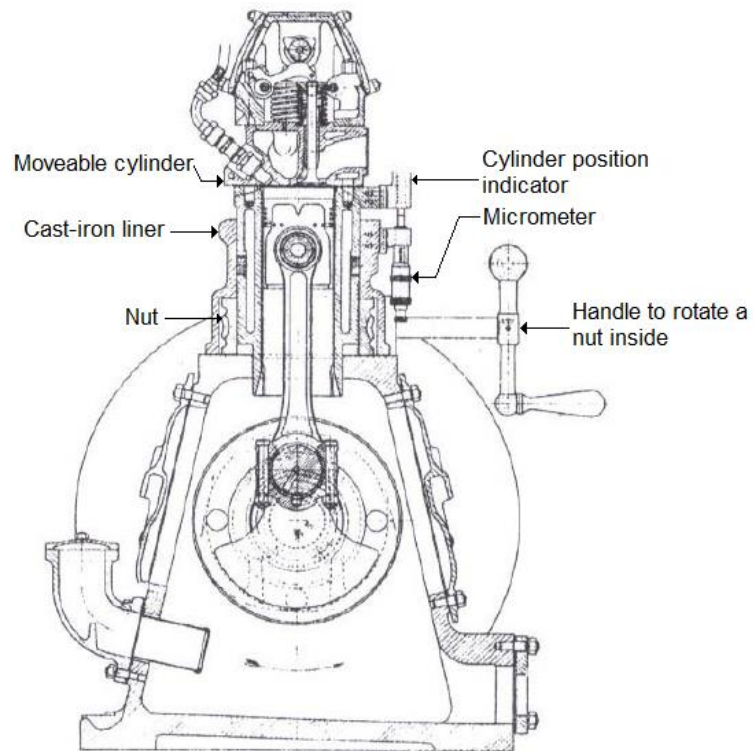
Figure 3-1: Ricardo E6 engine diagram

3.2.1 Lubrication and Coolant systems

The E6 engine has a wet sump type lubricating system that is filled up with mobil10W-40 oil. An oil pump mounted on the front cover of the engine directly delivers the oil to the crankshaft and the oil pressure is controlled by a relief valve. An oil pipe is connected to the top of the cambox to supply oil to the centre of the single camshaft and bearings. The oil is warmed up by an electrical heater of 0.5 KW rating that is located in the crankshaft case and an oil-water heat exchanger reduces the oil temperature when excess heating occurs during high load engine operations.

The coolant circulation comprises an electrically driven water pump and a 3kW immersion heater in the coolant circuit. Coolant temperature is controlled by a PID controller. A thermocouple that located approximately 200mm upstream of the outlet of the engine gives a feedback to the PID controller, which controls the solenoid valve in cold water pipeline to a heat exchanger.

3.2.2 Valve train

There are two poppet valves, one for intake and the other for exhaust. The valves are operated by an over-head camshaft that is driven from a crankshaft by means of two pairs of bevel gears. The original camshaft timing could only be changed by changing the position of bevel gears. A new camshaft was designed and installed to enable both intake/exhaust valves timing change and valve lifts to be done with minimum disassembling process by a pair of interchangeable cam lobs with opening duration of 195^0 CA and 8 mm of maximum valve lift for both intake and exhaust valves. Further details of the cam lob designs will be given in Chapter 4.

3.2.3 Port fuel injection system

A port fuel injection system is prepared to inject gasoline in the intake port shown in Figure 3-2. Gasoline is supplied to a fuel tank from an underground fuel thank by an air driven pump, and gasoline is delivered to a single Bosh fuel injector by a pump that is installed on the fuel pipe line. A pressure regulator controls gasoline injection pressure which is displayed by a pressure gauge. A pressure damping chamber is also installed between the pump and injector to provide steady injection pressure. An air release valve on the fuel tank is used to prevent negative pressure when the main fuel line is closed and to vent the air in the fuel tank when the main fuel line is opened. The PFI gasoline injection pressure is set to 2.5 bar using the fuel pressure regulator.
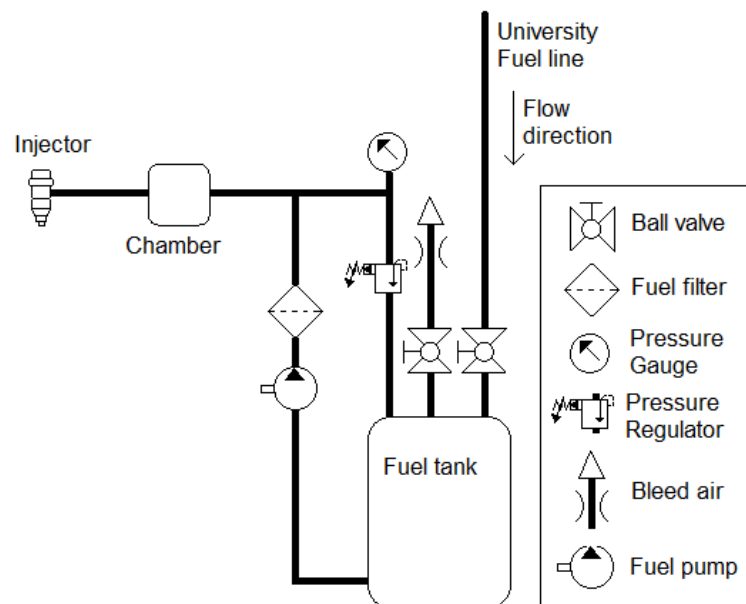
Figure 3-2: Port fuel injection system for gasoline

3.2.4 DME Direct injection system

The DME supply system shown in Figure 3-3 was designed to fulfil the health and safety requirement. All components in the DME supply system have higher working pressure than 110 bar. Ball valves are installed between every sections to isolate DME flow in case of leakage. Nitrogen cylinder and DME cylinder are located outside the lab. DME injection system utilises a gasoline direct injection (GDI: Bosh HDEV 5.1) injector to directly inject DME into the cylinder.
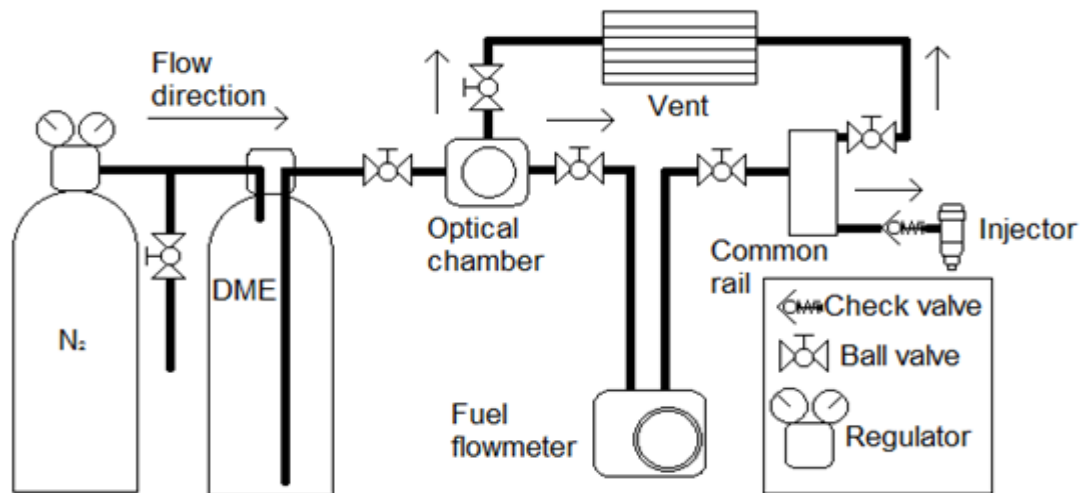
Figure 3-3: Direct injection system for DME

DME cylinder is supplied by BOC gas, and contains 5 kg of DME at 200 psi (13.8 bar) with pre-fitted dual port valve on top. The dual port valve consists of a vapour port and a liquid port. The vapour port connects a short pipe that ends at very close to the top of the DME cylinder, while the liquid port connects a long pipe that ends very close to the bottom of DME cylinder. The outer end of the vapour port of DME cylinder is connected to nitrogen cylinder to set the DME cylinder pressure from 0 to 110 bar by a pressure regulator. Tubing of 6 mm outside diameter tubes and 1mm wall thickness are used with a 420 bar working pressure. Both tubing and tube fittings are made of SS304 and supplied by Swagelok.

The pressurised DME is delivered through the liquid port of DME cylinder to an optical chamber near to the engine. The optical chamber has a cylindrical volume of 200 ml and both ends are sealed by quartz windows of 25 mm thickness for visual inspection. The optical chamber was tested hydrostatically to 150 bar. There are two outlets in the optical chamber. One outlet is located at the top of the

optical chamber and connected to a vent for ventilating air or unwanted nitrogen gas that may have entered into the optical chamber with DME. The other outlet on the right side of the chamber is connected to a Coriolis flow meter from which DME flows to the common rail. The common rail has a cylindrical volume of 500 ml. There are two outlets on the common rail. The top outlet is connected to a vent and the bottom outlet is connected to gasoline direct injector through check valve. A check valve is installed to prevent backflow from the injector to common rail.

3.3 ENGINE CONTROL SYSTEM

Apart from the mechanical parameters such as compression ratio and cam timings, the engine control system is necessary to vary software parameters such as engine speed, PFI and DI injection timing and duration. The engine is coupled to a Laurence Scott "NS" type swinging field AC Dynamometer. Dynamometer speed can be varied between 900 RPM and 3,000 RPM. The dynamometer is controlled by start and stop buttons on a main switch gear panel, which also controls the water circulating pump motor.

3.3.1 Crankshaft position system

A rotary encoder is mounted on the front end of the crankshaft to convert angular position of the crankshaft into digital signals. The rotary encoder is an optical absolute encoder, which consists of a LED (light-emitting diode), a coded disk, a mask, a photo detector on the opposite side of the disk and an electronic board as shown in Figure 3-4.
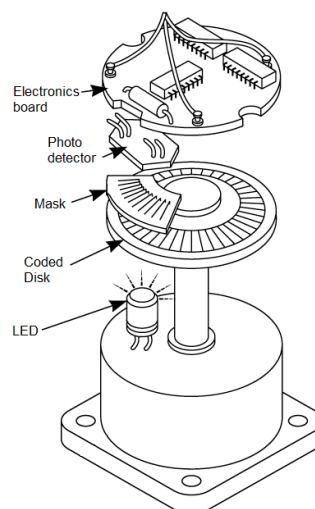

Figure 3-4: Crank shaft encoder

The coded disk has patterns with transparent and opaque area. A LED illuminates the pattern on the mask through coded disk that connects to the crankshaft. Electronics board generates square-wave pulses by reading the pattern on the mask using a photo detector. The encoder generates two signals. A clock signal pulse is generated by every segments of the encoder, and a reference signal is a single pulse per revolution. The encoder has 720 segments per revolution, thus encoder provides 0.5 ^{0}CA of resolution.

Since the engine is 4-stroke, two reference signals are generated per an engine cycle. A hall-effect sensor was installed on the camshaft to produce one reference signal per cycle. A half circle shape disk plate is connected to the camshaft, and rotates in a hall-effect sensor to block reference signal for half duration of the rotation. One of two reference signals from the encoder is blocked by the hall-effect sensor as crankshaft/camshaft ratio is 2:1. The clock signal and the remaining reference signal are transferred to an Injections control system and DAQ (data acquisition) card.

3.3.2 Injection control system

An injection control unit was built to control the both PFI (Figure 3-2) and DI (Figure 3-3). The injection control unit contains custom made 3-channel delay units and 3-channel timer units. The signals from the encoder is delayed to a set value by the delay unit and its pulse width is adjusted in the timer unit. The Injection control unit varies SOI (start of injection) timing and its duration with 0.5 ^{0}CA step for 0.1 ms to 12.5 ms. The minimum injection pulse duration depends on the performance of the injector. The pulse width of the PFI injector can be varied from1.5 ms to 12.5 ms and that of the DI injector from 0.6 ms to 12.5 ms, which are displayed on an oscilloscope. The DI injector driver was designed and supplied by Tianjin University. The driver is powered by 12 volts external DC power supply and receives the TTL signals from the control unit and sends the solenoid current to the injector.

3.4 DATA ACQUISITION (DAQ) SYSTEM

3.4.1 DAQ card

The DAQ system employs a NI (National instruments) USB-6353 DAQ card, which has 32 analogue inputs at a sampling speed of 1MS/s with 16-bit resolution. The DAQ card logs the following channels: (1.) In-cylinder pressure charge amplifier output (Voltage signal), (2.) Intake pressure (Voltage signal), (3.) Thermocouple amplifier (voltage signal), (4.) Fuel flow rate (4 to 20mA DC), (5.) Lambda sensor (Voltage signal), (6.) Encoder signal (Clock signal and reference signal). All of the data channels are logged at 0.5 ^{0}CA resolution as the encoder has 720 segments per revolution.

3.4.2 In-cylinder pressure measurement

The in-cylinder pressure is measured by means of a piezoelectric pressure transducer and a charge amplifier. A Kistler 7061B pressure transducer is installed in the M14 hole at the side of the combustion chamber between the valves. The Kistler 7061B is a water cooled quartz piezoelectric pressure transducer. Key components of the transducer are a deflected metal diaphragm exposed to the combustion chamber and quartz crystals in a housing. An increment in in-cylinder pressure compresses the quartz crystals through the diaphragm. The force acting on the crystals is converted into electrical charge, measured in pico-Coulombs (pC), a phenomenon known as the piezoelectric effect. The water cooling prevents the transducer output from being affected by changes in temperature, which affects the Yong's modulus and resonant frequency of the quartz crystals, the diaphragm and the housing. The transducer has a pressure range of 0 to 250 bar and temperature range of -50 ^{0}C to 350 ^{0}C.

Since the output of the transducer is in the form of very small electrical charge, the output is sent to a Kistler type 5001 charge amplifier via high insulation and low noise cable. The charge amplifier converts pC electrical charge to a proportional voltage signal by setting the appropriate calibration factor and range.
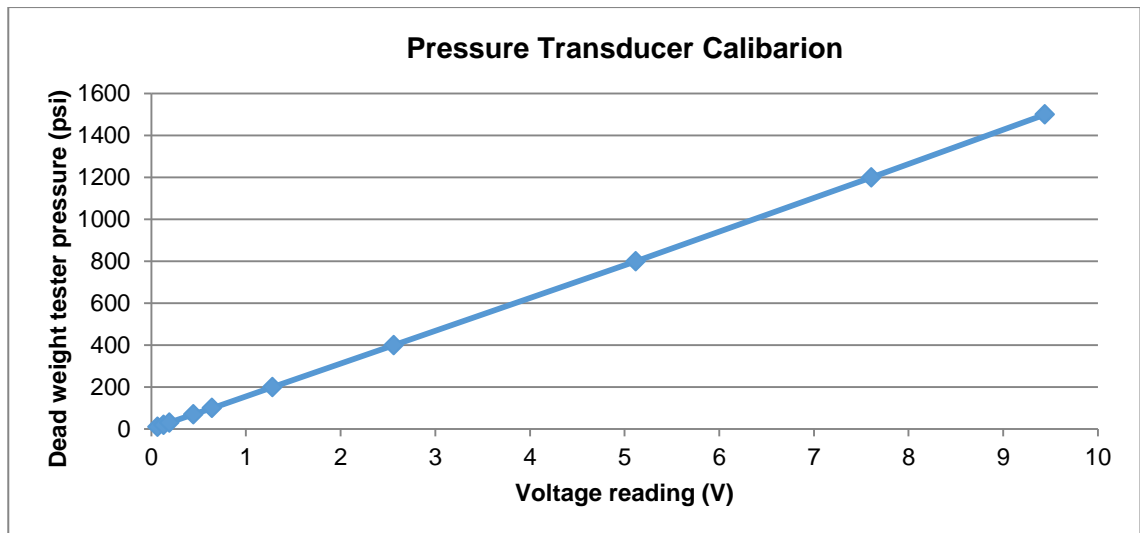
Figure 3-5: Calibration result of pressure transducer

The pressure transducer's calibration factor was checked before its calibration. During the calibration, the time constant on the charge amplifier was changed from short to the long-time constant, and then to the short-time constant for in-cylinder measurement. The charge amplifier was connected to an oscilloscope to read the voltage output from the amplifier, and the transducer was installed in a dead weight tester to pressurise the transducer. The sensitivity range of the charge amplifier was adjusted to give a voltage signal of 10 bar/V, and the linearity of the transducer was also tested as shown in Figure 3-5.

3.4.3 Intake pressure measurement

Intake pressure is measured by a Druck gauge pressure transducer (RS 746-3534) and has a response time of 10 ms with operation range from 0 to 4 bar. It is installed at 600mm from the engine intake port to measure the intake pressure.

3.4.4 Temperatures measurement

Five K-type thermocouples are installed in the engine to measure the Intake air temperature, exhaust gas temperature, engine oil temperature, and coolant temperature. There are two thermocouples to measure intake temperature. One thermocouple is used to obtain an air temperature for a calculation of air flow rate, and is located immediately down-stream of an air flowmeter. The other thermocouple near the engine intake valve port measures the air temperature into the cylinder, which is affected by the backflow during the valve overlap period. The exhaust thermocouple is located at approximately 300mm downstream of the

exhaust port. The engine oil temperature is measured in the oil sump. The coolant temperature is measured at approximately 100mm away from the engine inlet. Apart from the intake charge temperature that is displayed by a K type probe (RS 206-3722), the other four thermocouples outputs are connected to the DAQ card via a TCK-4 4-channel type-k thermocouple amplifier, which has 10mV/^{0}C output, and -200^{0}C to 1250^{0}C thermocouple range.

3.4.5 DME flow rate measurement

An Oval ALTImass Type U Coriolis Flowmeter (CA00A) is used to measure the mass flow rate of DME. The flowmeter operation range ranges from 0.4 g/min (gas: 0.2 g/min) to 40 g/min with up to 150 bar at 20 ^{0}C. The flowmeter consists of a sensor unit and a transmitter. As shown in Figure 3-3, the sensor unit is installed in the lowest position of the DME pipe line where no vibration is occurred. The location of the flowmeter is crucial to obtain accurate meter reading and to avoid a liquid-gas two phase flow, known as slug flow, which can be caused by the in-cylinder gas flow back from the injector to DME pipeline. The separate transmitter is connected to the sensor unit by a cable and its output sent to the DAQ card to record mass flow rate in g/min. The transmitter also provides the information on volume flow rate (L/min), density (g/ml), and temperature (^{0}C), but these are not recorded and are only monitored from a display screen of the transmitter.

3.4.6 Gasoline flow rate measurement

The gasoline flow rate was determined by carrying out a calibration measurement of the PFI injector in a glass flask. The pulse width was varied from 1.5 ms to 11 ms in 0.5 ms increment step. The total quantity of Injected gasoline was recorded in volume (ml) for each of the pulse width for 5 minutes, from which the injected gasoline volume per engine cycle (ml/cycle) could be determined. Then the volume was converted into mass by multiply a density of RON 95 gasoline (0.75 g/ml), shown in Figure 3-6.
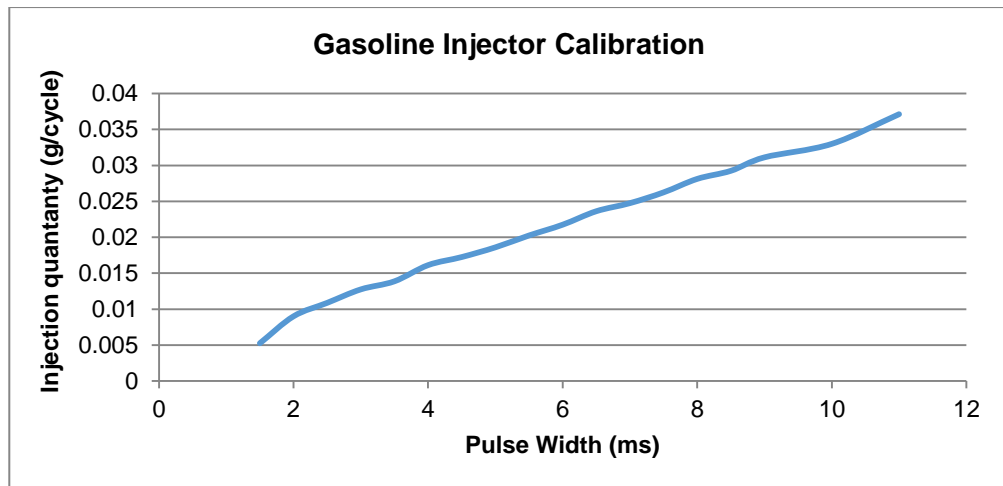
Figure 3-6: Calibration of PFI injection

3.4.7 Air flow rate measurement

An Alcock viscous flow air meter is used to measure the air flow rate downstream of an air filter. The flowmeter contains an orifice plate and two pipes are connected to the flowmeter where upstream and downstream of the orifice plate to measure differential pressure. The two pipes are connected to a multi-range manometer to provide the differential pressure unit in "Hg. The temperature that obtained by thermocouple, which located immediately down-stream of the air flowmeter, is used to read off temperature correction calibration graph (Appendix figure A3) that provided with the flowmeter. Final mass air in g/min is calculated by following equation, Equation 3-1.

$$Manometer\ reading\ ("\ Hg) \times Temperature\ correction$$
$$\times\ 1.62\ (calribration\ constant)$$
$$\times\ 36.6049\ (conversion\ from\ cf/\min\ to\ g/min)$$
$$=\ Air\ flow\ rate\ (g/\min)$$

<div align="right">Equation 3-1</div>

3.4.8 Lambda sensor

The air fuel ratio was measured using a Bosh lambda (λ) sensor LSU 4.2 and a MoTeC professional lambda meter (PLM). The lambda sensor LSU 4.2 is a wide band sensor that is designed to measure the concentration of oxygen in exhaust gases, which is then converted to the lambda value in the range of 0.7 to 32 by MoTeC PLM using the sensor's built in calibration resistor, manual table entry, and calibration constant. However it is impossible to calibrate the MoTeC PLM for this

study as the blended fuel component is constantly changed by the amount of each fuel. For that reason, the lambda value from the lambda sensor was only used for reference and the actual lambda value was determined by a use of mathematical approach that shown in Equation 3-2

$$\lambda_{gasoline} = \frac{\left(Air/_{Gasoline}\right)_{actual}}{\left(Air/_{Gasoline}\right)_{stoichiometric}} \quad \lambda_{DME} = \frac{\left(Air/_{DME}\right)_{actual}}{\left(Air/_{DME}\right)_{stoichiometric}}$$

$$\lambda_{total} = \frac{\lambda_{gasoline} \times \lambda_{DME}}{\lambda_{gasoline} + \lambda_{DME}}$$

3.4.9 Exhaust emissions measurement system

CO, CO2, and O_2 are measured by a Horiba MEXA-554JE analyser, while HC and NOx concentrations are measured by a Signal 3000HM analyser and Signal 4000VM respectively. Horiba MEXA-554JE measures the concentration of CO, CO_2, and O_2 in the range between 0 -10%, 0 - 20%, and 0 - 25% respectively. In order to obtain accurate measurement, MEXA-554JE requires some daily setting that includes replacing the three filter elements, HC hang-up test and leak check as well as calibration. The calibration is done by the use of calibration bottle of 3.48% CO, 1975 ppm HC, 14.05% CO_2 and 21.22% O_2 that supplied from Horiba.

MEXA-554JE adopts non-dispersive infrared (NDIR) technology to measure CO and CO_2, and galvanic cell to measure O_2. As shown in Figure 3-7, an IR detector measures the amount of infra-red absorbed by the sampled exhaust gas at the CO and CO2 absorption wavelength as an infra-red beam passes through the measurement cell, from which the concentration of CO and CO2 are determined.
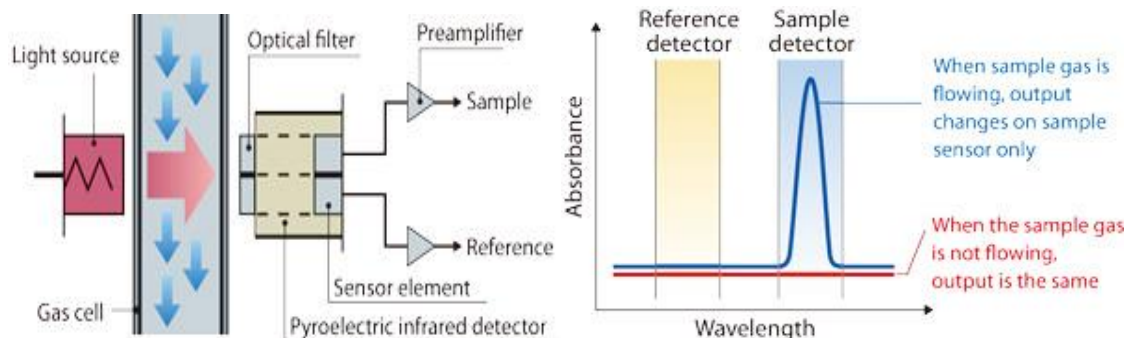

Figure 3-7: NDIR technology

Figure 3-8 shows the principle of FID technology used for HC measurement in Signal 3000HM. The exhaust gas is drawn via heated sample line at 191^{0}C in order to avoid condensation of hydrocarbon species. Air is also drawn into Signal 3000HM in order to convert into zero grade air by a catalyst into the flame chamber. The exhaust sample gas is delivered into hydrogen flame. When the sample gas is burnt in the flame, hydrocarbons in the sample produce ions that are detected by a high voltage ion collector. The current of high voltage ion collector is converted into the concentration of HC in the sample gas. 40% of hydrogen and 60% helium and zero grade air ensure accuracy of measurement as hydrogen flame is non-ionised.
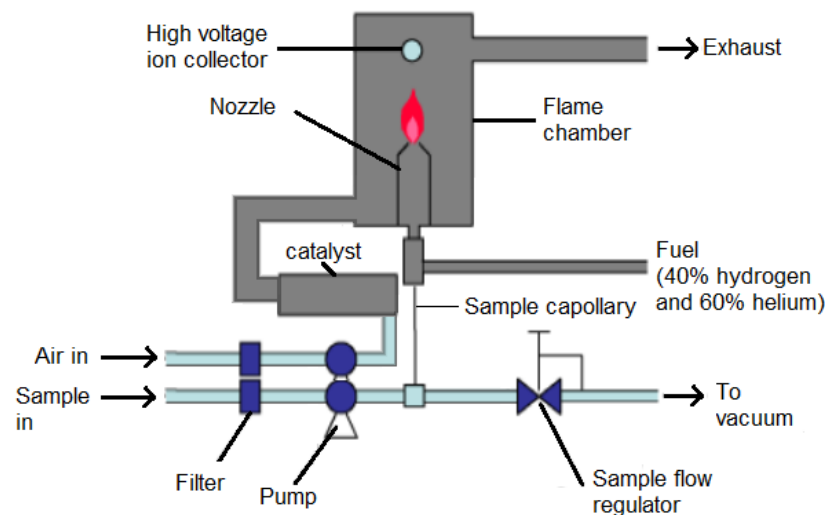
Figure 3-8: FID technology

Figure 3-9 shows the principle of chemiluminescence technology used for NOx measurement in Signal 4000VM. The exhaust gas is drawn into the reaction chamber via sample line while O_3 (ozone) that converted from O_2 via high voltage ozone generator is drawn into the reaction chamber. In the reaction chamber, NO react with O_3 and this reaction produces a quantity of light for each NO molecule that is reacted. PMT (photomultiplier) tube measure the light level in the reaction chamber as the light level is proportional the concentration of NO in the gas sample. In NOx measurement, exhaust gas is drawn into the reaction chamber via a heated catalyst that converts NO_2 to NO. This conversion allows to measure amount of NO_2 + NO in the sample.

Figure 3-9: Chemiluminescence technology (from Signal website)

3.4.10 In-Cylinder EGR measurement

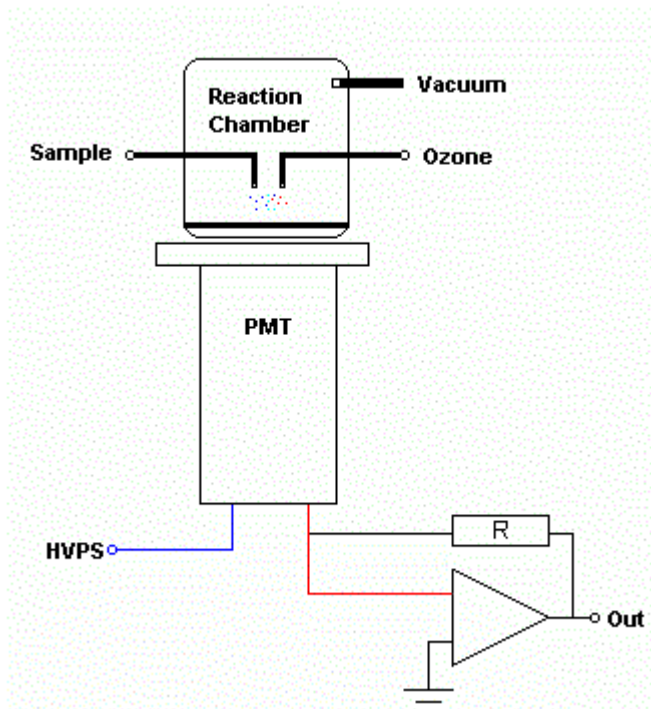The in-cylinder sampling technique coupled with exhaust CO_2 measurements were used to determine EGR (Exhaust Gas Recirculation) rate that is given by

$$\text{EGR rate} = \frac{CO_2 \text{ \% in cylinder}}{CO_2 \text{ \% in Exhaust}}$$

Equation 3-3

The in-cylinder CO2 concentration was measured by a high speed intermittent sampling valve developed at Brunel University [68]. The sampling valve adopts an electromagnetic system to operate a poppet valve of the sampling valve and the percussion principle to have faster response time. Figure 3-10 shows a diagram of the sampling valve. It can be seen that the anvil of poppet valve is not connected to the plunger of the electromagnet. Hence when the magnetic field accelerates the plunger of the electromagnet to impact the anvil, some of the plunger momentum is transferred to the anvil. This method is known as the percussion principle, and thus the opening amount and duration of the valve is controlled by varying the momentum imparted to the plunger. The electromagnet performance is important as it must rapidly build-up the magnetic flux before the valve is required to open and the plunger to build sufficient momentum. In this device, a single

voltage of 24 volts is supplied to the sampling valve to achieve adequate response. In order to seal the gap between the poppet valve and its seat, the poppet valve is made of hardened steel to seat on a seat made of copper that is soften by the hot in-cylinder gas passing though the seat.

Figure 3-10: The diagram of the intermittent sampling valve
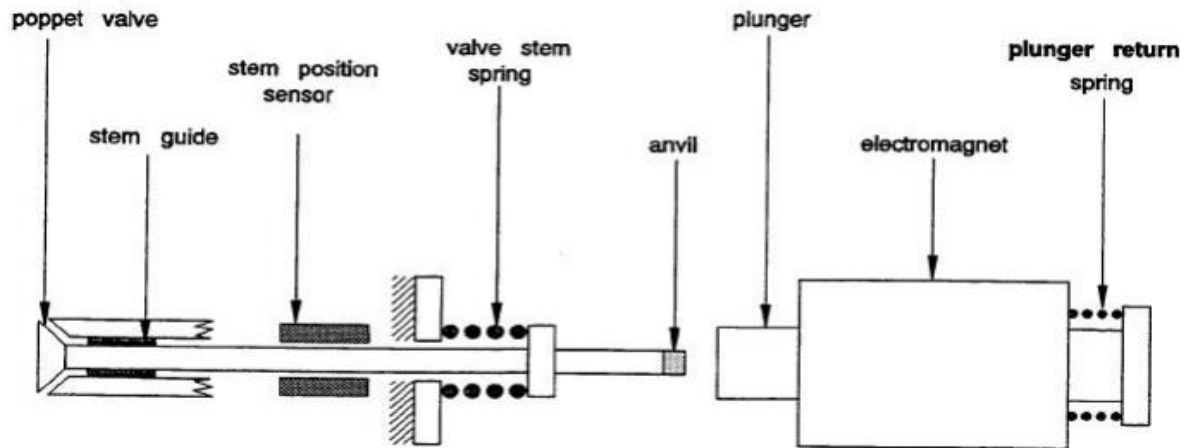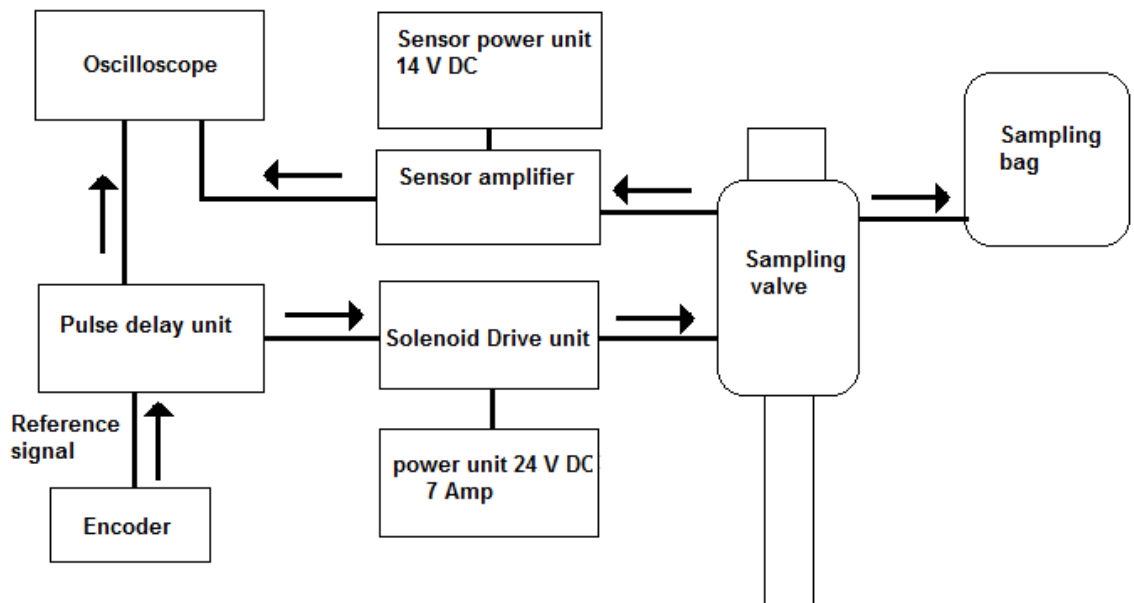

Figure 3-11: Sampling valve set up

Figure 3-11 shows the sampling valve set up. The sampling valve was installed in the cylinder head to extract a small volume of in-cylinder gas at a given time. The desired sampling timing and opening duration were controlled by the driving current sent to the solenoid actuator in the sampling valve from a signal delay unit.

The actual sampling valve opening time and duration were measured by a co-axial displacement sensor and then adjusted through the driving current signal from the signal delay unit. The sampling valve was set to open at 160^0 CA BTDC and closes at 140^0 CA BTDC during the compression stroke. The sampled gas was collected in a sampling bag and then analysed by the CO_2 analyser for cycle averaged CO_2 and hence EGR concentration measurements. Figure 3-12 shows the experimental setup diagram.
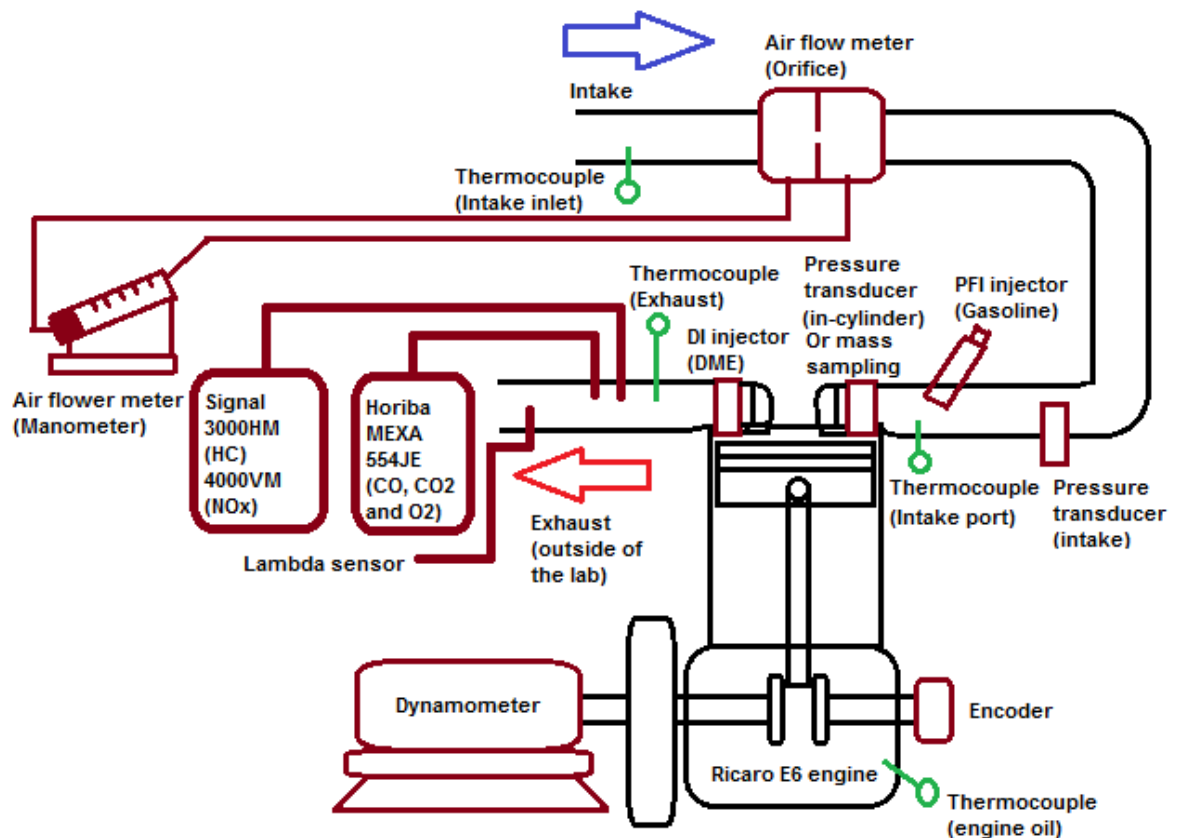
Figure 3-12: Experimental setup diagram

3.4.11 Data Acquisition and Post-processing

All the data that mentioned are recorded via a bespoke software package known as the Transient Combustion Analyser developed by Dr Yan Zhang. The P-V diagram is used to inspect if the motored data of peak cylinder pressure occur slightly before TDC. Motored data of Log p-V diagram is also inspected to see if a curvature appears during the first part of the compression line in order to confirm correct reference pressure being used.

In order to process the in-cylinder pressure data, firstly the charge amplifier output has to be converted into absolute pressure. The relationship between the output voltage and actual pressure is defined at any crank angle by

$$E(\theta) = \frac{p(\theta)}{C} + E_b$$

Where:

E = the charge amplifier output (v)

E_b = the bias voltage with zero pressure

C = the calibration factor of the system (bar/v)

A pegging process is needed to quantify the absolute pressure at a reference point in each engine cycle, which is selected at the inlet bottom dead centre (IBDC). Thus, by setting the in-cylinder pressure at IBDC equal to intake manifold absolute pressure (MAP), the absolute pressure is then determined from the output voltage at any crank angle by

$$P = C\,(E - E_{IBDC}) + P_{IBDC}$$

Where:

E_{IBDC} = the charge amplifier output at IBDC where the absolute pressure is determined

P_{IBDC} = intake manifold absolute pressure

In addition, the forced polytropic coefficient method is also included in the DAQ software based on the polytropic compression equation $PV^n = Constant$, in order to check the pegging method based on IBDC. In the forced polytropic coefficient method, the change in pressure between two points during compression is calculated by

$$\Delta P = P_i \left[\left(\frac{V_i}{V_{i+1}} \right)^n - 1 \right]$$

Where:

V_i = volume at a crank angle

V_{i+1} = volume increment to its next value

P_i = pressure at a crank angle

n = the slope of the PV diagram during compression

And

$$V_i = V_c \left\{ 1 + \frac{1}{2}(r_v - 1)\left[R + 1 - \cos\theta - (R^2 - \sin^2\theta)^{1/2} \right] \right\}$$

Where:

V_c = the clearance volume

r_v = the compression ratio

R = the ratio of connecting rod length to crank radius

Using Equation 3-4 the change in pressure between two points is written as

$$\Delta P = C[E(\theta_{i+1}) - E(\theta_1)]$$

Combining Equation 3-6 and Equation 3-8

$$E_b = E(\theta_i) - \frac{E(\theta_{i+1}) - E(\theta_1)}{\left[\left(\frac{V_i}{V_{i+1}} \right)^n - 1 \right]}$$

Pegging is performed every cycle to remove the problem of long-term drift inherent in piezoelectric devices. The converted absolute pressure is plotted against crank angle in ATDC and displayed in real time as shown in Figure 3-13.
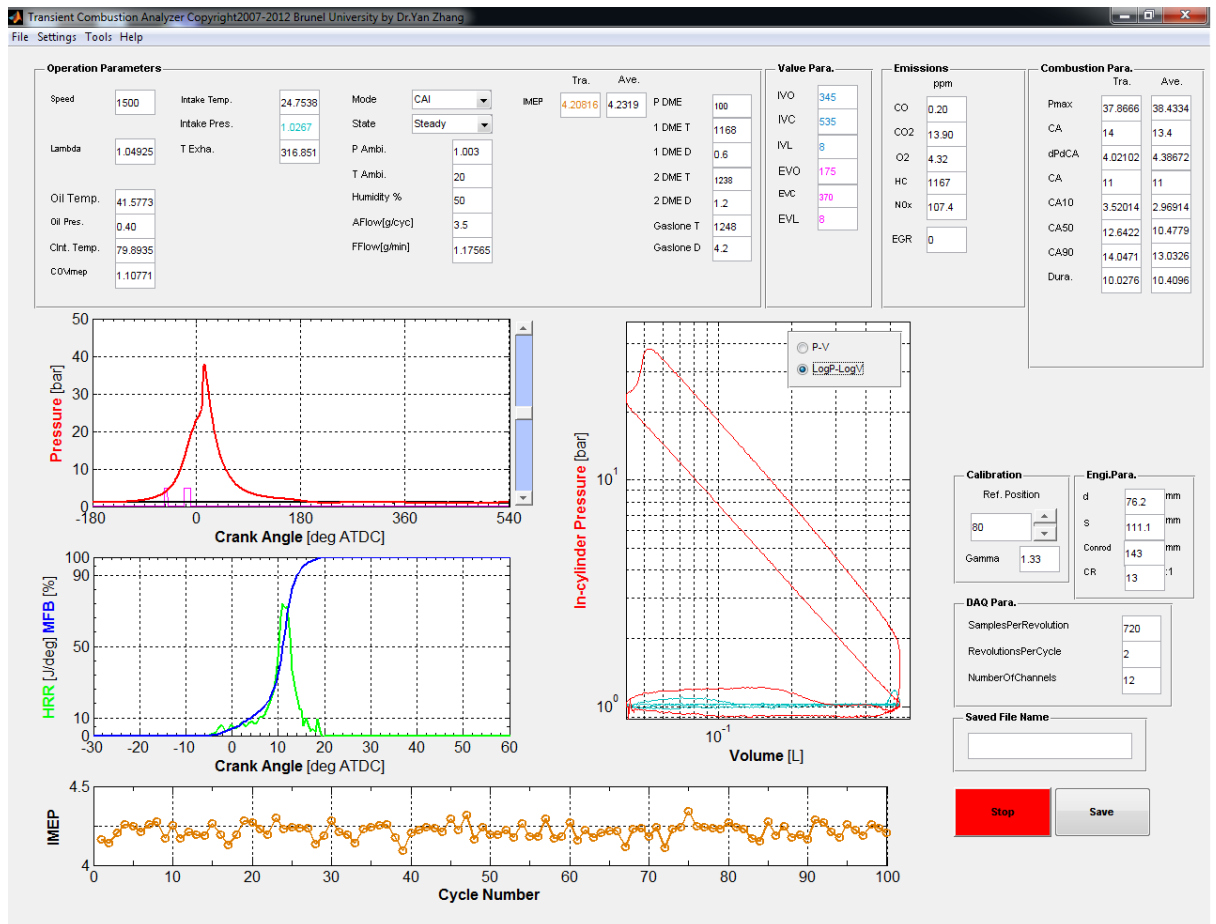
3.4.11.1 Operation parameters

Table 3-1 shows the operation parameters. The in-cylinder pressure is plotted against the cylinder volume and displayed in real time. It also allows to show logarithmic p-V diagram as shown in Figure 3-13. P-V diagram is used to obtain IMEP (Indicated Mean Effect pressure),

$$\text{IMEP} = \frac{1}{V_d} \oint PdV$$

Net IMEP and Gross IMEP are determined by the present of pumping work. If the sum of work done including entire 4 strokes (intake stroke, compression stroke, expansion stroke, and exhaust stroke), the result will be in Net IMEP, while Gross IMEP is calculated by the sum of work done during compression and expansion strokes only. Net IMEP is updated on a cycle to cycle basis in IMEP Tra. And the ensemble-averaged IMEP is displayed as IMEP Ave. as shown in Figure 3-13.

Statistical analyses is applied to analyses the coefficient of variation (COV = standard deviation/mean) in individual IMEP value, COV_{IMEP} (%), which is calculated

$$COV_{imep}\ (\%) = \frac{\sigma_{IMEP}}{\sum_1^{100} IMEP_i} \times 100$$

Where σ_{IMEP} is the standard deviation in IMEP.

Table 3-1: Parameters in operation parameters

Updated via DAQ card parameters		
Parameters	**Term**	**unit**
Lambda	Obtained from lambda sensor	λ
Oil Temp.	Engine oil temperature from thermocouple	^0C
Clnt.Temp.	Engine coolant temperature from thermocouple	^0C
COV_{imep}	Coefficient of variation of IMEP	%
Intake Temp.	Intake temperature from thermocouple	^0C
T Exha.	Exhaust temperature from thermocouple	^0C
Intake Pres.	Intake pressure from pressure transducer	bar
FFlow[g/min]	Total DME flow rate from fuel flowmeter	g/min
Manually entered parameters		
Parameters	**Term**	**unit**
Speed	Engine speed	Revolution/min
Oil Pres.	Engine oil pressure	bar
P Ambi.	Ambient pressure	bar
T Ambi.	Ambient temperature	^0C
Humidity %	Ambient humidity	%
AFlow [g/cyc]	Air flow manometer reading	"Hg
P DME	DME injection pressure	bar
1 DME T	1st DME injection Timing	Encoder clock count (1 -1440)
1 DME D	1st DME injection pulse duration	ms
2 DME T	2nd DME injection Timing	Encoder clock count (1 -1440)
2 DME D	2nd DME injection pulse duration	ms
Manually entered parameters		
Parameters	**Term**	**unit**
Gasoline T	Gasoline injection timing	Encoder clock count (1 -1440)
Gasoline D	Gasoline injection pulse duration	ms

3.4.11.2   Emissions

The concentration of CO, CO_2 and O_2 in % and the concentration of HC and NOx in ppm are entered into the software and used to calculate the specific emissions by

$$ISCO \ (g/kWh) = \frac{mass \ / \ kWh}{MW_{total} \ \times CO \ (\%) \times 0.01 \times MW_{CO}}$$

$MW_{CO} = CO \ molecular \ (28.0101 \ g/mol)$

$$ISHC \ (g/kWh) = \frac{mass \ / \ kWh}{MW_{total} \ \times HC \ (ppm) \times 0.000001 \times MW_{HC}}$$

$MW_{HC} = HC \ molecular \ (44.06 \ g/mol)$

$$ISNOx(g/kWh) = \frac{mass \ / \ kWh}{MW_{total} \ \times NOx \ (ppm) \times 0.000001 \times MW_{NO}}$$

$MW_{NO} = NO \ molecular \ (30.00614 \ g/mol)$

$$MW_{total} = \frac{\dot{m}_{gasoline} \times MW_{gasoline} + \dot{m}_{DME} \times MW_{DME} + \dot{m}_{air} \times MW_{air}}{\dot{m}_{gasoline} + \dot{m}_{DME} + \dot{m}_{air}}$$

Where:

$\dot{m}_{gasoline}$ = gasoline flowrate (g/min)

$MW_{gasoline}$ = molecular weight of gasoline = 144 g/mol

$\dot{m}_{DME}$ = DME flowrate (g/min)

MW_{DME}= molecular weight of DME = 46 g/mol

$\dot{m}_{air}$ = air flowrate (g/min)

MW_{air} = molecular weight of air = 28.97 g/mol

$$mass \ / \ kWh = \frac{\dot{m}_{gasoline} + \dot{m}_{DME} + \dot{m}_{air}}{Net \ power \ (kW) \times 60}$$

Equation 3-16

$$Net\ power\ (kW)$$

$$= \frac{NET\ IMEP\ (bar)}{10} \times \frac{swept\ volume\ (cm^3)}{1000} \times \frac{engine\ speed\ (rpm)}{60} \times 2$$

Equation 3-17

3.4.11.3   Combustion parameters

Combustion parameters displayed include the Maximum cylinder pressure (P_{max}), the crank angle at which this maximum pressure occurs (CA below P_{max}), the maximum rate of pressure rise (dPdCA = dP/dΘ), the crank angle at which this maximum rate of pressure rise (CA below dPdCA),10%, 50 % and 90% mass fraction burn rate (CA10, CA50, CA90), and combustion duration (Dura. = CA90 – CA 10).

The graph of MFB (Mass fraction burnt) curve and heat release rate are shown in Figure 3-13. In this experiments, MFB analysis will be to determine the energy-release aspects of combustion: 1. Ignition delay (2nd DME injection timing to 10% of MFB), 2. Start of combustion (10% of MFB), 3. Combustion phasing (50% of MFB), 4. End of combustion (90% of MFB) and 5. Combustion duration (10% of MFB to 90% of MFB).

The MFB (Mass fraction burnt) is calculated by using the Rassweiler and Withrow method (Equation 3-18).

$$\Delta P = \Delta P_v + \Delta P_c$$

Equation 3-18

Where:

ΔP = total the cylinder pressure rise

ΔP_v = the pressure rise due to volume (Equation 3-6)

ΔP_c = the pressure rise due to combustion

Combining Equation 3-6 and Equation 3-18 ΔP_c is evaluated as

$$\Delta P_c = P_{i+1} - P_i \left(\frac{V_i}{V_{i+1}}\right)^n$$

Equation 3-19

Where:

V_i = volume at a crank angle (Equation 3-7)

V_{i+1} = volume increment to its next value (Equation 3-7)

P_i = pressure at a crank angle

P_{i+1} = pressure increment to its next value

As the combustion process does not occur at constant volume, ΔP_c is not directly proportional to the mass of fuel burnt. Therefore the pressure rise due to combustion is referred to the clearance volume at top dead centre V_c to include the volume effect,

$$\Delta P^*_c = \Delta P_c \left(\frac{V_i}{V_c}\right)$$

Where

ΔP^*_c = the pressure rise due to combustion (including volume effect)

ΔP_c = the pressure rise due to combustion

V_i = volume at a crank angle

V_c = the clearance volume

Since ΔP^*_c includes the pressure rise due to combustion, it can be assumed that ΔP^*_c is proportional to the mass fraction burnt (χ), then the mass fraction burnt at the end of the interval $\Delta\theta$ is given by

$$\chi = \frac{MFB_i}{MFB_{total}} = \frac{\sum_1^i \Delta P^*_c}{\sum_1^N \Delta P^*_c}$$

Where

MFB_i = Mass fraction burnt at a crank angle

MFB_{total} = Mass fraction burnt from start to end

N = the pressure rise due to combustion becoming zero

ΔP^*_c = the pressure rise due to combustion (including volume effect)

It must notice that this method based on several assumptions. Firstly it assumes the effect of heat transfer does not affect to polytropic constant, however in reality constant specific heat is in a different result from compression stroke to expansion stroke. Secondly the constant volume specific is constant, which is not constant as it depends on the fuel and air mixture condition in reality. In addition the pressure rise due to combustion is not related to the mass of mixture burnt, but is proportional to the amount of fuel chemical energy released.

The result of MFB is plotted with HRR (heat release rate) on the window in real time as shown in Figure 3-13. Heat release rate analysis is based on the first law of thermodynamic, and yields directly the rate of heat release using cylinder pressure.

$$\frac{dQ}{d\theta} = \frac{\gamma}{\gamma - 1} P \frac{dV}{d\theta} + \frac{1}{\gamma - 1} V \frac{dP}{d\theta}$$

Where:

Q = heat release rate

θ = a crank angle

γ = specific heat ratio (C_p/C_v)

V = volume at a crank angle (Equation 3-7)

Above HRR equation ignores crevices flow as well as using fixed gamma value. In practical gamma is varied during compression and expansion stroke as the mean charge temperature increases during compression and then decreases during expansion. In order to obtain the most accurate heat release result, it is known as the gamma value must be set to its value of during combustion. For the experiment gamma value is fixed to 1.33.

The result of MFB is shown in CA10 = 10% MFB, CA50 = 50%, CA90 = 90% and Dura. = 10% MFB – 90% MFB are shown in Figure 3-13: Transient combustion analyser DAQ software interface. Combustion para. in Figure 3-13, Pmax shows the results of the peak cylinder pressure and CA shows a crank angle at maximum pressure occurrence. These data are useful to inspect if the motored data of peak cylinder pressure occur slightly before TDC. Motored data of Log p-V diagram is

also inspected to see if a curvature appears during the first part of the compression line in order to confirm correct reference pressure being used.

Knocking combustion is defined by means of the maximum rate of cylinder pressure rise per a crank angle (dPdCA = dP/dϴ). Knocking probability that shows the percentage of knocking cycle is coupled with average of dP/dϴ. Knocking combustion was defined by dP/dϴ > 10 bar, and knocking probability is calculated by

$$\text{Knock probability} = \frac{number\ of\ knocking\ cycles}{number\ of\ tototal\ cycles\ (100\ cycles)}$$

3.4.11.4   Calibration, Engine and DAQ parameters

Theses sections in Figure 3-13 allow to manually input calibration, engine and DAQ parameters in order to process the data. Calibration parameter consists of reference position, and gamma. Reference parameter is used to define TDC position of an encoder, while gamma (ratio of specific heats) is used for heat release calculation as explained in combustion parameter.

Engine parameter requires to calculate a volume at a crank angle. Engine parameter In Figure 3-13, D represents a bore (76.2 mm), S represents a stroke (111.11 mm), Connrod represents a Connecting rod (143 mm), and CR represents compression ratio.

In DAQ parameter, samples per revolution is defined to 720 as the encoder has 720 segments and revolution per cycle is 2 as the engine is 4 stroke. Number of channels shows how many channels are being recorded via DAQ card as explained in DAQ car section.

3.4.11.5   Post-processing (Efficiencies calculation)

Figure 3-14 shows the efficiency of the internal combustion engine. The efficiencies were calculated by follow equations.
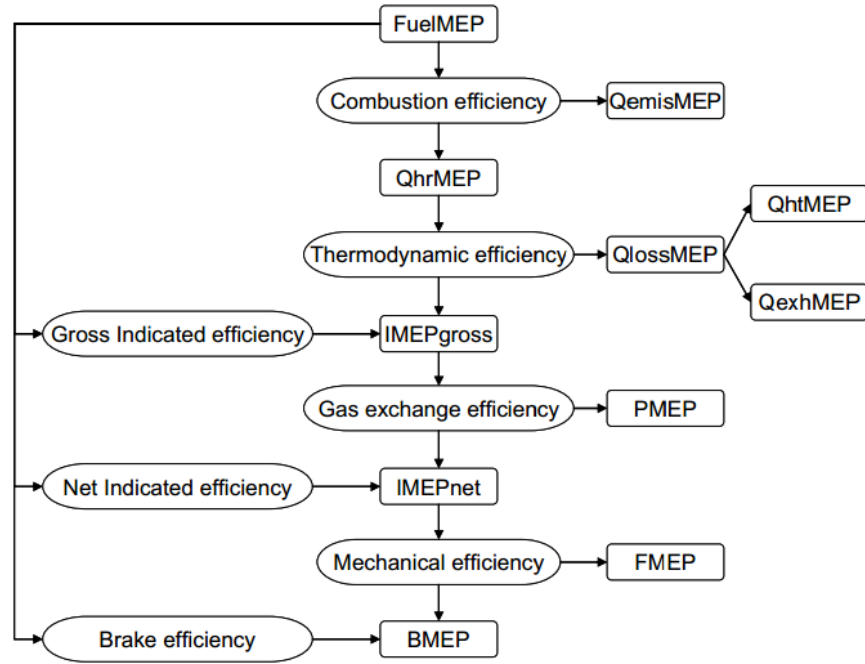
Figure 3-14: Energy flow in an IC engine

$$FuelIMEP = \frac{m_{gasoline} \times LHV_{gasoline} + m_{DME} \times LHV_{DME}}{V_d}$$

Where

$m_{gasoline}$ = mass of gasoline in one cycle

m_{DME} = mass of DME in one cycle

LHV_{DME} = lower heating values of DME (28.882 MJ/kg)

$LHV_{gasoline}$ = lower heating values of gasoline (43.448 MJ/kg)

$$Q_{hr}MEP = \eta_c \times FuelMEP$$

η_c= Combustion efficiency

$$IMEP_{gross} = \frac{1}{V_d} \int_{compression}^{expantion} PdV$$

Equation 3-26

$$BMEP = \frac{4 \times \pi \times T}{V_d}$$

Equation 3-27

$$\eta_t \text{(thermal efficiency)} = \frac{IMEP_{gross}}{Q_{hr}MEP}$$

Equation 3-28

$$\eta_c = 1 - \frac{\sum_i x_i \times LHV_i(m_{gasoline} + m_{DME} + m_{air})}{m_{gasoline} \times LHV_{gasoline} + m_{DME} \times LHV_{DME}}$$

Equation 3-29

Where:

η_c = Combustion efficiency

x_i = mass fractions of CO and HC

LHV_i = lower heating values of CO (10.1 MJ/kg) and HC (44 MJ/kg)

LHV_{DME} = lower heating values of DME (28.882 MJ/kg)

$LHV_{gasoline}$ = lower heating values of gasoline (43.448 MJ/kg)

$$\eta_g \text{(gross efficiency)} = \frac{IMEP_{gross}}{FuelMEP}$$

Equation 3-30

$$\eta_n \text{ (net indicated efficiency)} = \frac{IMEP_{Net}}{FuelMEP}$$

Equation 3-31

$$\eta_b \text{ (brake efficiency)} = \frac{BMEP}{FuelMEP}$$

Equation 3-32

$$\eta_{ge} \text{ (gas exchange efficiency)} = \frac{IMEP_{Net}}{IMEP_{gross}}$$

Equation 3-33

$$\eta_m(\text{mechanical efficiency}) = \frac{BMEP}{IMEP_{Net}}$$

Equation 3-34

3.5 SUMMARY

Ricardo E6 engine and its set up for DME assisted gasoline CAI combustion experiment have been described. The E6 engine has prepared both the direct DME injection system and the port fuel gasoline injection system that can be controlled at 0.5 CA resolution. The technology of NDIR, FID and chemiluminescence that used to measure CO, HC and NOx respectively, have been explained. The high speed intermittent sampling valve that used to extract in-cylinder gas for measuring EGR rate and its operating method has been described. DAQ system utilises bespoke software package to log the in-cylinder pressure, fuel flowrate, air flowrate, intake pressure and many temperatures at 0.5 CA resolution. The detailed description of the post-processing and analysis are also present.

Chapter 4   DESIGN OF RE-BREATHING CAM LOBE AND ENGINE OPERATION

4.1 INTRODUCTION

This chapter documents the procedure of designing a re-breathing cam lobe and engine operation to carry out an experiment. Re-breathing cam lobe was designed to obtain 35% EGR. Ricardo WAVE 1-D simulation was adopted to predict the amount of the trapped residual gas in the cylinder, and then the predicted profile was used to produce technical drawing by a use of Solid works. The test procedure was also described in this chapter.

4.2 DESIGN OF RE-BREATHING CAM LOBE

4.2.1 Cam lobe description

Since E6 engine is 4 stroke engine, a cam lobe rotates at half the speed of the crank shaft. A cam lobe lifts a valve by pressing its rocker arm, which locates under the cam lobe. There is a clearance between a base circle and a rocker arm to prevent mechanical friction when the cam lobe is expanded by heat.
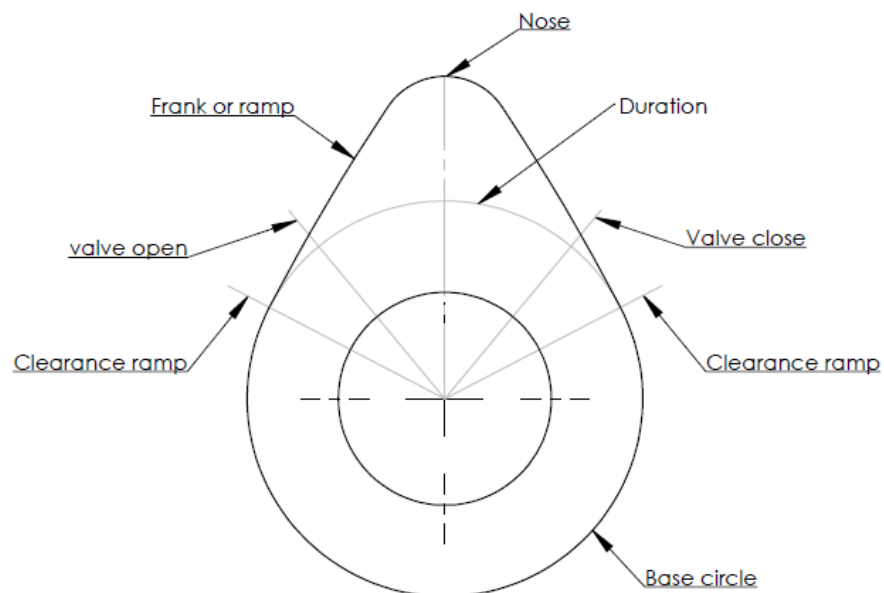

Figure 4-1: Description of cam lobe

Figure 4-1 describes cam profile terms. As the cam rotates in clockwise, a valve is lifted by frank or ramp of cam. The valve open and close timing are not considered

as soon as the valve lift because narrow passage limits the flow, thus the valve open and close timing are considered at 0.5mm valve lift. Since the intake re-breathing strategy utilises intake valve event during the exhaust stroke, a cam profile requires an extra nose before the main valve event.

In WAVE simulation, the duration and the height of pilot valve intake was varied to determine the effects of re-breathing valve in terms of trapped residual gas rate and volumetric efficiency. And then the obtained re-breathing valve profile was used to produce CAD drawing for CNC (Computer Numerical Control) machining. Cam lobe was made of tool steel and was hardened (tempered in an oven) to increase Rockwell scale to be above 50.

4.2.2 Ricardo E6 engine modelling on WAVE

Since WAVE simulation does not allow to have dual fuel neither DME as the main fuel, gasoline fuelled a single cylinder SI was modelled as shown in Figure 4-1. In general parameter section, simulation duration was defined as 40s to allow enough cycles to auto converge.
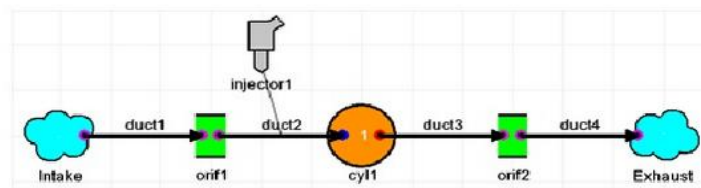

Figure 4-2: E6 model on Wave build

The Intake port and the exhaust port were defined by using two duct elements, and each two ducts were connected by orifice elements. Each duct lengths and diameters are defined by measuring the length of each pipe on E6 engine and initial conditions of ducts were defined as shown in Table 4-1. These initial conditions data were obtained by carrying out an experiment on real engine.

Table 4-1: Definition of ducts for WAVE modelling

Initial conditions	Intake port (duct 1 and duct 2)	Exhaust port (duct 3 and duct 4)
Pressure	1 bar	1.05 bar
Temp	300 K	900 K
Wall temp	310 K	910 K
Friction coefficient	0	0
Heat transfer coefficient	1.5	1.5

In the engine general panel, geometry of the engine, combustion, operating parameter and heat transfer were defined. Geometry data were entered according to the engine specification that mentioned in the previous chapter, while the other parameters were obtained from a test. Figure 4-3 shows the defined geometry and combustion model. In SI Weibe combustion model, location of 50% was defined to 23 degrees ATDC, which is quite late for optimised combustion phasing. This is because the test that carried out to obtain SI combustion parameter for WAVE model used single DME injection to initiate combustion instead of spark discharge, early DME injection timing leaded to CAI combustion which is not allowed in WAVE simulation.
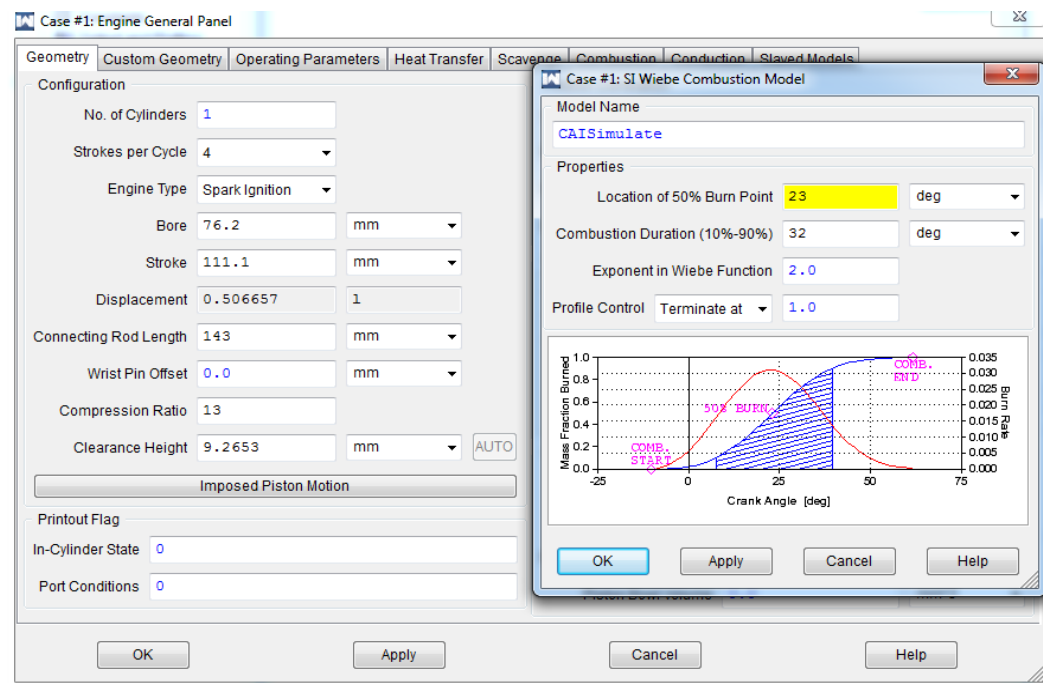
Figure 4-3: Defining the geometry and combustion

Operation parameter section required to define engine speed, 1500 rpm was entered as the speed that used for the test. Heat transfer tab only allows to use the Woschni correlative model, which assumes simple heat transfer from area that exposed to the combustion chamber.

Table 4-2 shows the data that entered in heat transfer tab. Values of heat transfer were used to calibrate the simulation data to the test data. Increasing heat transfer was result in decreasing peak pressure. Surface area multiplier for piston top and cylinder head were determined by piston face and cylinder head shape. Since the engine has flat surface for both piston face and cylinder head, value 1 was used.

56

All the temperature data were used default value as they were not possible to measure temperature from the test. Swirl ratio, which only used for compression ignition engine for improve fuel vaporisation was set to 0 as the engine has straight intake port.

Table 4-2: Defining heat transfer

Woschni model	Value
Heat transfer when intake valves are open	1.1
Heat transfer when intake valve are closed	1.2
Piston top surface area multiplier	1
Cylinder head surface area multiplier	1
Piston top temperature	520 K
Cylinder head temperature	520 K
Cylinder liner temperature	400 K
Intake valve temperature	420 K
Exhuast valve temperature	480 K
Swirl ratio	0

As the simulation was to found out the optimised re-breathing valve profile with 35% EGR rate, various valve profiles were used to define the valves. Firstly, the profiles of an intake and an exhaust cam lobes of E6 engine were measured by means of a dial indicator and then the profiles were plotted as shown in Figure 4-4.
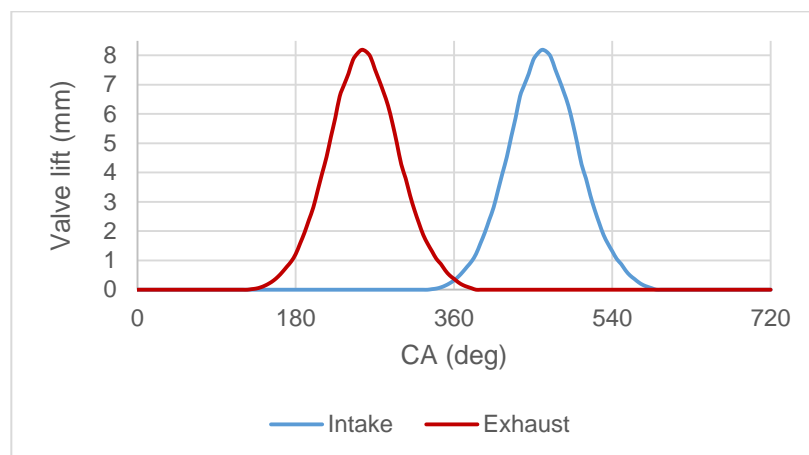
Figure 4-4: Measured cam lobe profiles for the intake

And then various pilot valve profiles were added on the intake valve profile as well as modified intake valve profile. Series of simulations were carried out by using various valve events. The maximum pilot valve lift was varied from 1.5 mm to 4 mm, while the duration was varied from 100 ^{0}CA to 160 ^{0}CA. Pilot valve opening

and closing timing was also varied to minimise pumping loss. WAVE required to define flow coefficient profile that describe how restricted the flow through the valve is at different lift position, this data is obtained through a process of port flow testing using a steady airflow rig. Since it was not possible to test, CFTYP option, which pre-formatted external file, was used to define the coefficient profile for all the simulation work.

The last part of modelling E6 engine on WAVE was to add a PFI injector, which added on duct 2 as shown in Figure 4-2. Defining injector requires three parameters, a position of injector, a temperature for the injected fuel and an amount that will vaporise upon injection into the fluid stream, and an air fuel ratio. The position of injector was defined to 40 mm from the left end on duct 2 on position tab, while 330 K was entered for mixture temperature, and 0.3 for the liquid fraction evaporated after injection on the properties tab. AFR was defined as 14.7, which is stoichiometric for gasoline fuel.

The simulation result of motored in-cylinder pressure graph was compared to the result of experiment to verify E6 WAVE model has been calibrate.

4.2.3 Simulation results and discussion

The first simulation was carried out to determine the effect of the lift height of pilot intake valve that has shorter valve event than the main valve event with PVO (Positive Valve Overlap) on trapped residual gas. As shown in Figure 4-5, the main intake valve duration was increased from 185 ^{0}CA to 295 ^{0}CA to achieve PVO. Pilot intake valve duration was also fixed at 120 ^{0}CA while its height was varied from 2.7 mm to 3.7 mm in increment step of 0.2 mm.

The simulation results indicated that increasing the lift height of pilot valve increased the EGR rate from 36% to 59%. Mass flux, which is the rate of mass flow per unit area, at duct 2 was examined to determine the flow rate and its direction at every crank angle. In Figure 4-6, negative mass flux indicates reverse flow into the intake whereas, positive mass flux indicates flow inducted into the cylinder. It can be seen that although the start point of decreasing mass flux was slightly varied by the lift height of pilot valve, the decreasing mass flux occurred at the lift height of pilot valve was around 0.5 mm rather as soon as valve start moving. The decreasing mass flux back to zero, and then it started decreasing

again before it turns to positive value, after that the mass flux back to zero when the lift height of intake valve reached to 0.5 mm. The first negative peak was occurred by pilot valve event, while the second negative peak was caused by PVO. It was noticed that the variation of mass flux was greater in the second negative peak although the duration of PVO was fixed to all the test. The result also point out that having pilot intake valve event would provide well mixed the mixture of air and the exhaust gas as it allows time to mix in the intake port before inducted into the cylinder, thus homogeneous EGR will be obtained.

Another simulation was carried out by using the valve profile that shown in Figure 4-7. For this simulation, Pilot valve profile was added without positive valve overlap while the lift height of pilot intake valve was varied from 1.5 mm to 4 mm in increment step of 0.5 mm as shown in Figure 4-8.
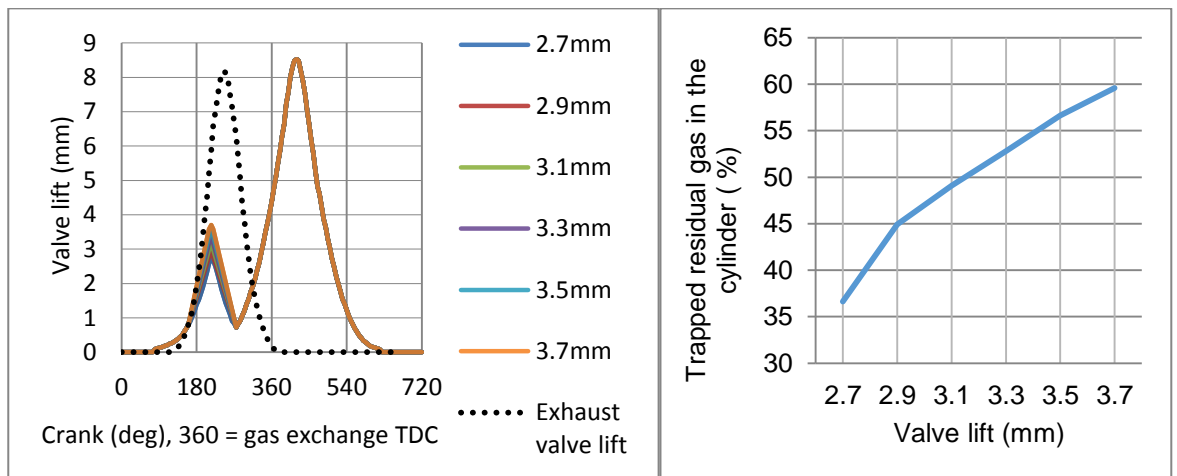
Figure 4-5: Intake re-breathing valve lift variation with PVO and simulation result of EGR rate
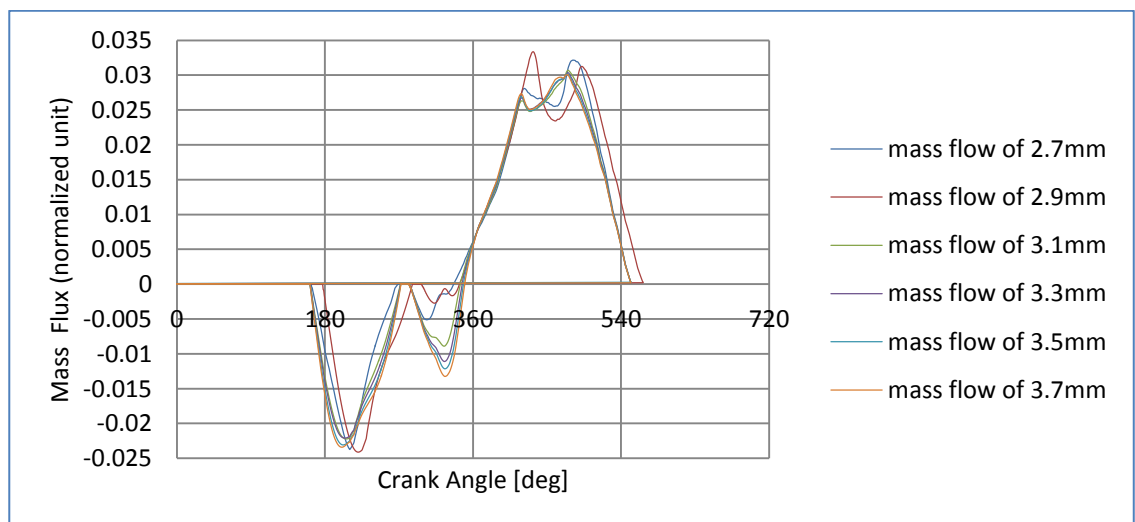
Figure 4-6: The variation of Intake mass flow, 360 = gas exchange TDC
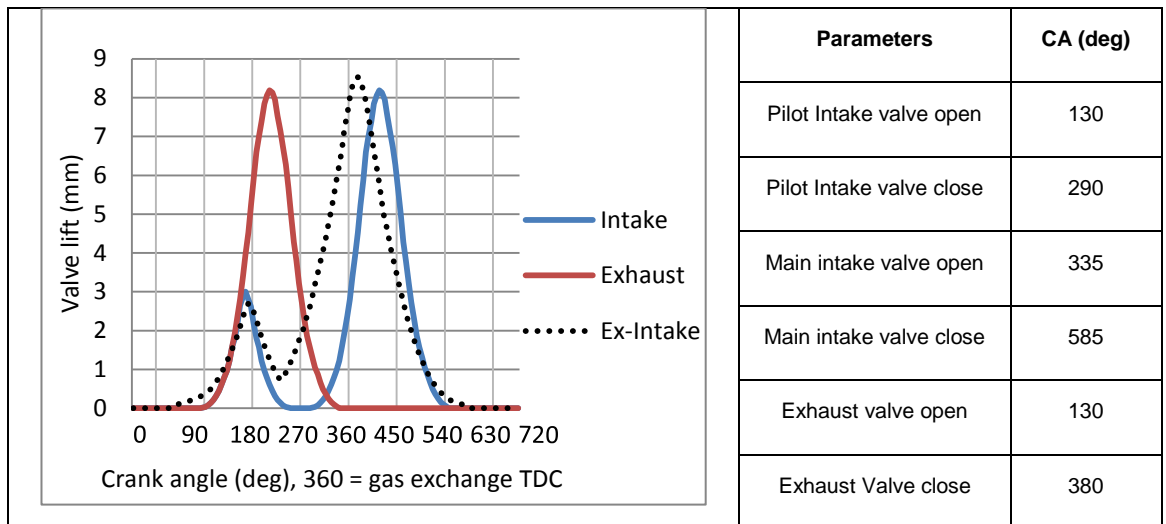
Figure 4-7: Valves profile for simulation

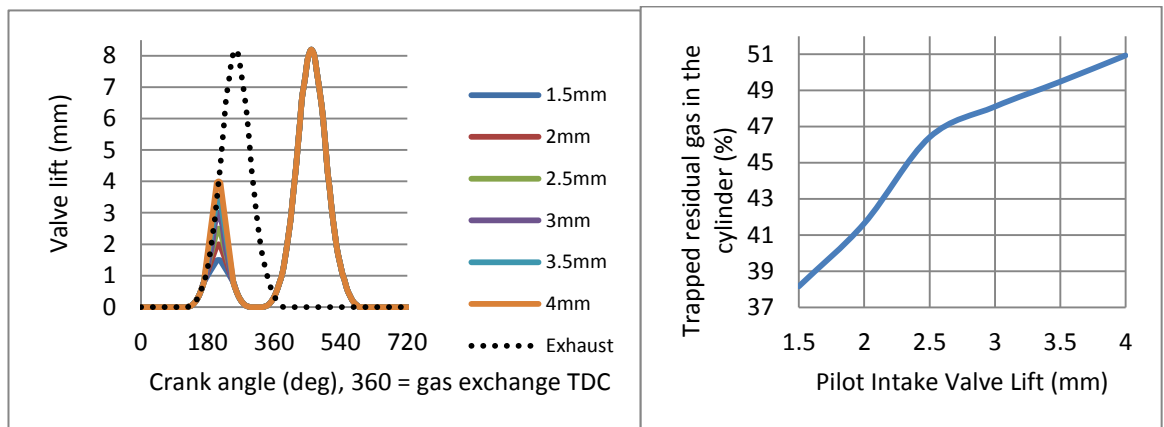| Parameters	CA (deg)
Pilot Intake valve open	130
Pilot Intake valve close	290
Main intake valve open	335
Main intake valve close	585
Exhaust valve open	130
Exhaust Valve close	380

Figure 4-8: Intake re-breathing valve lift variation without PVO and simulation result of EGR rate

The maximum EGR rate of 51% was obtained by 4 mm lift height of the pilot valve, while 1.5 mm lift height of the pilot valve provides the minimum EGR rate of 38%. Since 1.5mm lift height of pilot was the minimum valve open due to the 0.5 mm valve threshold, another simulation was carried out by varying the pilot valve open duration from 100 ^{0}CA to 160 ^{0}CA at fixed maximum lift height of the valve as shown in Figure 4-5.
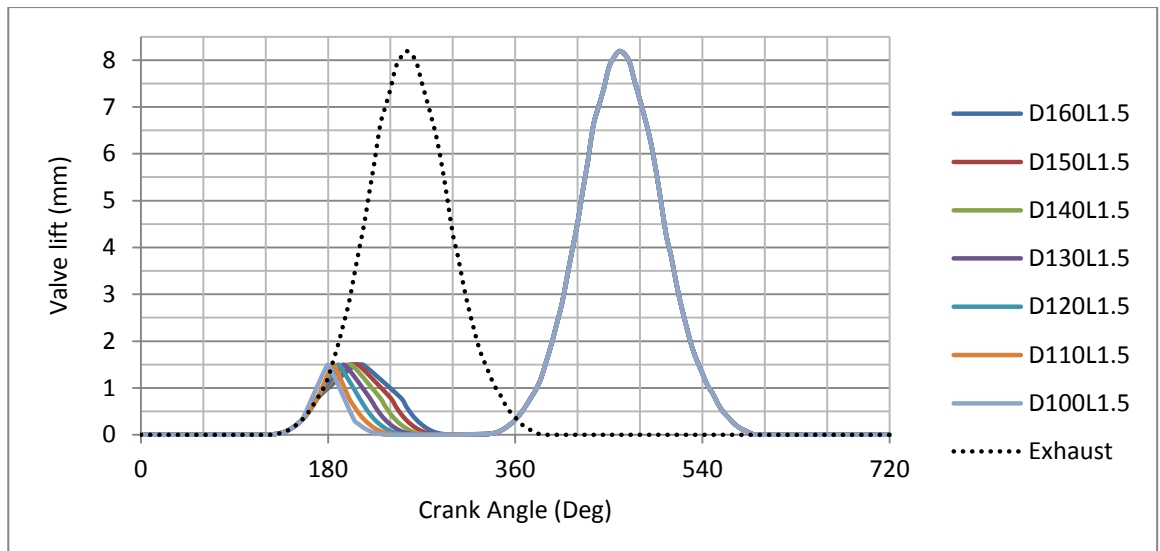
Figure 4-9: Valve profiles for pilot intake duration variation simulation

Figure 4-10 shows the simulation result of EGR rate by the variation of pilot intake valve duration. EGR rate was increased by increasing pilot intake valve duration from 27% to 38%. The EGR rate variation due to the variation of duration was minor compare to the lift height of pilot intake valve. Although the duration of 140 ^{0}CA provides 35% EGR, it was decided to use the duration of 130 ^{0}CA in order to match with the exhaust valve open speed. Another simulation was carried out at fixed duration of 130 ^{0}CA while the lift height was varied from 1.5 mm to 4 mm in increment of 0.5 mm step as shown in Figure 4-11.
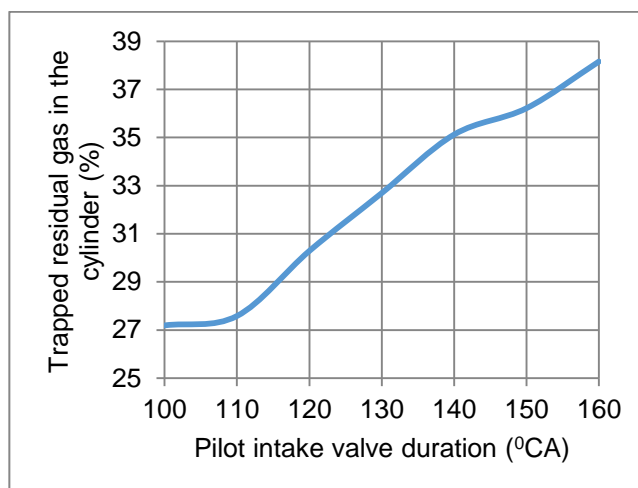
Figure 4-10: Simulation result of EGR rate by the variation of pilot intake valve duration
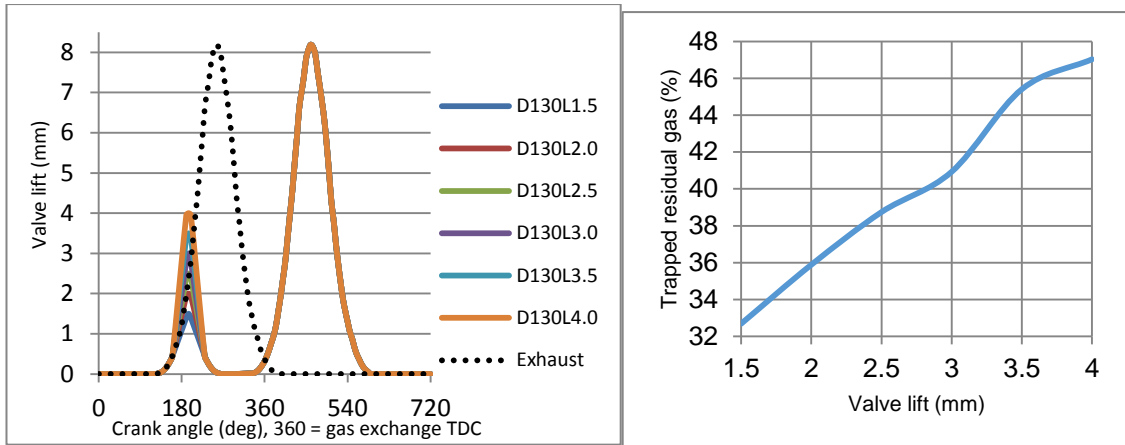
Figure 4-11: The profile of vales that used for simulation and the result of EGR

The simulation result predicted that the lift height of pilot intake need to be around 1.8 mm and the obtained valve parameters are shown in Table 4-3.

Table 4-3: WAVE predicted valve parameter to obtain 35% EGR

For 35% EGR	
Pilot Intake valve open	CA 130 deg
Pilot Intake valve close	CA 260 deg
Pilot Intake valve lift	1.8 mm
Main intake valve open	CA 335 deg
Main intake valve close	CA 585 deg
main Intake valve lift	8 mm

Since re-breathing valve will be achieved by one intake poppet valve, dwell duration between the pilot valve and the main valve would not be possible to change once the cam lobe is made. Another simulation was carried out to determine the optimum dwell duration between the valve events. Figure 4-12 shows the valve profiles that used for the simulation. It has to be noticed that in this simulation, T = represents the pilot IVO timing, which the valve start lift rather than 0.5 mm of valve threshold and L represent the lift height of valve. The timing of exhaust valve open matched to the timing of pilot intake valve although only two exhaust valve profiles are shown in Figure 4-12. This was to minimise the variation of EGR rate by varying pilot intake valve open timing.
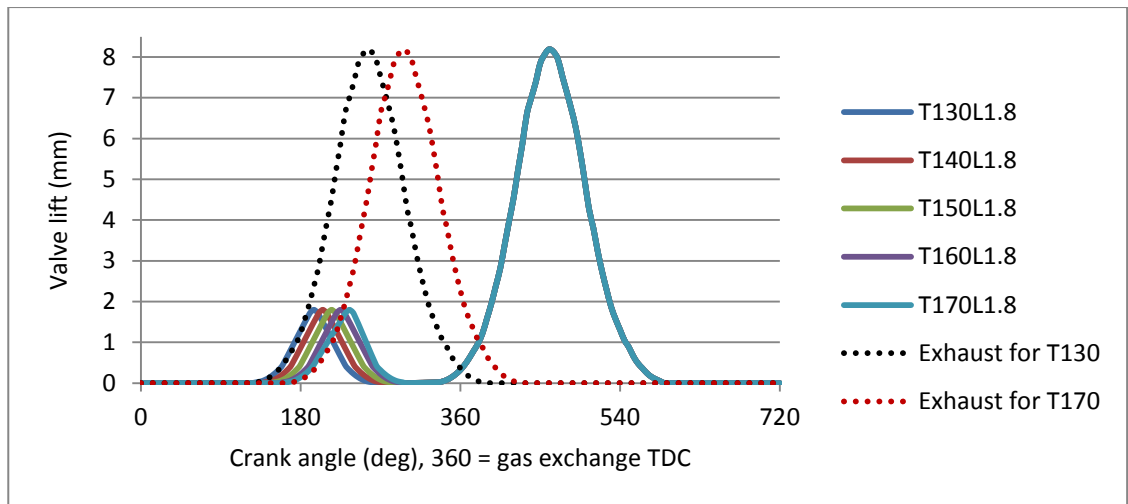
Figure 4-12: Pilot valve open timing (T = pilot valve open timing, L= the lift height of pilot valve)
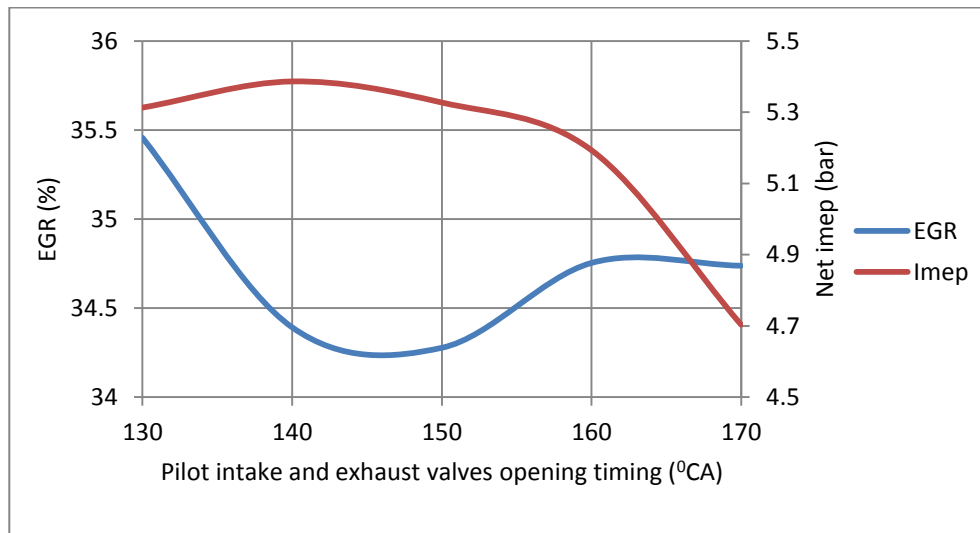

Figure 4-13: Simulation result of IMEP and EGR rate

Figure 4-13 shows the simulation result of IMEP and EGR rate. The maximum EGR rate of 35.4 % and the minimum EGR rate of 34.4 % were obtained while the net IMEP value was varied from 5.4 bar to 4.7 bar. IMEP was slightly increased by retarding pilot IVO timing from 130 ^{0}CA to 140 ^{0}CA, and then IMEP was decreased by retarding pilot IVO timings. As the exhaust valve timing was retarded with pilot IVO timing, IMEP curve represents the trade-off in selecting the exhaust valve timing. It is known that the exhaust valve requires to open before the piston reaches the Bottom dead centre (BDC), this is to reduce the exhaust pumping work during exhaust stroke by using exceeds in-cylinder pressure during exhaust stroke, otherwise the positive work will waste to push the exhaust gas. However too early exhaust valve timing leads to reduction in the effective expansion ratio and expansion work, and is not compensated for by reduced the pumping work.

63

Figure 4-14 shows the PV diagram of the pilot IVO timing of 140 ^{0}CA, which considered to be early EVO, and 170 ^{0}CA, which considered to be late EVO. It is notice that early EVO of 140 ^{0}CA was in the result of smaller exhaust pumping loss. Therefore, the pilot IVO timing of 140 ^{0}CA was considered to be the optimised timing of the pilot IVO timing and EVO timing for net indicated efficiency.
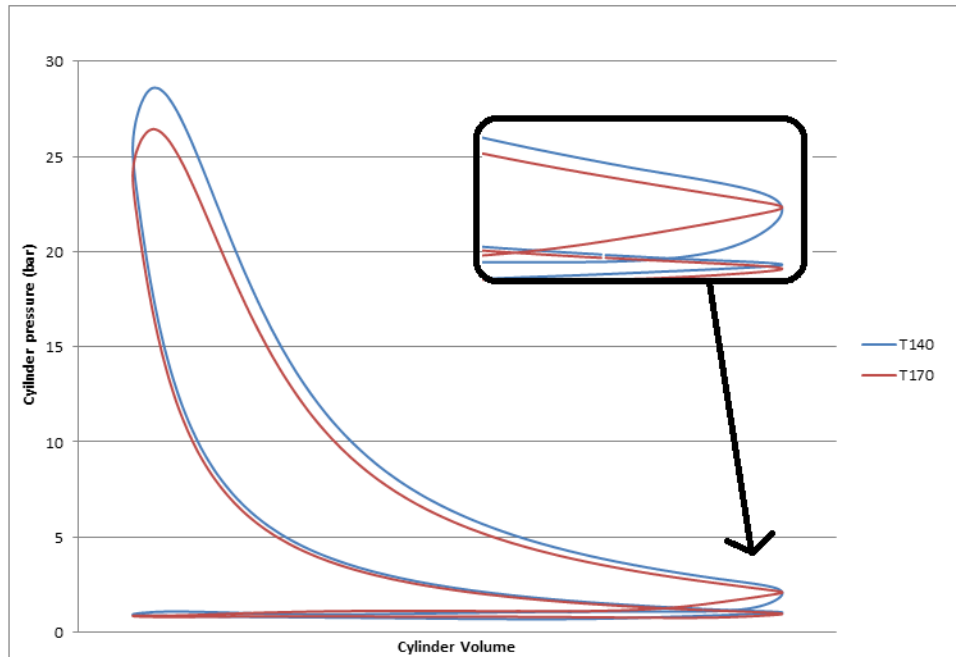

Figure 4-14: Comparison of PV diagram for early and late timing of EVO

Table 4-4: Final re-breathing valves parameters that predicted by WAVE

For 35% EGR	
Pilot Intake valve open	CA 140 deg
Pilot Intake valve close	CA 270 deg
Pilot Intake valve lift	1.8 mm
Main intake valve open	CA 335 deg
Main intake valve close	CA 585 deg
main Intake valve lift	8 mm
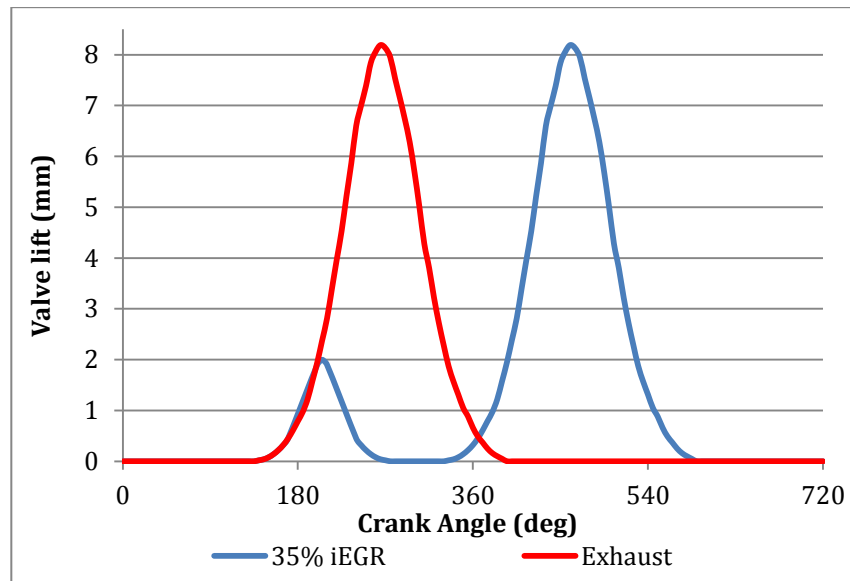
Figure 4-15: Final re-breathing valves profiles that predicted by WAVE

4.2.4 Cam lobe design

The predicted cam lobe profiles were used to produce technical drawing by means of Solid works. Figure 4-16 shows the diagram of 35% cam lobe. Since pilot intake valve open indicates the point where a valve starts lifting, the duration of each valve events were defined by a half duration of the crank angle.

The maximum valve lifts of pilot and main valve event needed to add the tappet clearance of 0.2mm, and their position were defined on the half of their duration to have exact same acceleration and deceleration during the valve opening and closing. The noses radius were defined by comparing the profile of simulation and the technical drawing. The nose of pilot valve event was define to 2 mm and its main valve was to 5.5mm. Figure 4-17 shows the comparison of CAD valve profile and simulation valve profile.
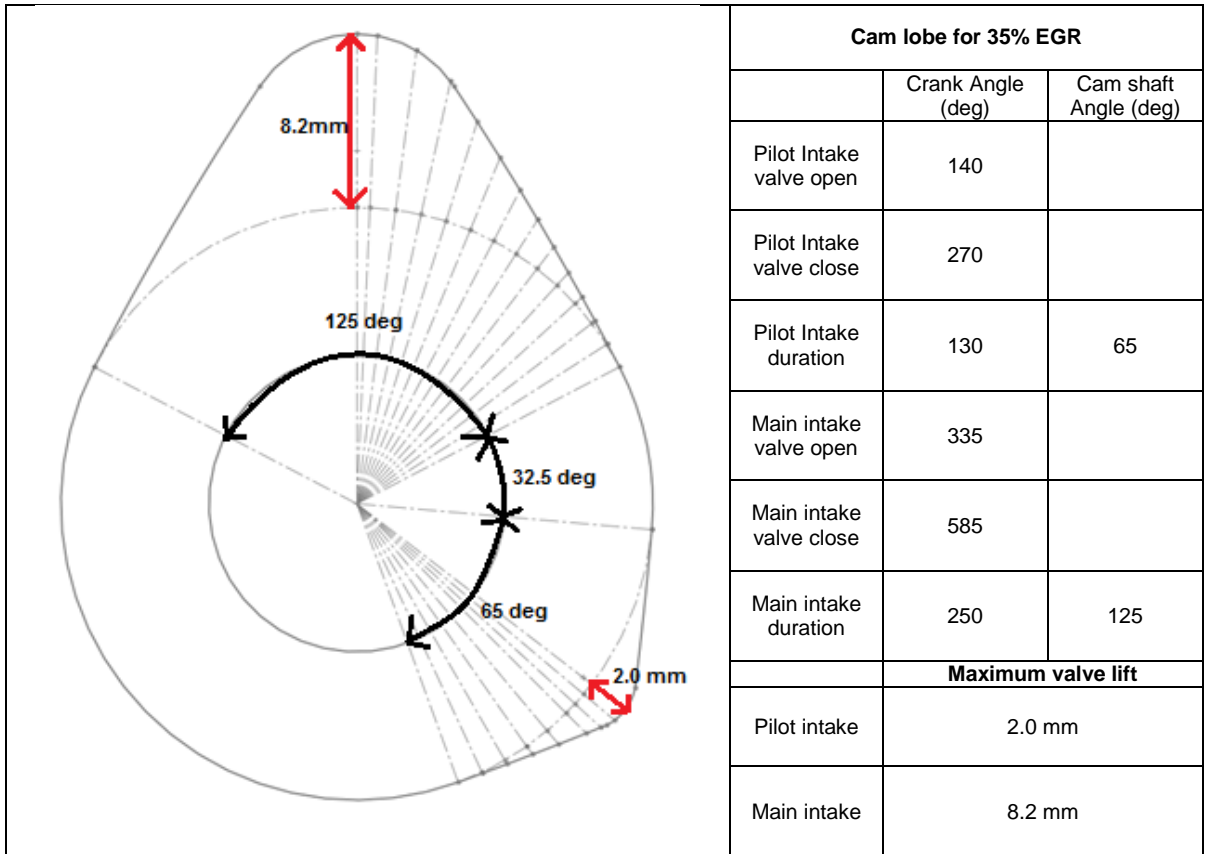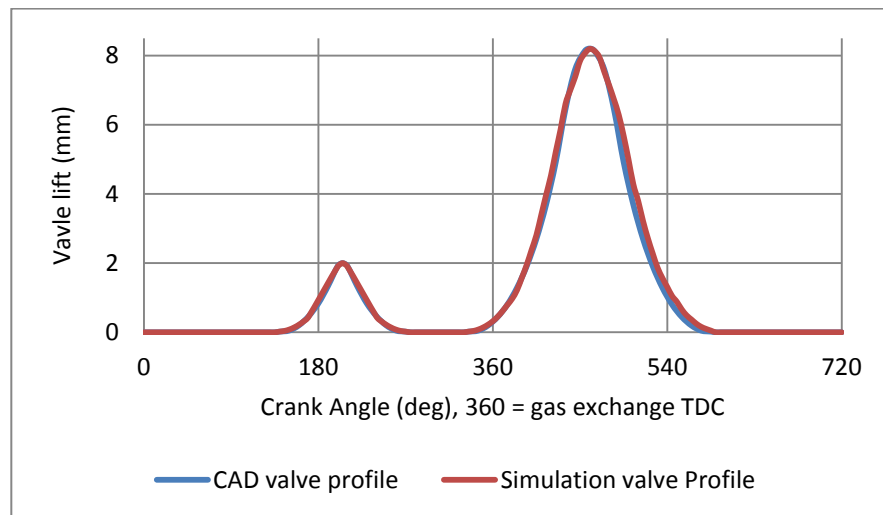
Cam lobe for 35% EGR		
	Crank Angle (deg)	Cam shaft Angle (deg)
Pilot Intake valve open	140	
Pilot Intake valve close	270	
Pilot Intake duration	130	65
Main intake valve open	335	
Main intake valve close	585	
Main intake duration	250	125
Maximum valve lift		
Pilot intake	2.0 mm	
Main intake	8.2 mm	

Figure 4-16: Diagram of re-breathing cam lobe for 35% EGR

Figure 4-17: Comparison of CAD valve profile and simulation valve profile for 35% EGR
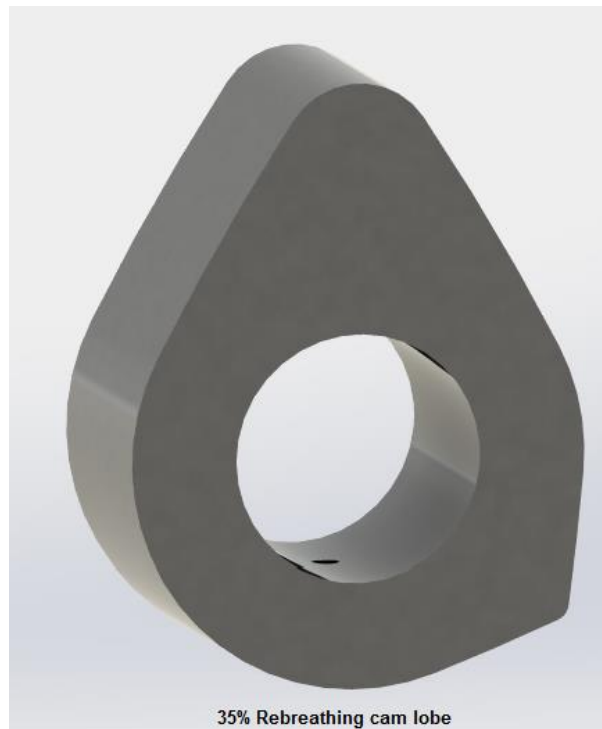
Figure 4-18: Rendered view of 35% re-breathing cam lobes

4.3 ENGINE OPERATION

4.3.1 Warm-up the engine

Before carrying out an experiment, the engine was warmed up to operating temperature of 80 ^{0}C by means of an immersion heater (3 kW) in the water circulation system, and an electrical heater (0.5 kW) that located in the crankshaft case. This is because initially with a cold engine, air mass flow rate was around 10% higher than its operating temperature, thus air/fuel ratio was reduced as the engine reached to its operating temperature. Motored peak in-cylinder pressure seemed to be reduced with a cold engine as leakage between a piston and in-cylinder wall is greater than when the engine reaches to operating temperature. In addition, auto-ignition timing of CAI combustion and its timing highly depended on temperature and the mixture strength, hence maintain the engine temperature at steady state was one of key obtain accurate data.

4.3.2 Preparing the emission analysers

Horiba MEXA-554JE, which used to measure CO, CO_2 and O_2 required replacing three filters, pre-filter, strainer and dust filter as well as HC hang-up test and leak check on a daily basis. The MEXA-554JE was serviced every year, and the

calibration was done by the use of calibration bottle of 3.48% CO, 1975 ppm HC, 14.05% CO_2 and 21.22% O_2 that supplied from Horiba when it indicated calibration symbol.

Both Signal 3000HM, measuring HC and signal 4000VM, measuring NOx required to warm up an oven to 191 ^{0}C. Once the oven is warmed up, the fuel of 40%/60% mixture of hydrogen and helium was supplied to the 3000HM with the pressure of 2.07 bar (207 kPa). The 3000HM ignited the mixture with zero grade air, and when the flame temperature reached to above 550 ^{0}C the calibration was carried out by using propane span gas. The 4000VM required to connect a zero gas supply in 0.7 bar (70 kPa), and air supply in 0.7 bar (70 kPa) to generate O_3. Once 4000VM temperature reached to generate O_3, calibration was carried out. This process ensure the measured emission data are accurate.

4.3.3 Test procedure

A test was carried out when the engine was warmed-up and the emission analysers were ready to sample. Firstly, engine condition was checked, such as external EGR valve, throttle, coolant temperature and compression ratio. Once the engine condition was adjusted to desire setting, gasoline and DME injection timing and their injection duration were adjusted. Secondly the engine was motored to 1500 rpm as all of the experiments were carried out at 1,500 rpm. After that injection switches were on to inject the fuels, the coolant heater was turned off when the combustion took place. As gasoline was used as main fuel, gasoline injection duration was adjusted for air/fuel ratio to lambda 1, while 1st DME injection duration was used to control combustion duration and its phasing, and 2nd DME injection timing was adjusted to achieve stable combustion, which defined as COV_{IMEP} in below 10%. The combustion parameters, such as CA 10, CA 50, and CA90, and combustion stability were monitored through the DAQ software that mentioned in Chapter 3. Once the all the control parameters were set to the test point, 100 cycles of test points were recorded and the data was used to analyse the test. All the test points were measured in this test procedure.

4.4 SUMMARY

In this chapter, designing re-breathing cam lobe and the engine operation procedure have been descried. The E6 engine was modelled on WAVE, and the model was used to predict the EGR rate. The simulation results showed that the burnt gas flowed into intake during pilot valve event and then flow inducted into the cylinder during main intake valve event. When positive valve overlap (PVO) presented after the pilot intake valve, the lift height of pilot valve affected to the amount trapped residual gas during PVO. Dwell duration between the pilot valve and the main valve was also examined by the variation of pilot intake valve open timing and exhaust valve opening timing. Too early pilot IVO timing was result in the waste of positive work during expansion stroke, but too late IVO timing increased pumping work during the exhaust stroke. It was found that the optimised timing of EVO and pilot IVO timing was located around 10 ^{0}CA before bottom dead centre of exhaust stroke. The predicted valve profiles to obtain 35% EGR was used to produce CAD drawing by a use of solid works. Test procedure was described from warming up the engine and preparing the emission analysers to obtain the data.

Chapter 5 EXPERIMENTAL INVESTIGATION OF DME ASSISTED GASOLINE CAI COMBUSTION WITH INTAKE RE-BREATHING

5.1 INTRODUCTION

The 35% re-breathing cam lobe described in Chapter 4 was installed in the E6 engine to enable the intake re-breathing operation. Gasoline combustion has been achieved during this research by means of direct DME injection and trapped residual gas that obtained by the re-breathing valve strategy.

In this chapter, DME assisted gasoline CAI combustion has been experimentally researched to determine effects of intake valve timing, DME injection timing, split DME injection ratio, compression ratio and air/fuel ratio. A series of experiments were carried out. The first experiment varied intake valve timing to determine the optimised intake valve timing for net indicated efficiency, and then the optimised intake valve timing was employed to determine the effects of DME injection timing on various split DME injection ratio. Finally, the optimised intake valve timing and the DME injection timings were employed to study the performance, combustion and emission characteristics of DME/Gasoline operations at different compression ratios, air/fuel ratios and split DME injection ratios.

5.2 THE EFFECT OF INTAKE VALVE TIMING

5.2.1 Experiment condition

Since CAI combustion is realised by compressing premixed charge to auto-ignite, initial charge temperature is one of dominant factors to control the CAI combustion. In this research intake charge heating was mainly obtained by the trapped residual gas which depended on the rebreathing process of exhaust gas during the initial opening of the intake valve in the exhaust stroke, as shown in Figure 5-1. Thus intake valve timing test was first carried out. The variation of intake valve timing would result in the variation of both the pilot intake valve and main valve intake opening timings. The intake re-breathing timing test was carried out at a fixed engine speed of 1,500 rpm, lambda 1.3, CR 15 and 4.2 bar net IMEP while intake valve opening (IVO) was varied from 15^0CA BTDC to TDC (gas

exchange TDC) with fixed EVO (exhaust valve opening) at 185 ^{0}CA BTDC and EVC (exhaust valve close) at 10 ^{0}CA ATDC. Both intake and exhaust valve opening/closing timings were defined by 0.5mm valve lift.
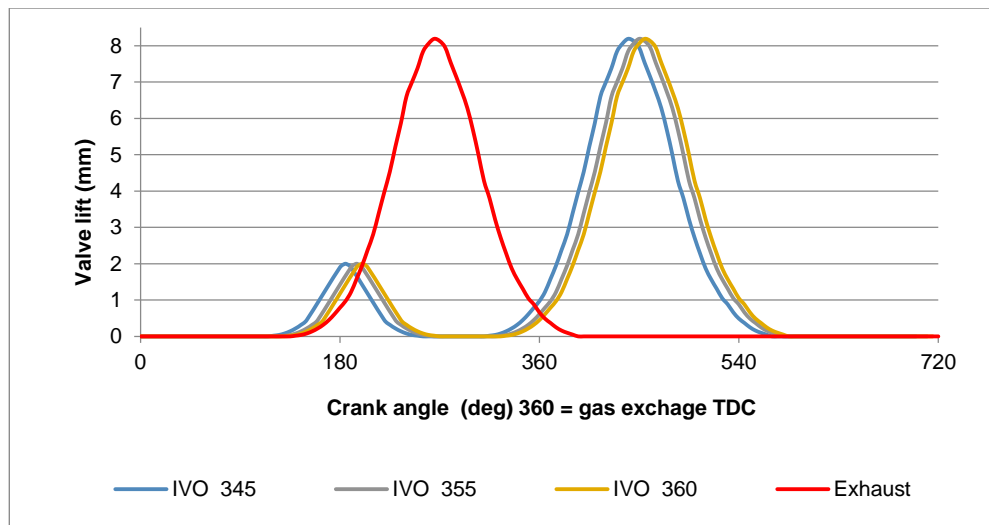

Figure 5-1: Tested valve profiles

Table 5-1: Gasoline and DME injection quantity and timing for the test

Parameters	Value
Compression ratio	15:1 (geometric)
Engine speed	1,500 rev/min
Coolant temperature	80 ^{0}C
Intake pressure	Naturally Aspirated (1bar)
Atmosphere temperature	25 ^{0}C
Gasoline Injection pressure	2.5 bar
DME injection pressure	100 bar
Net IMEP	4.2 bar
1st DME SOI timing (adjusted to each case)	309 ^{0}CA ~ 312 ^{0}CA
2nd DME SOI timing (adjusted to each case)	340.5 ^{0}CA ~ 342.5^{0}CA
Total mass of DME injection	1.826 mg/cycle to 2.541 mg/cycle
Gasoline SOI timing	344 ^{0}CA
Mass of gasoline	15.225 mg/cycle

Table 5-1 shows the test condition. The variation of intake valve timing affected the gas exchange efficiency and hence the volumetric efficiency. In order to compare the indicated efficiency at a constant load, it was necessary to vary the gasoline/DME ratio from 93%:7% to 86%:14% by increasing the DME injection quantity at a fixed gasoline injection quantity. The increased mass of DME

injection was only used to compensate for the change in the volumetric efficiency in order to keep the overall air/fuel ratio to lambda 1.3. 60%:40% split injection strategy was applied to the DME injection. The first DME injection during the early compression stroke was used to increase the reactivity of the premixed gasoline/air mixture, and the second DME injection near TDC was introduced to trigger the start of auto-ignition combustion.

5.2.2 The effect of intake re-breathing timing on performance

The variation in the intake valve timing has affected the EGR rate, volumetric efficiency, and intake temperature. As shown in Figure 5-2 and Figure 5-3, the EGR rate and the volumetric efficiency were increased by retarding IVO timing from 25% to 29%, and 51% to 55% respectively. Both the higher EGR rate and the volumetric efficiency could be attributed to the lower intake charge temperature as shown in Figure 5-4, which was measured at the intake port close to the back of the intake valve. With both main IVO and the pilot IVO retarded, the temperature of the burned gas into the intake port would be lowered and hence the lower intake charge temperature, which leads to the increased volumetric efficiency.

In order to compensate for the increased air in the cylinder at a constant relative air/fuel ratio of 1.3 and IMEP of 4.2 bar for a fixed mass of gasoline, the mass of DME was increased as shown in Figure 5-5.
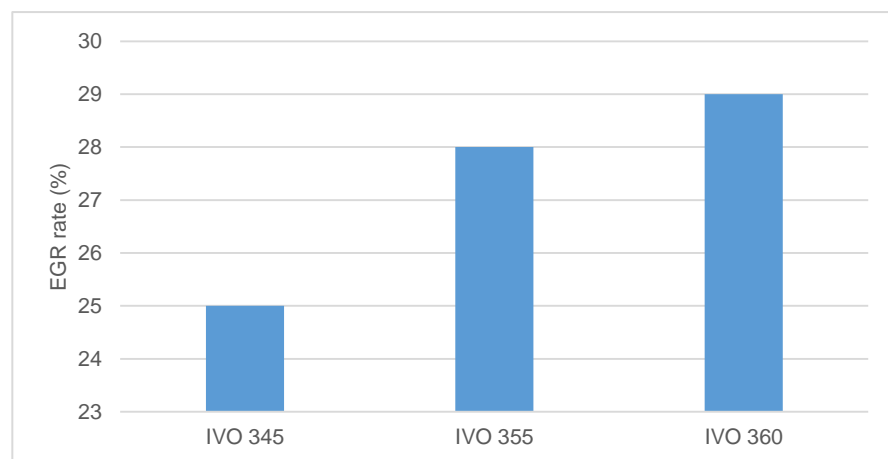
Figure 5-2: Measured EGR rate
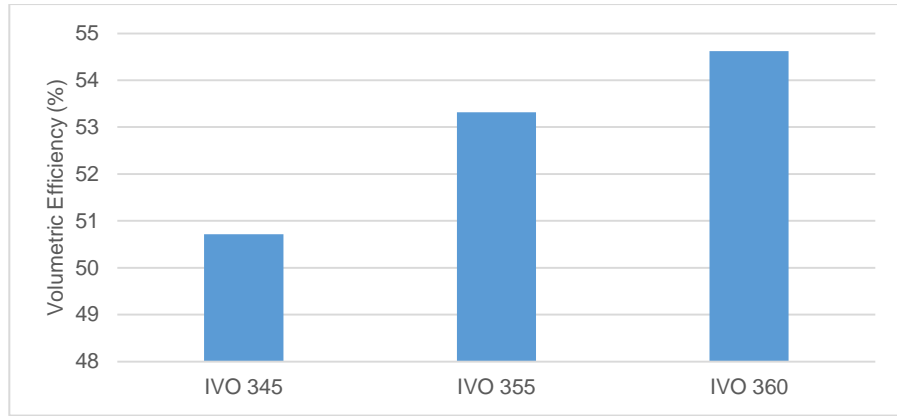
Figure 5-3: Volumetric efficiency variation by the change of IVO
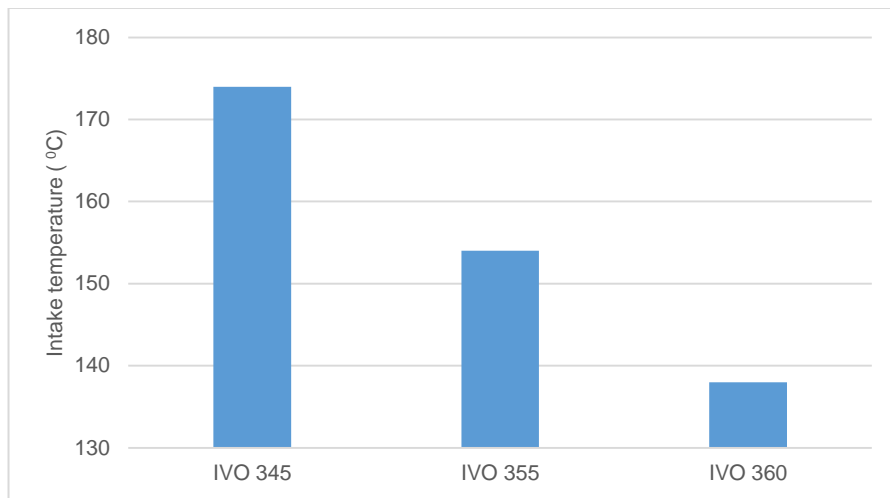
Figure 5-4: Intake charge temperature
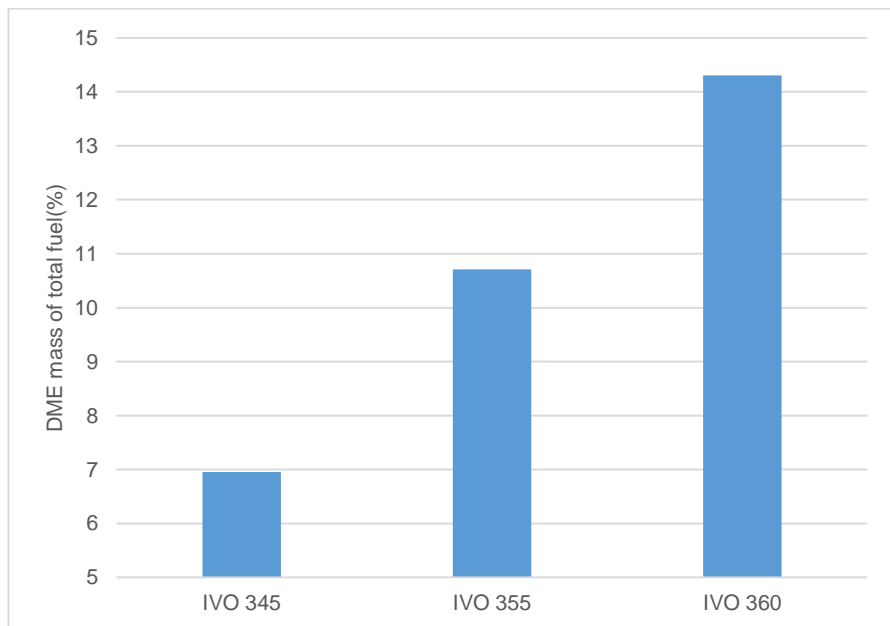
Figure 5-5: Percentage of DME mass
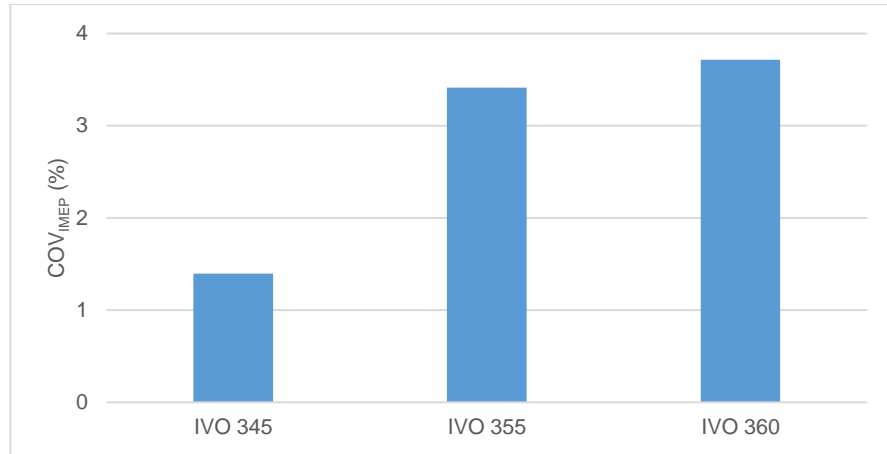
Figure 5-6: COV$_{imep}$

As shown in Figure 5-6, COV$_{IMEP}$ increased slightly with retarded IVO. Initially it was expected to achieve lower COV$_{IMEP}$ with higher DME injection mass because DME was more flammable than gasoline. This could be caused by the combined effect of the decreased intake temperature and the higher concentration of EGR rate, which slowed down the auto-ignition reactions.

Figure 5-7 shows the in-cylinder pressure traces at the three IVO timings. Both 1st and 2nd DME injection timings were optimized for minimum fuel consumption in each case. The peak in-cylinder pressure of IVO 345 was the highest and there was little difference between peak cylinder pressures of IVO 355 and IVO 360. In addition, IVO 360 case was characterized with a lower charge pressure than the other two cases between 330 ^{0}CA to 350 ^{0}CA despite of its higher volumetric efficiency, indicating more heat release reactions had taken place with the IVO 345 and IVO 355 due to higher charge temperature.
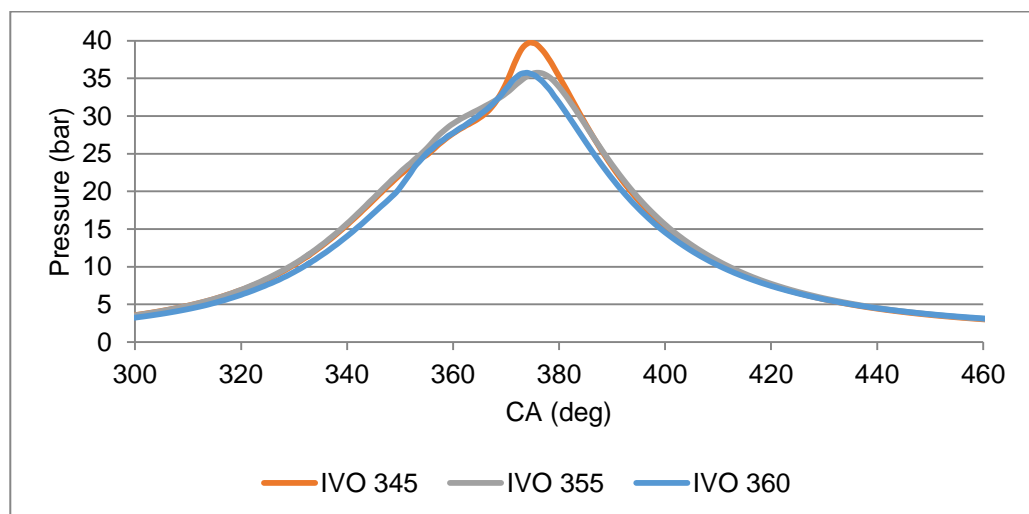
Figure 5-7: In-cylinder pressure traces (360 = firing TDC)

Figure 5-8 shows the 2nd DME injection timing and CA10, CA50 and CA90 of MFB (mass fraction burned). Here, 2nd DME injection is considered as the ignition source and the duration between the start of 2nd DME injection timing and CA 10 is defined as the main ignition delay period. As more DME was injected with retarded IVO, 2nd DME injection timing was slightly retarded in order to avoid violent combustion. The ignition delay was shortened with retarded IVO timings. In comparison, the combustion duration (Figure 5-9) defined by CA10 – CA90 became longer with the retarded IVO. This may be explained by the lower charge temperature and higher percentage of EGR at retarded IVO.

2nd DME injection timing
IVO 345 = -19.5 ATDC
IVO 355 = -18.5 ATDC
IVO 360 = -17.5 ATDC
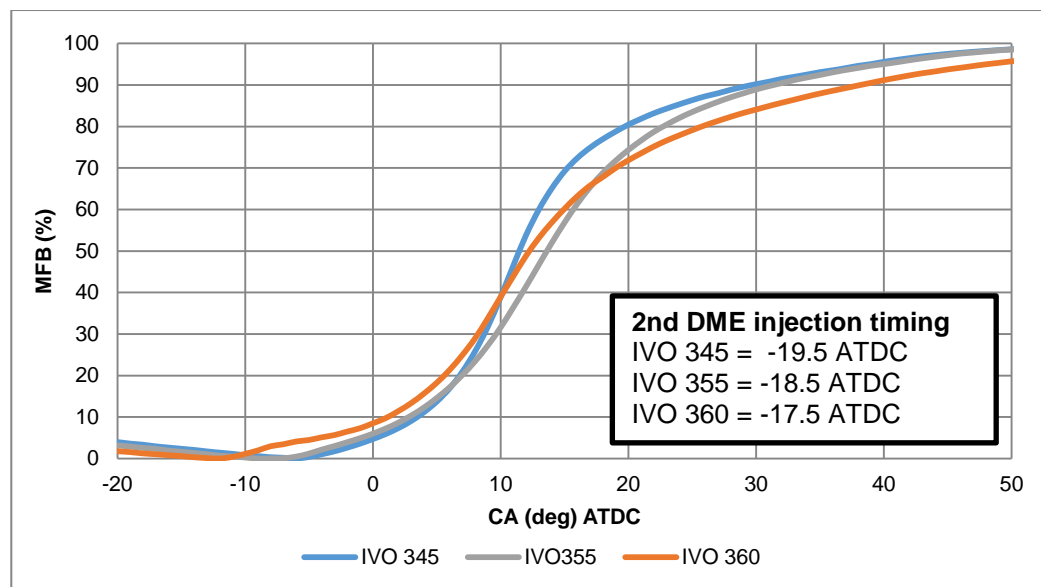
Figure 5-8: 2nd DME injection timing, 10%, 50% and 90% MFB
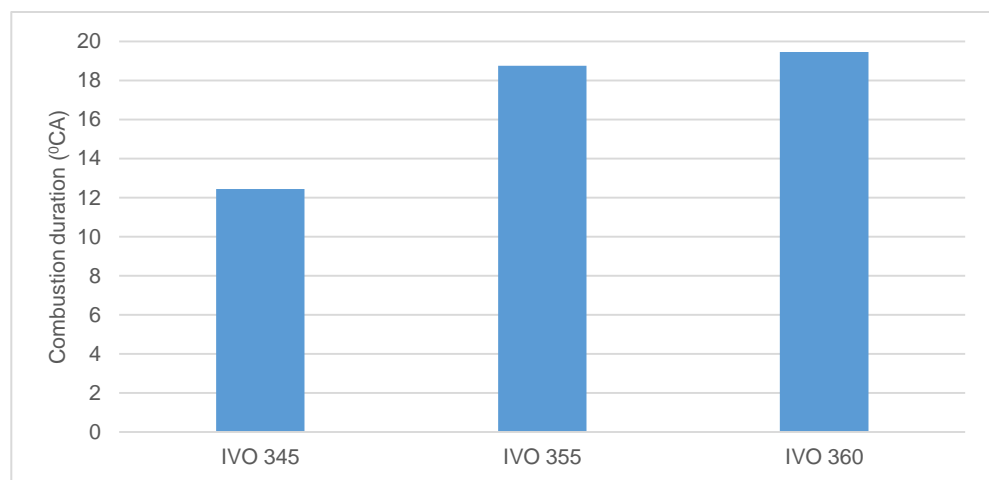
Figure 5-9: Combustion duration

5.2.3 The effect of intake re-breathing timing on emissions and efficiencies

The measured exhaust emissions (indicated specific emissions) for the three IVO timings are shown in Figure 5-10, Figure 5-11 and Figure 5-12. Interestingly, CO emission and HC emission exhibited opposite trends as IVO timings were changed. CO emission increased from 6 g/kWh to 8 g/kWh and HC emission slightly decreased from 11.5 g/kWh to 11.28 g/kWh with the retarded IVO timing. Increased CO emission seems to be correlated to the lower initial charge temperature and higher COV_{IMEP} at the retarded IVO. The slight increase in uHCs could be caused by the slower and delayed combustion at the retarded IVO. NOx emission was very low and varied from 0.5 g/kWh to 0.4 g/kWh.
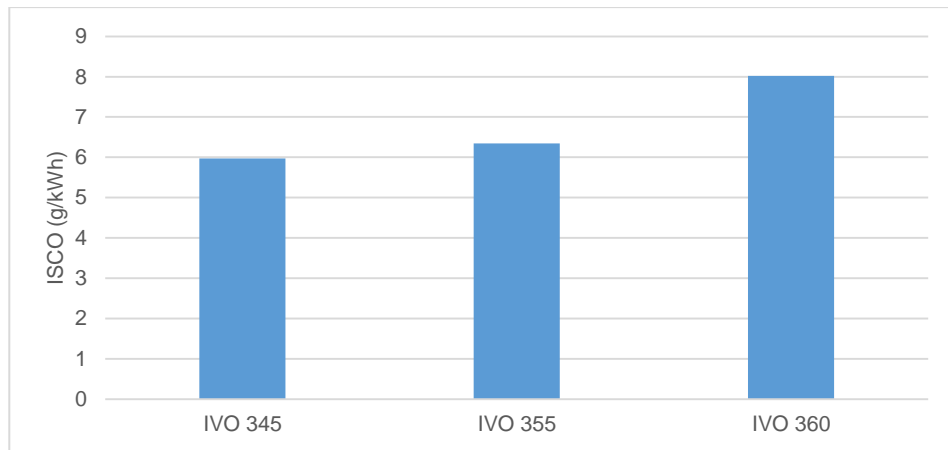
Figure 5-10: ISCO emission
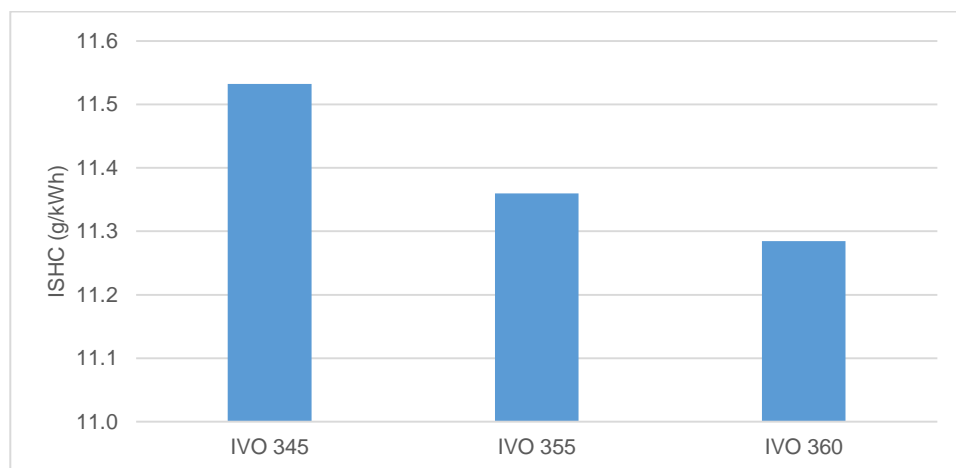
Figure 5-11: ISHC emission
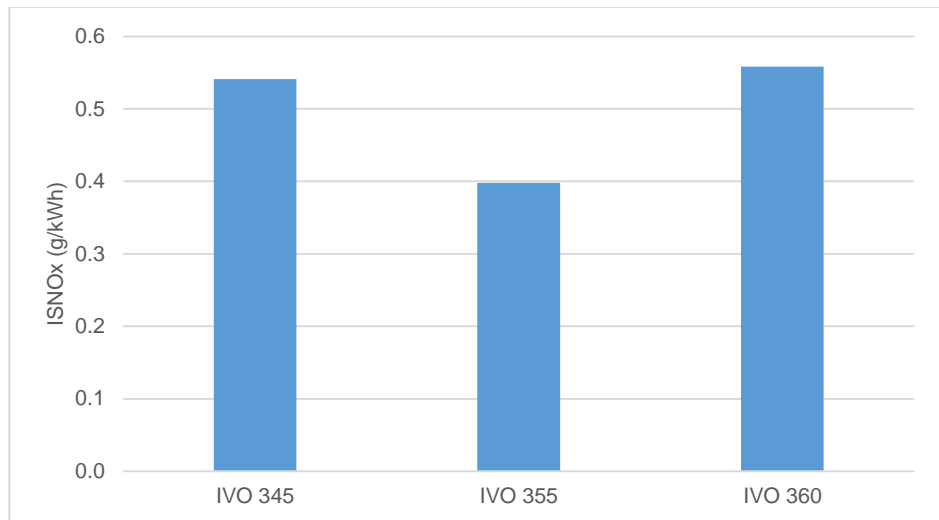
Figure 5-12: ISNOx emission

Figure 5-13 and Figure 5-14 show the combustion, thermal gas exchange and net indicated efficiencies. The combined effect of higher CO emission but lower HC with the retarded IVO rendered the combustion efficiency constant. The thermal efficiency decreased slightly due to lower effective compression ratio. As the test was carried out at the wide open throttle (WOT), all tested IVO timings showed above 96% of the gas exchange efficiency. The gas exchange efficiency slightly decreased from 98.3% to 96.6% with the retarded IVO timing. The gas exchange efficiency and volumetric efficiency exhibited opposite trends as a function of IVO timings. Therefore, the decreased intake temperature and the increased EGR seems to be the dominant factors for the increased volumetric efficiency with the retarded IVO timing.
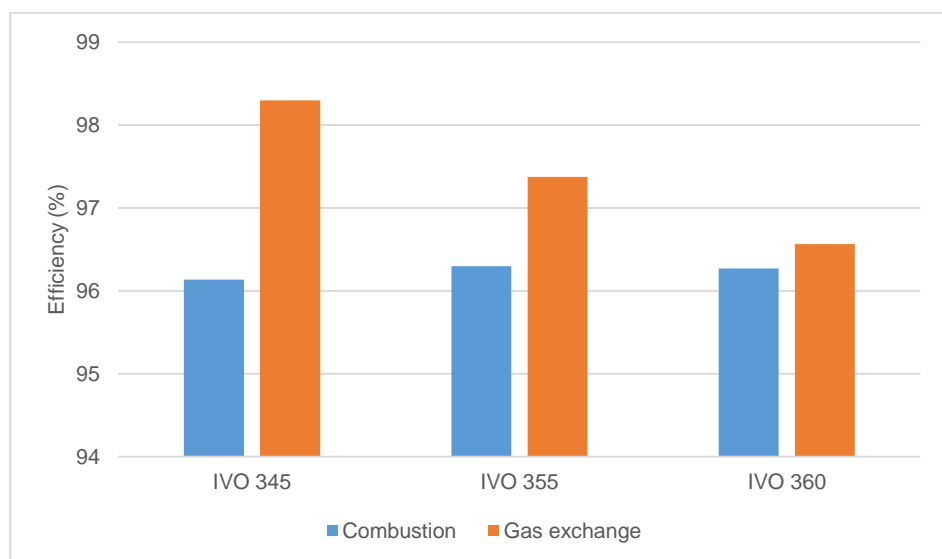
Figure 5-13: Combustion and gas exchange efficiencies
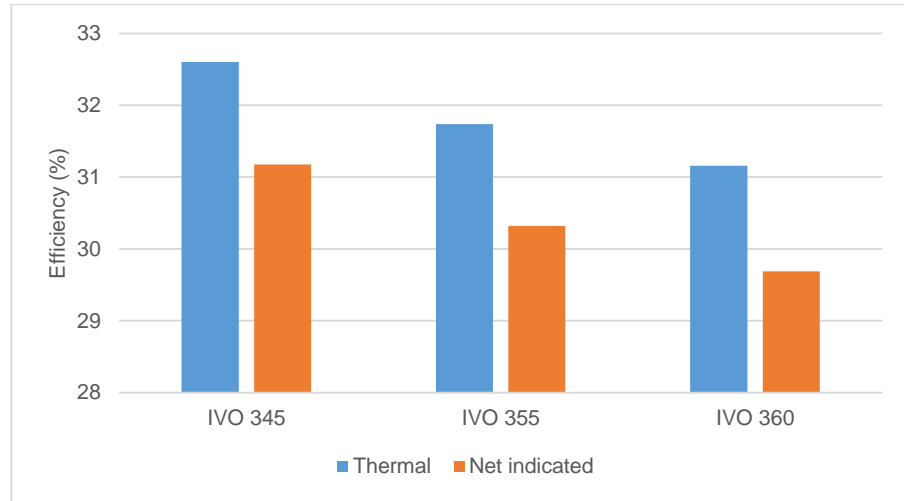
Figure 5-14: Thermal and net indicated efficiencies

5.3 THE EFFECT OF DME INJECTION AND SPLIT DME INJECTION RATIO

5.3.1 Experiment condition

During the preliminary experiment, 1st DME injection and 2nd DME injection showed opposite effects on the start of combustion and combustion phasing. The quantity of the first DME injection showed greater effect than its timing, whereas the injection timing of 2nd DME injection has a more dominant effect than its quantity. Thus, the 2nd DME injection timing was varied on various split DME injection ratio at a fixed DME/gasoline of 10%:90%. The test was carried out at the fixed engine speed of 1,500 rpm, CR 15 and lambda 1.3 with 90%:10% gasoline/DME ratio while 2nd DME injection timing was varied from 7 ^{0}CA BTDC to 25 ^{0}CA BTDC with various split DME injection ratios as shown in Table 5-2.

Table 5-2: DME injection timing test condition

Parameters	Value
Compression ratio	15:1 (geometric)
Engine speed	1,500 rev/min
Coolant temperature	80 ^{0}C
Gasoline Injection pressure	2.5 bar
DME injection pressure	100 bar
lambda	1.3
1st DME SOI timing	56 ^{0}CA BTDC
2nd DME SOI timing (adjusted to each case)	7 ^{0}CA BTDC – 34 ^{0}CA BTDC
Split DME injection ratio	67%:33% – 0%:100
Gasoline SOI timing	16 ^{0}CA BTDC

As the IVO 345 profile showed the highest efficiency with the most stable combustion among the test parameters, it was employed for this test as shown in Figure 5-15.
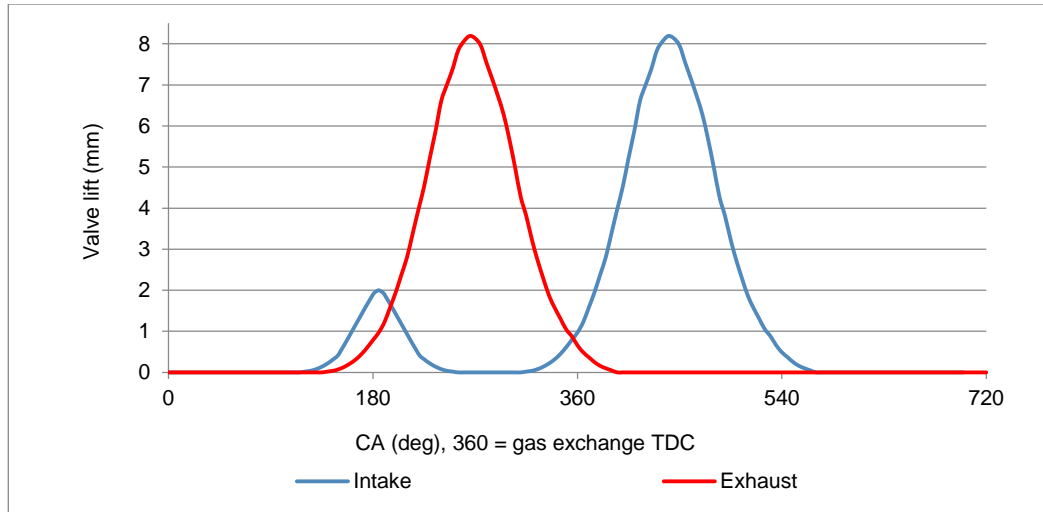

Figure 5-15: Intake and exhaust valve profiles for DME injection timing test

5.3.2 The effect of DME injection & split DME injection ratio on performance

Figure 5-16 shows that the net IMEP varied from 3.7 bar to 4.1 bar as the DME injection timing was changed. Similar maximum net IMEP values were obtained by each split DME injection ratio. The 2nd DME injection timing had a similar effect on the engine output to that of the spark discharge timing in a SI (spark ignition) engine, as if the 2nd DME injection acted as an ignition source. When 2nd DME injection was too late, the net IMEP decreased due to reduced work done during the expansion stroke. Too early 2nd DME injection reduced the net IMEP due to the increased negative work during the compression stroke. Therefore the optimised 2nd DME injection timing is equivalent to the MBT (minimum advanced for the best torque) timing in a SI engine.

The MBT timing of 2nd DME injection was retarded by the increased 1st DME split injection ratio. This could be explained by that fact that the increased 1st DME injection ratio improved the reactivity of the premixed gasoline/air mixture at the fixed relative air/fuel ratio and DME/gasoline ratio, thus the 2nd DME injection had to be retarded for avoiding excessive pressure rise during the compression stroke. As a greater 1st DME injection ratio of the premixed DME/gasoline/air mixture is more ignitable than the lower 1st DME injection ratio, the ignition delay was decreased by the increased 1st DME injection ratio as shown in Figure 5-17.

Figure 5-18 shows COV_{IMEP} that used to define the stability of combustion ($COV_{IMEP} < 10\%$). The stable combustion was achieved by all test points. COV_{IMEP} was increased by either too early or too late 2nd DME injection regardless of the split DME injection ratio. Too late 2nd DME injection caused the incomplete combustion whereas too early 2nd DME injection caused the knocking combustion. As shown in Figure 5-19, the combustion duration was increased by the retarded 2nd DME injection and vice versa.

The split DME injection ratio also affected the net IMEP. The stable combustion region was retarded by the increased 1st DME injection ratio due to the increased reactivity of the premixed gasoline/air mixture. The increased 1st DME injection ratio shortened the ignition delay and the combustion duration. In the case of single late DME injection (0:100% of the split DME injection ratio), the combustion duration was distinctively longer combustion duration than the others split DME injection ratio. In this case, the premixed charge did not contain any DME and the combustion would be dominated by slower flame propagations originating from the stratified DME regions rather than simultaneous combustion of premixed charge with DME from the early injection of split injections. In addition, it is noted that the ignition delay remained constant when the single DME injection was changed from -34 ^{0}CA ATDC to -28 ^{0}CA ATDC although the combustion duration was gradually decreased. This seems to suggest that the combustion mode changed from multiple auto-ignition combustion of the mixture of a more homogeneous reactivity (DME) to local flames around the stratified DME autoignition sites formed by the later injected DME after a very short ignition delay when injection took place near TDC.
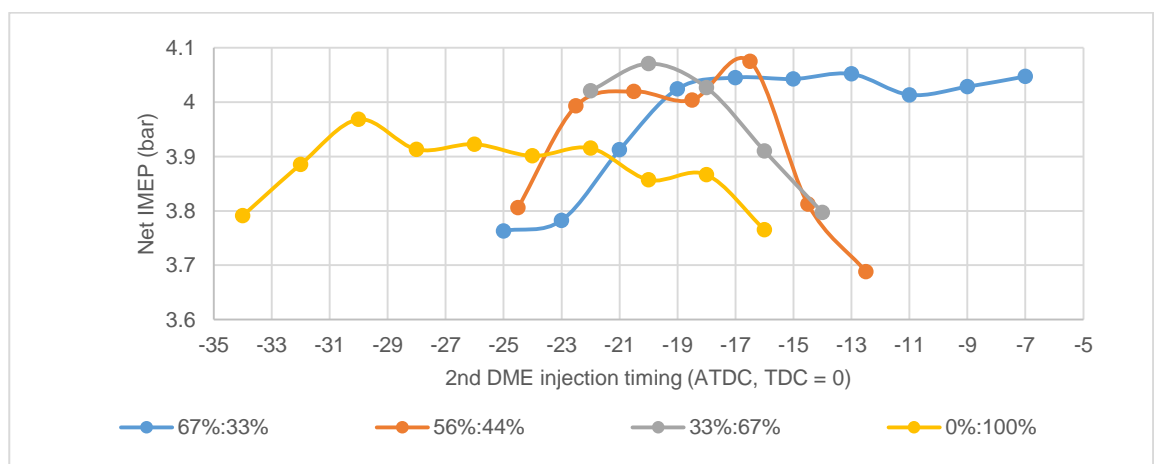
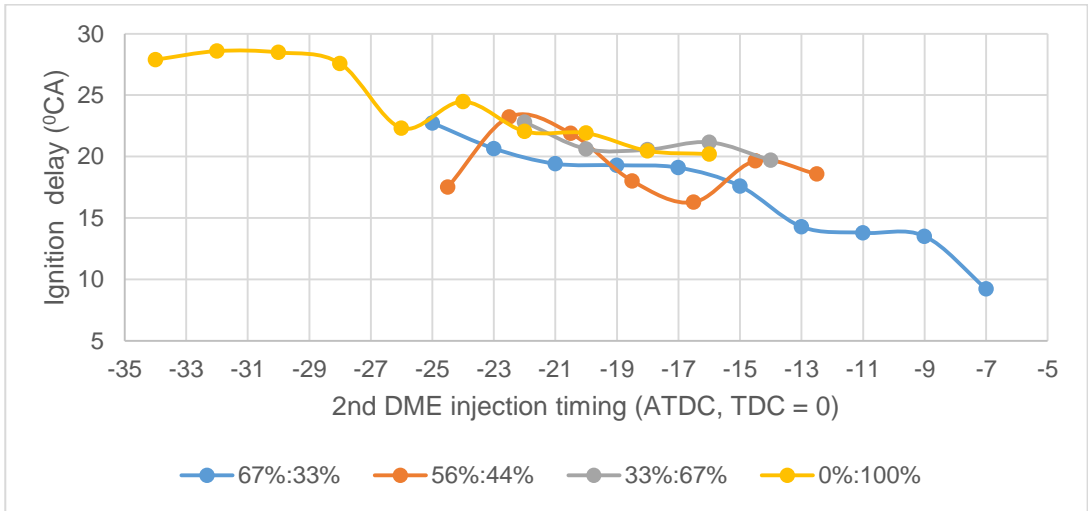Figure 5-16: Net IMEP variation by DME injection timing

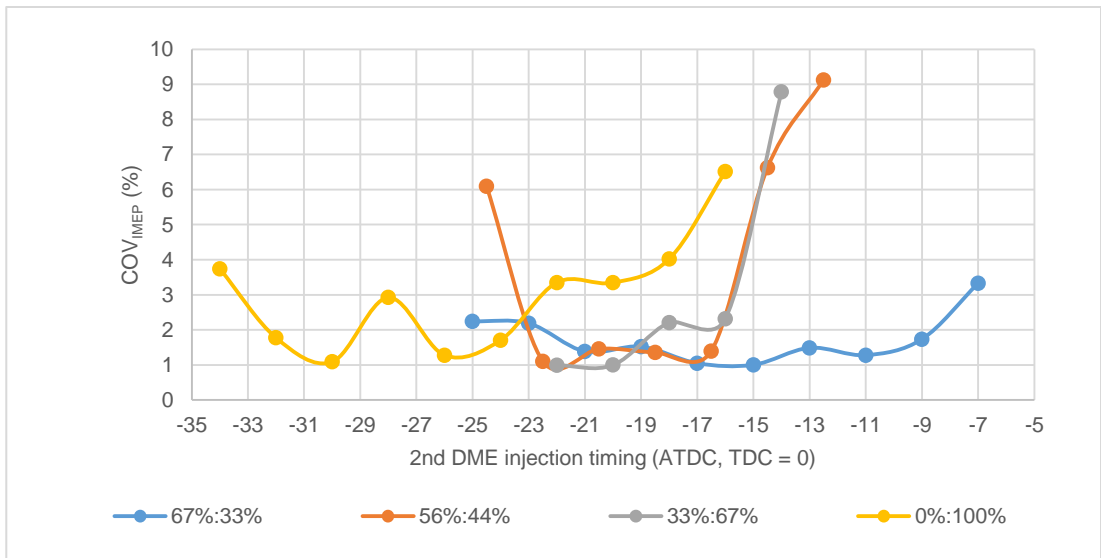Figure 5-17: Ignition delay by DME injection timing

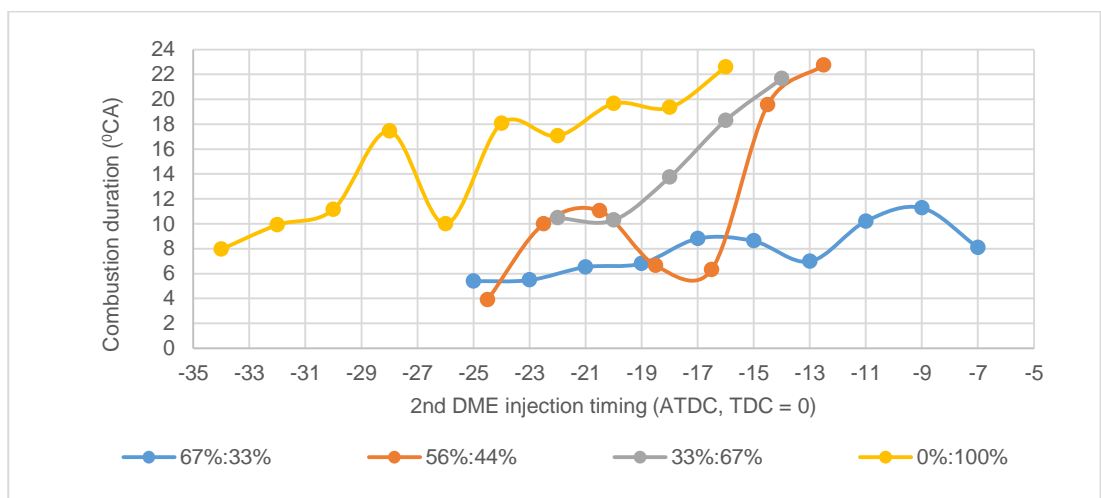Figure 5-18: COVI$_{MEP}$ variation by DME injection timing

Figure 5-19: Combustion duration variation by DME injection timing

81

In order to determine the knocking combustion, knocking probability and average in-cylinder pressure rise between each crank angle were examined. Figure 5-20 shows the result of knocking probability that is defined by the percentage of cycles whose dP/dΘ was over 10 bar. Figure 5-21 shows the average dP/dΘ of 100 consecutive cycles. As expected the average dP/dΘ was increased by the advanced 2nd DME injection timing and further advancing 2nd DME injection timing eventually increased the knocking probability. As 1st DME injection ratio was increased the average dP/dΘ became higher and 2nd DME injection timing had to be retarded to avoid the knocking combustion.

In the case of 67%:33% split DME injection ratio, both knocking probability and dP/dΘ went up with the most retarded second injection. This is thought to be the combined effect of the intake re-breathing and the increased 1st DME injection ratio. The late DME injection caused partial burn as shown by the higher COV$_{IMEP}$ in Figure 5-18. Those unburned hydrocarbon gas was retained in the cylinder and their high reactivity would increase the reactivity of the charge and promote the early autoignition, leading to rapid and violent knocking combustion.
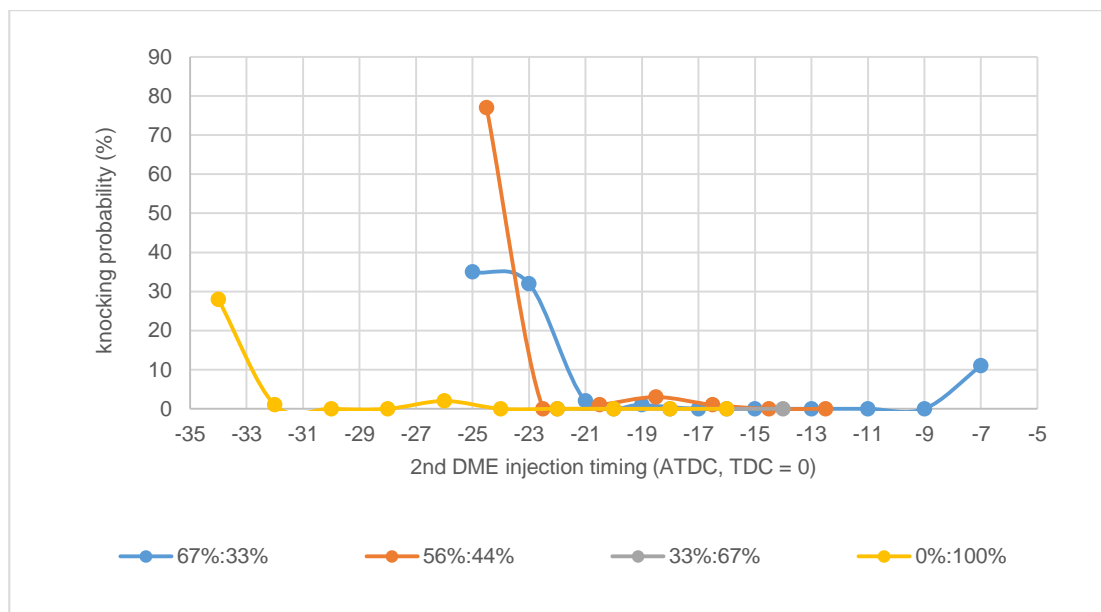
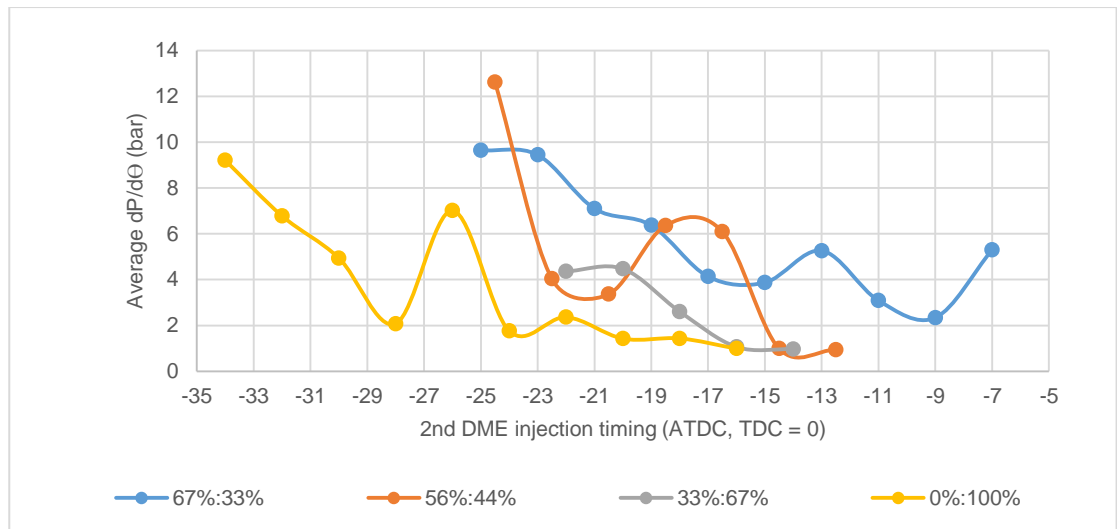Figure 5-20: Knocking probability variation by DME injection timing

Figure 5-21: Average dP/dθ variation by DME injection timing

5.3.3 The effect of DME injection and split DME injection ratio on emissions and efficiencies

Figure 5-22, Figure 5-23 and Figure 5-24 show indicated specific emissions of CO, HC and NOx, respectively. ISCO emission varied from 4 g/kWh to 11 g/kWh, while ISHC emission varied from 11 g/kWh to 19 g/kWh. Both CO and HC emissions increased with the most retarded 2nd DME injection because of the increasing fuel rich diffusion combustion due to shorter ignition delays. When more DME was injected in the first injection, both HC and CO emissions also increased with the most advanced 2nd DME injection because of the over-diluted DME mixture formed after the early DME injection and its subsequent incomplete combustion. In comparison, both CO and HC emissions decreased monotonically as the DME injection was advanced when most or all DME were injected in the second injection, because of the absence of the over-dilution DME mixture formed from the earlier DME injection.

In the most stable combustion conditions in the middle, Increasing 1st DME injection ratio reduced both CO and HC emissions. This is considered as the increased mass of the DME (high reactive fuel) to the premixed gasoline/air mixture made the premixed charge to be more flammable, thus occurrence of the rapid heat release assisted to reduce both CO and uHC emissions as combustion duration was shortened by the increased 1st DME injection ratio.

On the other hand, the increased 1st DME injection ratio slightly increased NOx emission due to the rapid heat release rate and hence increased in-cylinder

temperature. NOx emission also increased with advancing 2nd DME injection timing as advanced 2nd DME injection increased peak in-cylinder pressure and peak temperature.
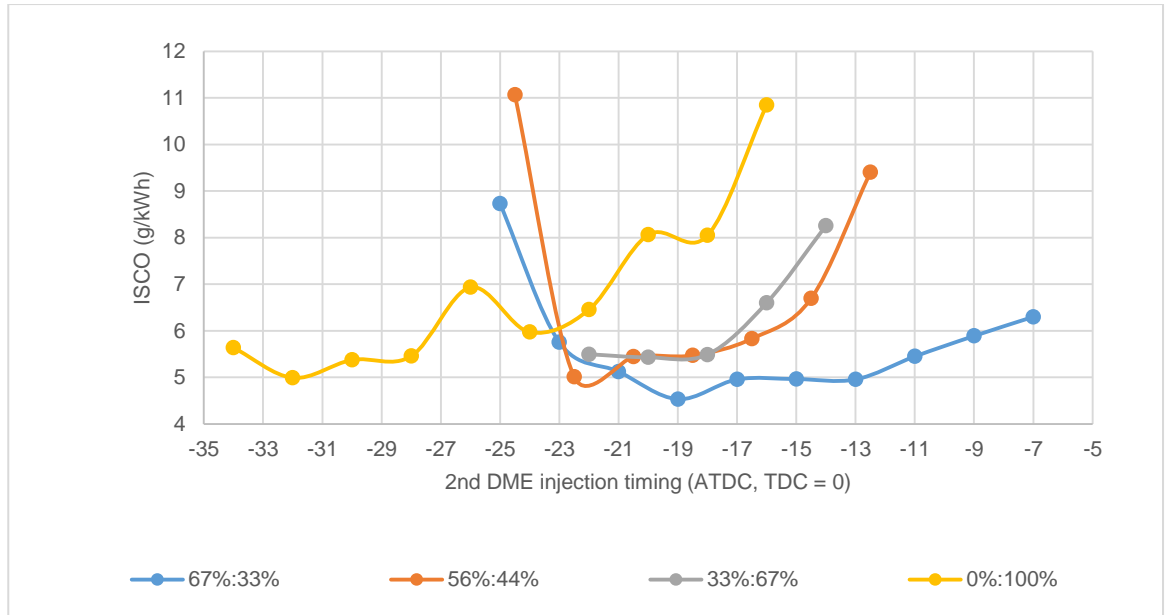

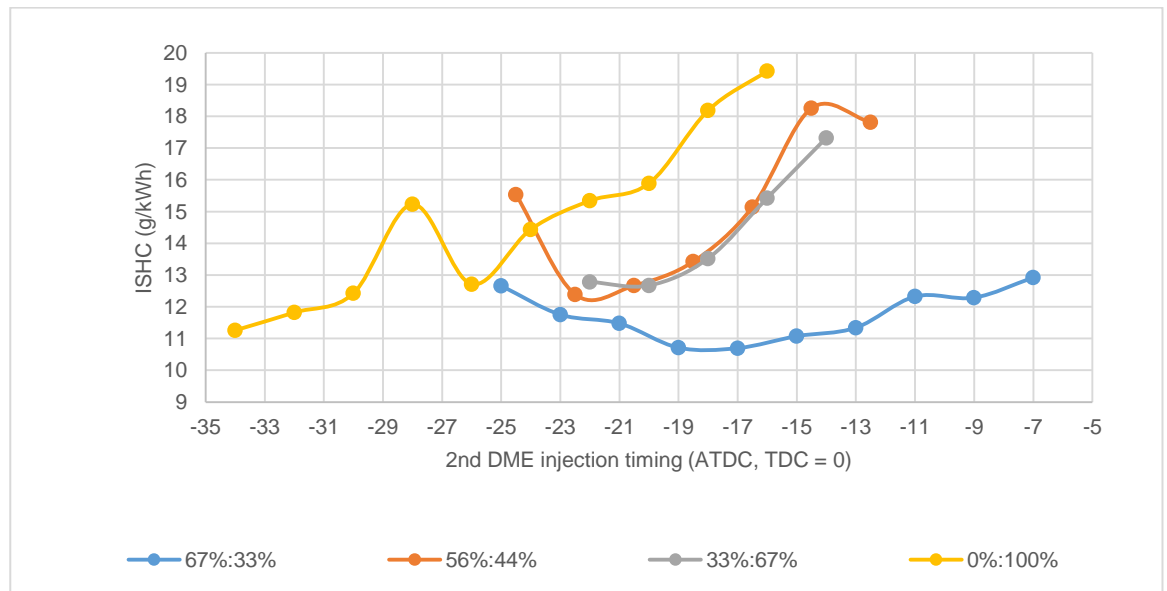Figure 5-22: ISCO emission variation by DME injection timing

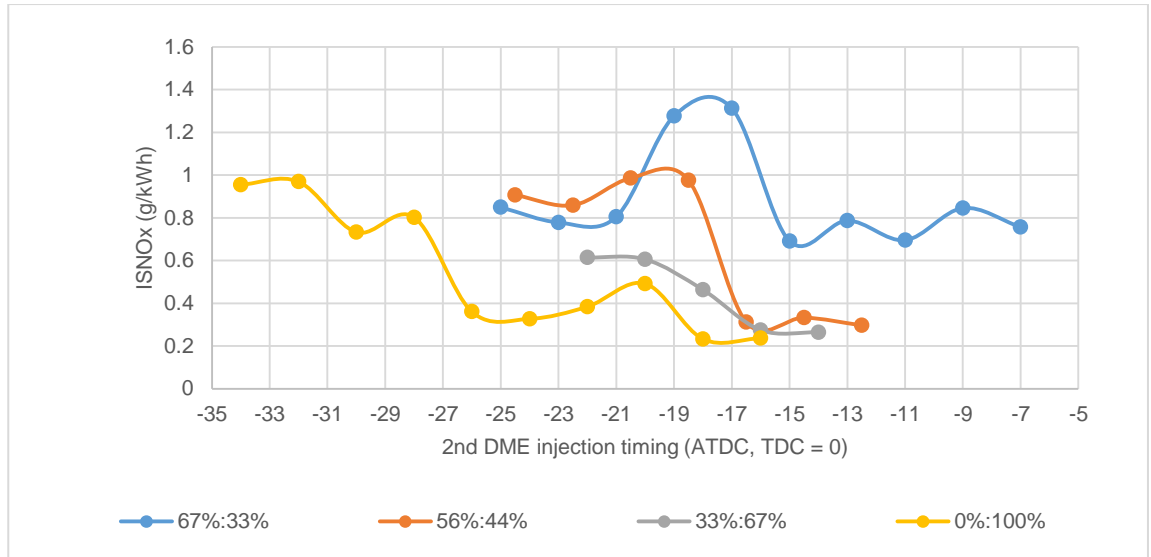Figure 5-23: ISHC emission variation by DME injection timing

Figure 5-24: ISNOx emission variation by DME injection timing

Figure 5-25 and Figure 5-26 show the combustion efficiency and the thermal efficiency respectively. As the combustion efficiency was determined by the CO and HC emissions, the combustion efficiency was reduced by either too early or too late 2nd DME injection with split injections. The single DME injection showed improved combustion efficiencies with more advanced DME injections. Increased 1st DME injection ratio improved the combustion efficiency in the most stable engine operating regions because of the higher reactivity and more complete combustion, which is also reflected by the lower exhaust temperature in Figure 5-27. The higher combustion efficiency and optimized combustion phasing resulted in higher thermal efficiencies shown by each case examined.

Figure 5-28 shows that the net indicated efficiency varied from 30% to 34% with 2nd DME injection timings in the same way as the thermal efficiency, as the pumping loss was constant.
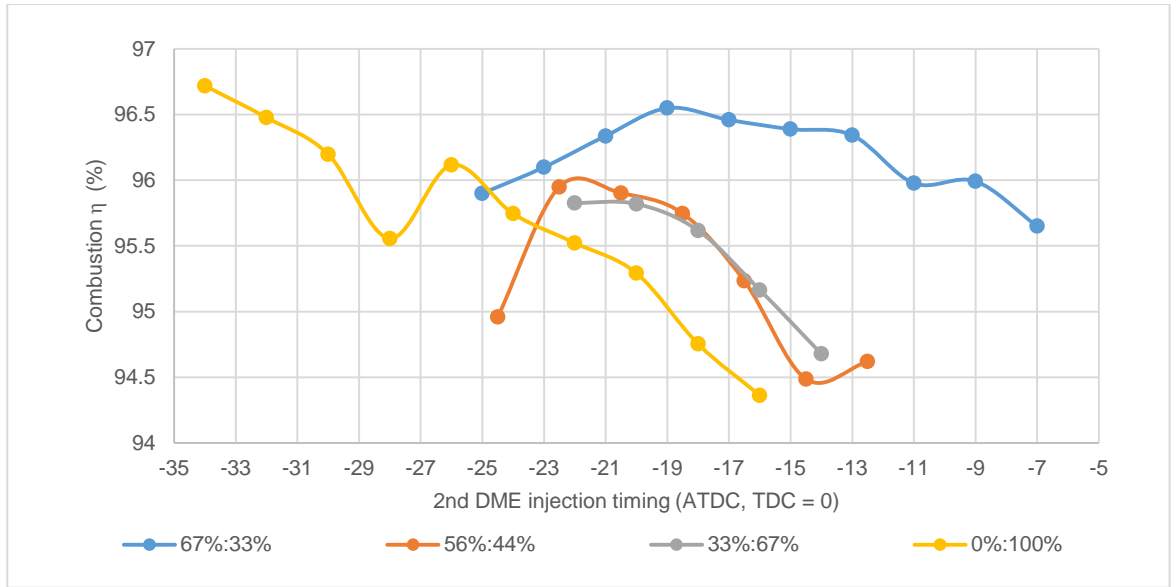
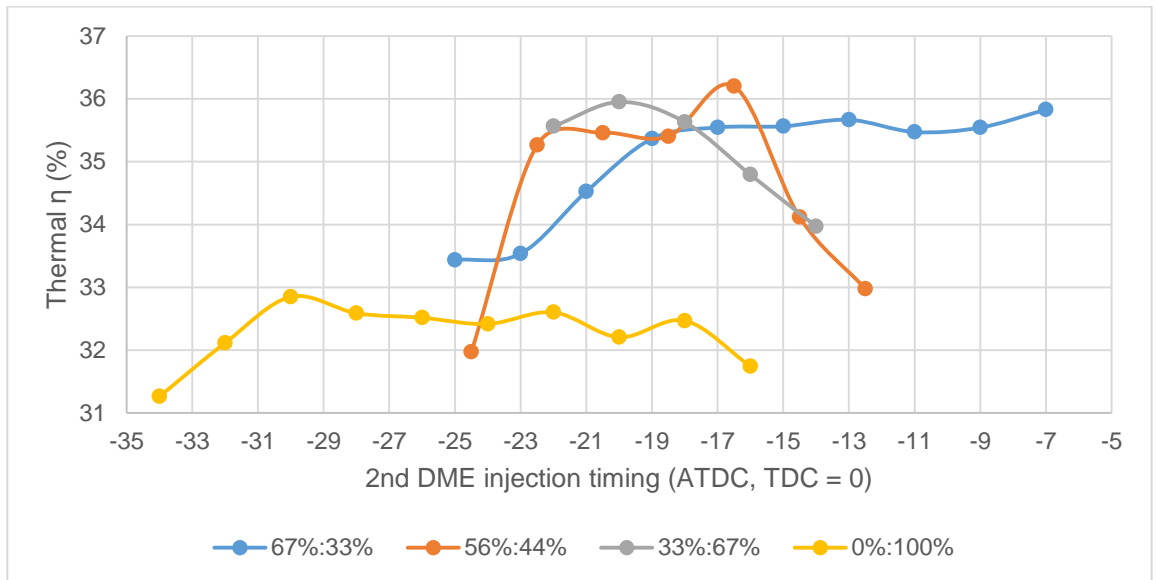*Figure 5-25: Combustion efficiency variation by DME injection timing*

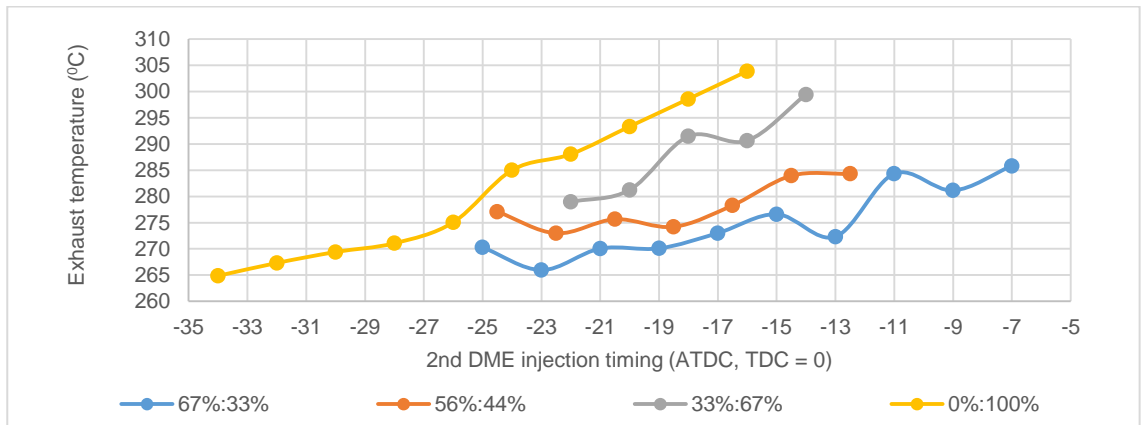*Figure 5-26: Thermal efficiency variation by DME injection timing*

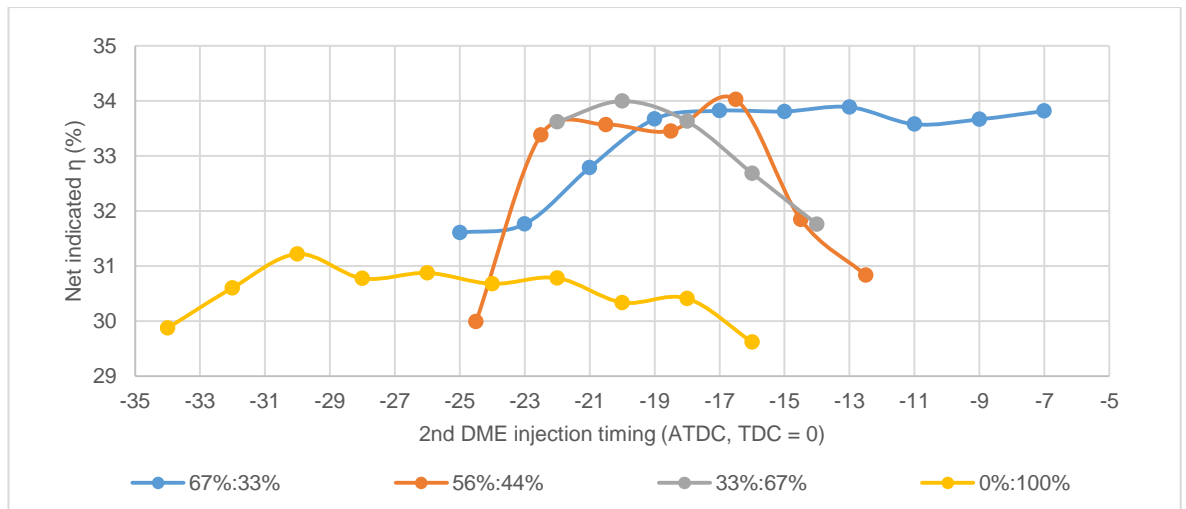*Figure 5-27: Exhaust temperature variation by DME injection timing*

Figure 5-28: Net indicated efficiency variation by DME injection timing

5.4 EFFECTS OF COMPRESSION RATIO AND AIR/FUEL RATIO

5.4.1 Experiment condition

The compression ratio is one the most important parameters that controls in-cylinder condition to initiate the chemical reactions by changing the pressure and the temperature of an in-cylinder. The air/fuel ratio was varied to control engine output and the operation range at each compression ratio. The air/fuel ratio was changed by the quantity of gasoline at a given quantity of DME injection. Hence the DME/gasoline ratio was varied from 8%:92% to 13%:87% while the air/fuel ratio was varied from λ 0.9 to λ 1.45. Initially it was planned to keep the DME/gasoline ratio at 10%:90%, but it was very difficult to achieve precised control over the small quantity of DME injected. At 10%, DME injection quantity was about 1.33 mg/cycle that needed to be increased or decreased by 0.13 mg/cycle in order to satisfy 10%:90% of DME/gasoline ratio at various air/fuel ratios. The DME injection quantity was also affected by its injection timing. The injection quantity was slightly increased by the advanced DME injection and was slightly decreased by the retarded DME injection timing due to back-pressure. It was possible to decrease DME injection quantity by the narrowed pulse width at advanced DME injection timing, however the widened pulse width did not increase DME injection quantity and it only increased the DME injection cyclic variation. For these reasons, DME was injected at a fixed pulse duration and the air/fuel ratio was controlled by the gasoline injection pulse width. In addition, 33%:67% and

67%:33% split DME injections were employed to determine the effects of the split DME injection ratio on the operation range.

Table 5-3 shows the test condition. The test was carried out at a fixed engine speed of 1,500 rpm, relative air/fuel ratios from 0.9 to 1.4, compression ratios of 13 to 15 and 33%:67% and 67%:33% split DME injection ratios. 1st DME injection timing was fixed at 56 ^{0}CA BTDC while 2nd DME injection was optimised for each case.

Table 5-3: Test conditions for CR, air/fuel ratio, and split DME injection ratio

Parameters	Value
Compression ratio	13:1 to 15:1 (geometric)
Engine speed	1,500 rev/min
Coolant temperature	80 ^{0}C
Intake pressure	Naturally Aspirated (1bar)
Throttle	WOT
lambda	0.9 to 1.4
Gasoline Injection pressure	2.5 bar
DME injection pressure	100 bar
1st DME SOI timing	56 ^{0}CA BTDC
2nd DME SOI timing (adjusted to each case)	10 ^{0}CA BTDC – 38 ^{0}CA BTDC
Split DME injection ratio	33%:67% and 67%:33%
Gasoline SOI timing	16 ^{0}CA BTDC

Valve opening/closing of intake and exhaust was defined by 0.5mm threshold and the used valves profiles are shown in Figure 5-29.
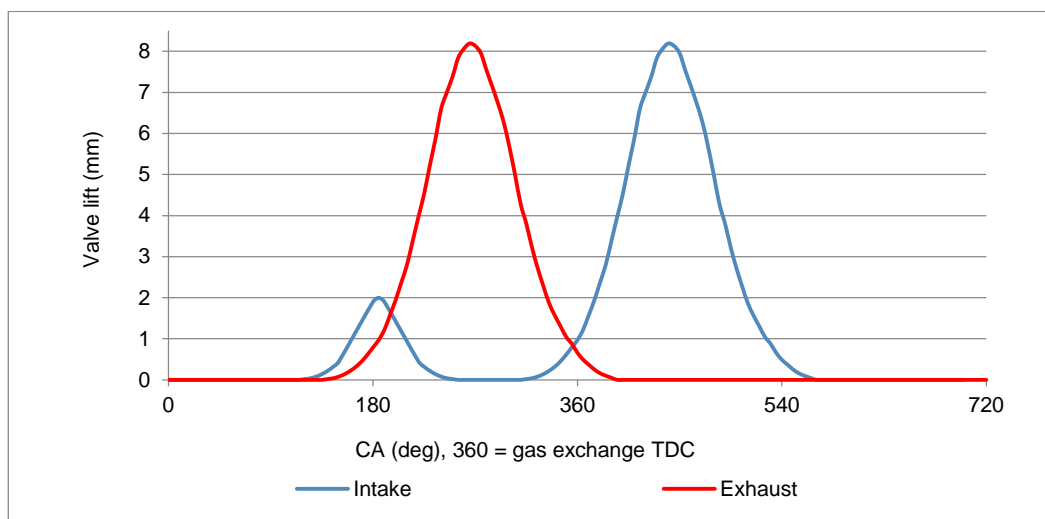

Figure 5-29: Valves profiles for CR, air/fuel ratio, and split DME injection ratio test

5.4.2 Effects of CR, air/fuel ratio and split DME injection ratio on performance

Figure 5-30 shows net IMEP contour maps for the two split DME injection ratios, as a function of the relative air/fuel ratio and the compression ratio. The high load boundary was limited by the knocking combustion ($dp/d\theta$ > 10bar/CA), whereas the low load boundary was limited by the unstable combustion (COVimep > 10%). Since the engine was operated at wide open throttle, the engine output was mainly controlled by the amount of fuel or the relative air/fuel ratio. The compression ratio had direct impact on the auto-ignition and combustion process. As the compression ratio was increased, higher charge temperature and pressure extended the low load boundary because of more complete combustion but reduced the high load boundary due to increased heat release rate.
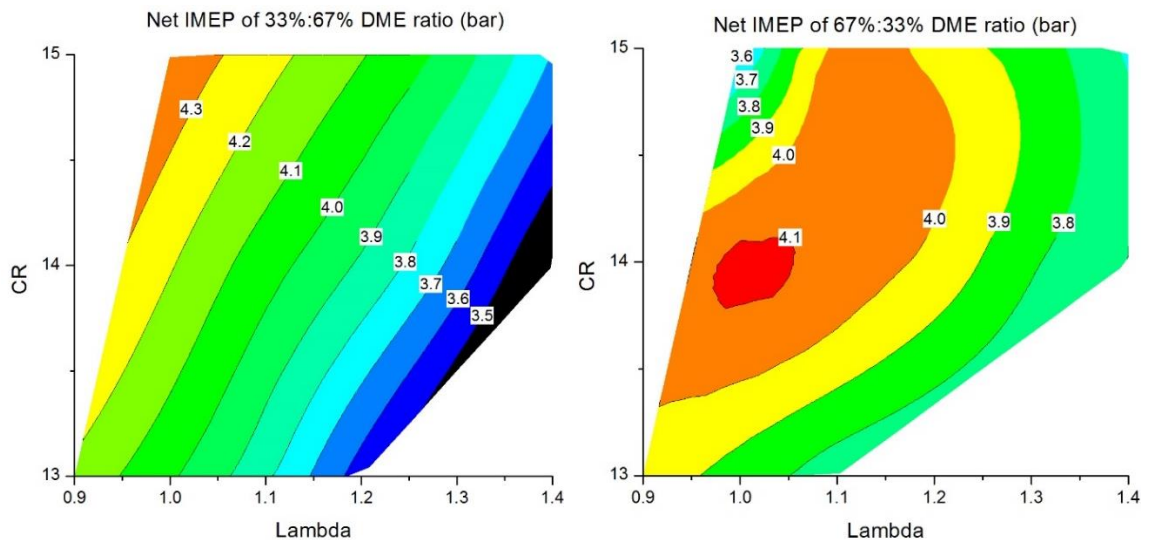
Figure 5-30: The results of net IMEP by CR, air/fuel ratio and the split DME injection ratio variation

In the case of 33%:67% split DME injection ratio, the net IMEP decreased from slightly fuel rich mixture to leaner mixtures as expected. But the maximum net IMEP of 4.3 bar was achieved at the highest compression ratio of 15 and the stoichiometric mixture, instead of a compression ratio of 13 and λ=0.9 when knocking combustion is less likely to occur at a lower compression ratio and maximum output obtained with slightly fuel rich mixture. However, it was found that the volumetric efficiency and hence the amount of charge for a given air/fuel ratio increased with the compression ratio. The volumetric efficiency increased from 42.91% at CR=13 to 45.51% at CR=14 and 48.11% at CR=15. As the result, more

fuel was burned at the same air/fuel ratio at the higher compression ratio, producing more engine output.

Similarly the volumetric efficiency increased with the compression ratio with 67%:33% split DME injection. But the maximum net IMEP was obtained at the intermediate compression ratio of 14 with a near stoichiometric mixture.

The difference between the two cases can be explained by the results shown in Figure 5-31 to Figure 5-33. In the case of the 33%:67% DME split injection, combustion remained stable in most region other than the boundaries. The relative air fuel ratio had a more dominant effect on both combustion stability and heat release rate. In comparison, the increased amount of DME in the first injection caused substantial variation and higher values in the COVimep and the maximum rate of pressure rise. As more DME was injected in the first injection, the compression ratio had great effects on the combustion process than the relative air/fuel ratio because of more heat was released by multiple auto-ignition combustion of the premixed DME/gasoline mixture, which was more affected by the change in compression temperature and pressure brought about by the compression ratio.
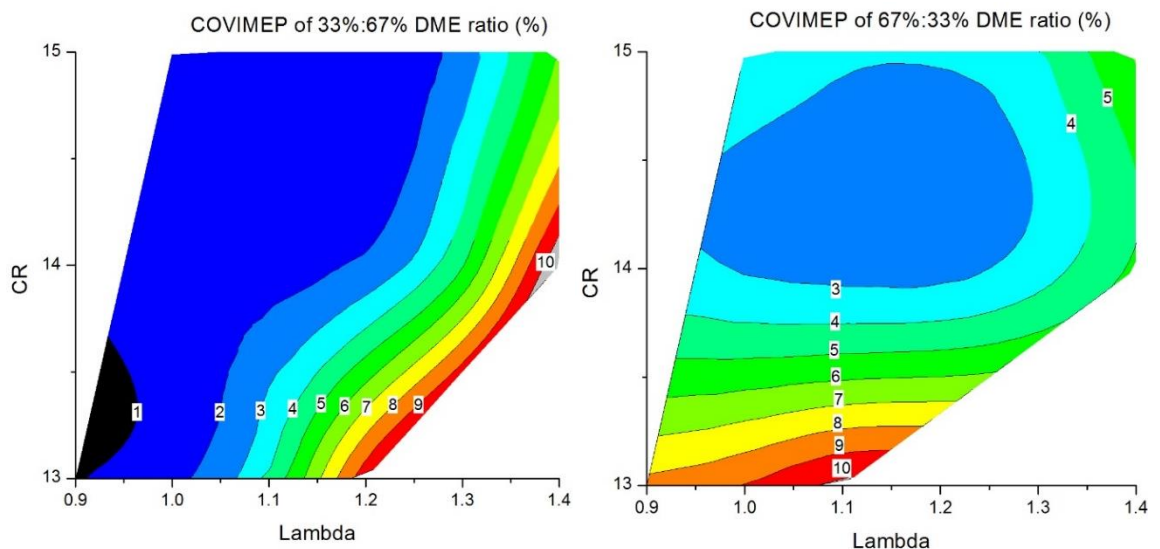

Figure 5-31: The results of COVIMEP by CR, air/fuel ratio and the split DME injection ratio variation

In the case of the 33%:67% split DME injection ratio, the COV_{IMEP} increased slightly with the increased relative air/fuel ratio. The lowest COV_{IMEP} was achieved at 0.9 λ and CR 13 as determined by the cyclic variation of DME injection. The

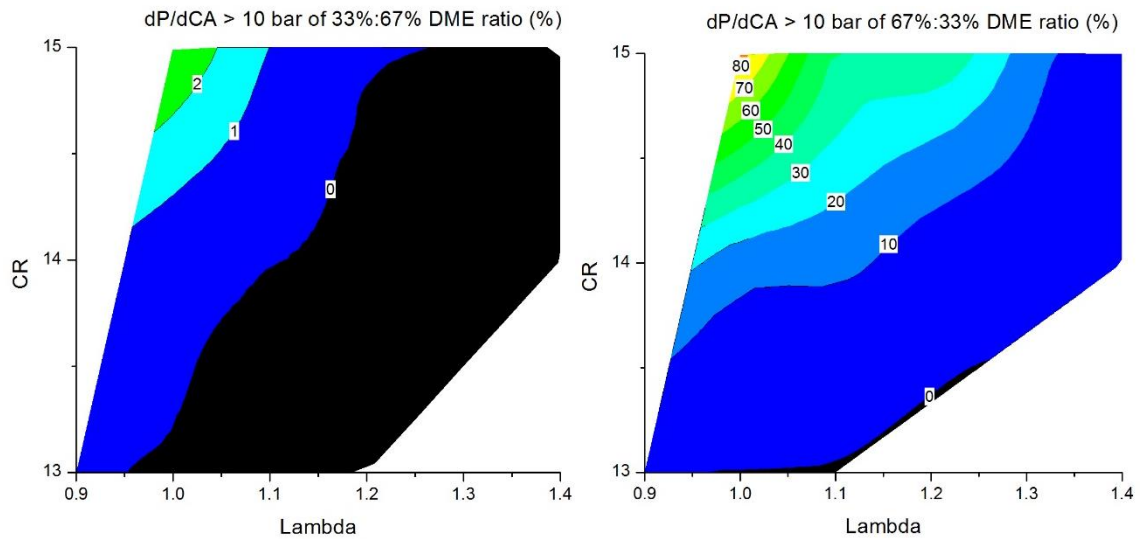lowest COVimep of 3% was achieved at CR=14 and λ <1.3 with 67%:33% split DME injection.

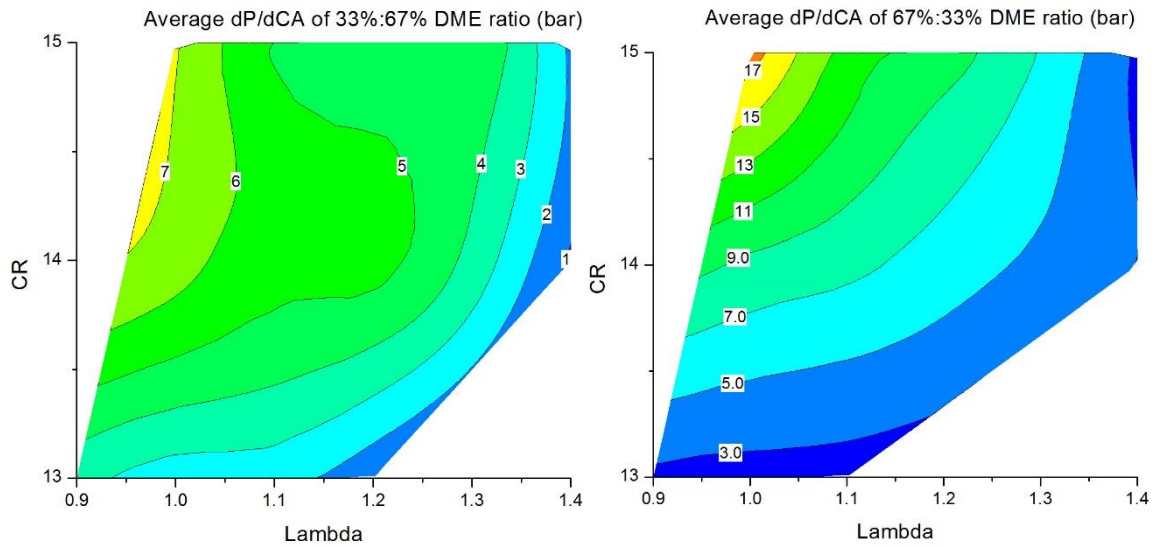Figure 5-32: dP/dθ to determine the knocking combustion

Figure 5-33: Average dP/dθ by CR, air/fuel ratio and the split DME injection ratio variation.

As shown in Figure 5-32 and Figure 5-33, percentage of knocking cycles and average of the maximum pressure rise were increased by increased compression ratio or decreasing the relative air/fuel ratio. The highest knocking cycle of 2% was observed at CR 15 and the average of maximum pressure rise was below 10 bar. This is because the start of auto ignition timing was mainly manipulated by the 2nd DME injection timing, thus the combustion phasing was also able to be optimised at various condition. On the other hands, knocking combustion was present in every conditions with more DME injected later, although the average of the maximum pressure rise was below 10 bar.
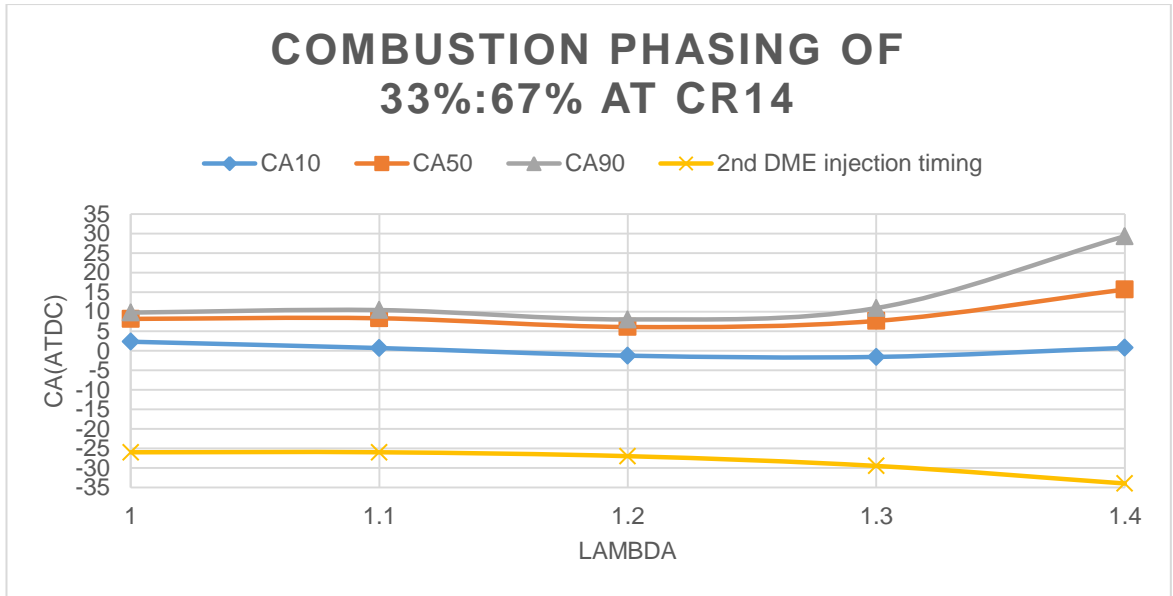
Figure 5-34: Combustion phasing of 33%:67% DME ratio at CR 14
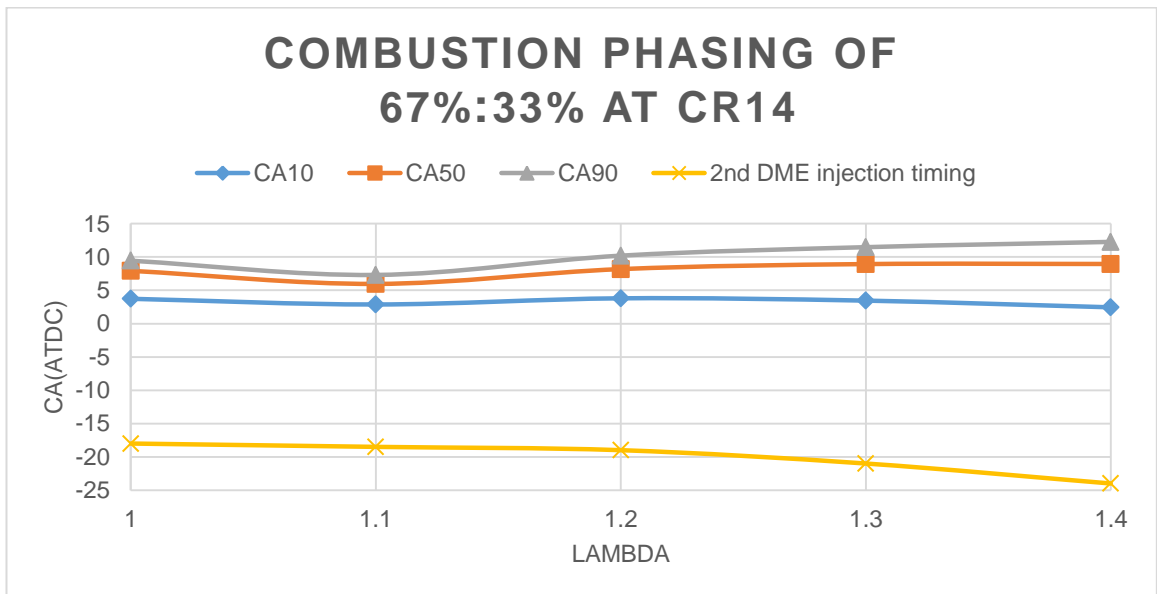

Figure 5-35: Combustion phasing of 67%:33% DME ratio at CR14

Figure 5-34 and Figure 5-35 show the combustion phasing of 33%:67% and 67%:33% of split DME injection ratios at CR14. Start of auto ignition (combustion) timing was defined as MFB 10% (CA10) and the end of combustion was defined as MFB 90% (CA90), while the ignition delay was defined as from 2nd DME injection timing to CA10. 67%:33% split DME injection showed ignition delay and combustion duration than their 33%:67% split DME injection ratio.

As shown in Figure 5-36, the combustion duration depended as MFB (mass fraction burned) CA 10 to CA 90, was increased by increasing lambda when one

third of DME was included in the first injection. Compression ratio also affected to combustion duration, but the effect was almost negligible from CR 15 to CR14 and became greater from CR14 to CR13. Combustion duration seems related to COV IMEP and knocking combustion. A combustion duration shorter than 10 CA increased the number of knocking combustion cycles whilst longer combustion duration than 20 CA led to unstable combustion as mixture was too lean to complete the combustion. As more DME was injected earlier, combustion duration became shorter as more heat was released by the multiple auto-ignition combustion of premixed DME/gasoline mixture.
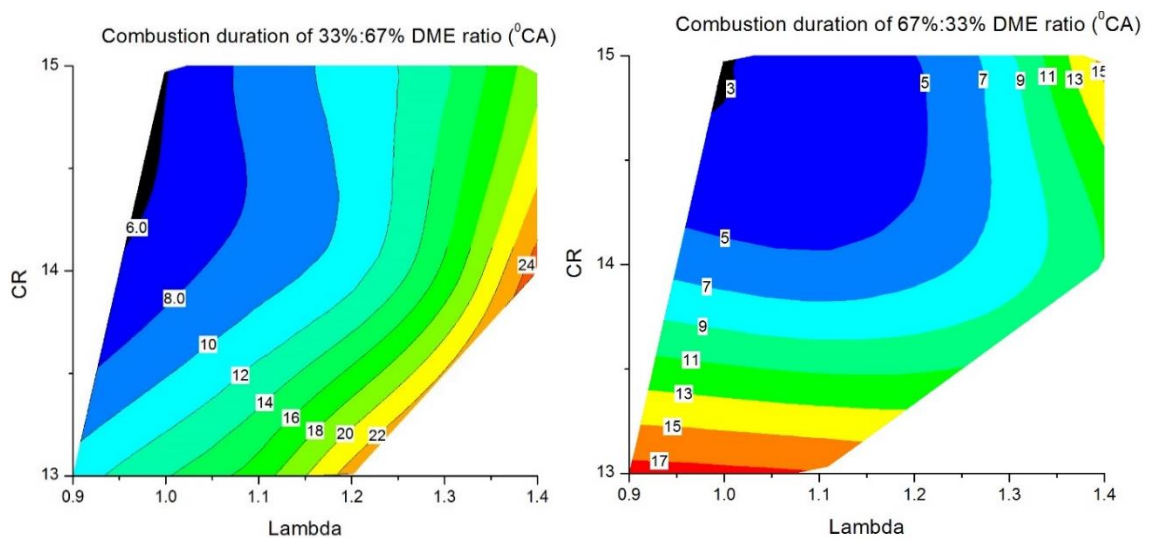

Figure 5-36: Combustion duration of 33%:67% and 67%:33% DME ratio

5.4.3 Effects of CR, air/fuel ratio and split DME injection ratio on emission and efficiencies

As shown in Figure 5-37, the CO emission decreased as the mixture became leaner with 67%:33% DME ratio as CO is mainly produced from fuel rich combustion. In the case of 33%:67% of the split DME injection ratio, the specific CO emission reached its minimum around λ=1.1-1.2. As more DME was included in 1st injection, specific CO emissions became much higher, because of the combined effects of lower IMEP and unstable combustion.
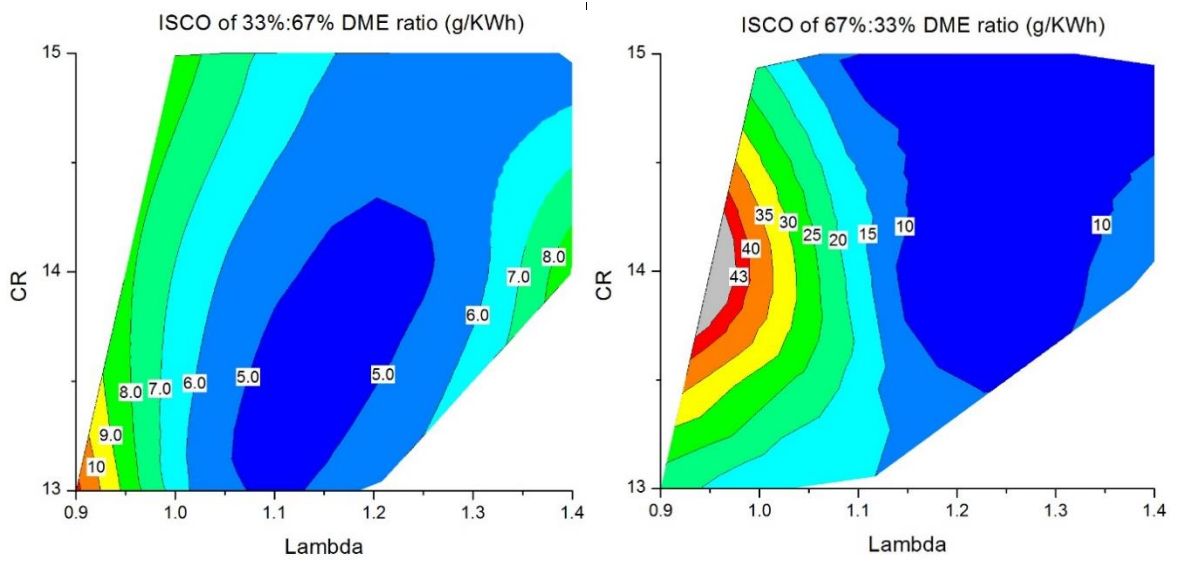
Figure 5-37: ISCO of 33%:67% and 67%:33% split DME ratio

Figure 5-38 shows indicated specific HC emissions for both split DME injection ratios. In the case of 67%:33% split injection, specific HC emissions increased with fuel rich mixture and reduced compression ratio when the lower charge temperature and hence longer ignition delay caused more over-dilution of early DME injection. In comparison, higher specific HC emission of the 33%:67% injection was mostly caused by the incomplete combustion of the leaner mixture in the cylinder and decreasing net IMEP.
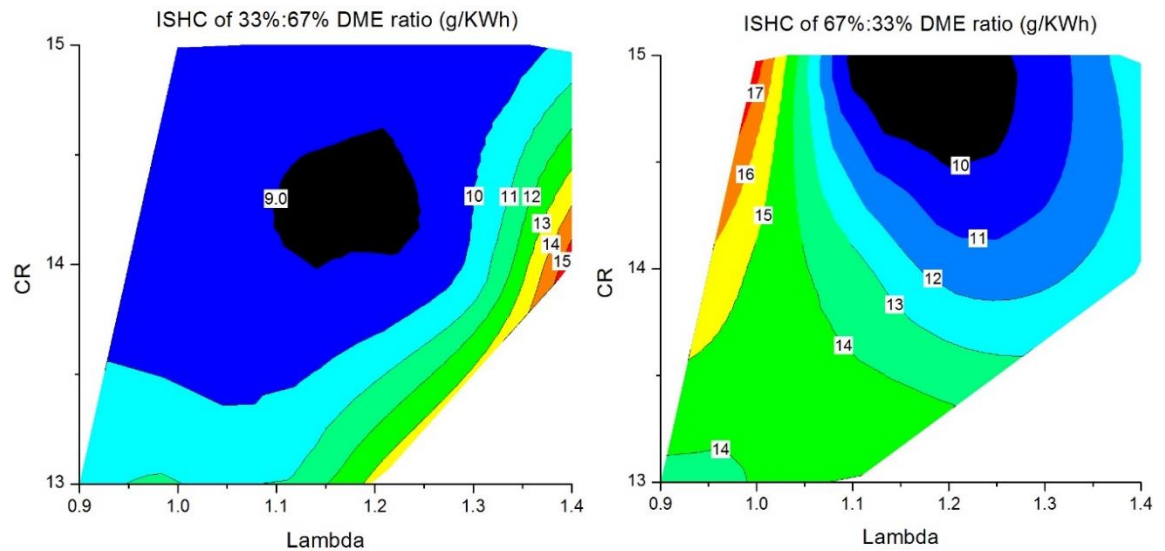

Figure 5-38: ISHC of 33%:67% and 67%:33% split DME ratio

Figure 5-39 shows the ISNOx emission results. As the formation of NOx strongly depends on the flame temperature, highest NOx emission was produced at higher compression ratios and with near stoichiometric mixture. Much lower NOx

94

emission was produced by 33%:67% of split DME injection ratio than 67%:33% split DME injection ratio due to the decreased dp/dθ.
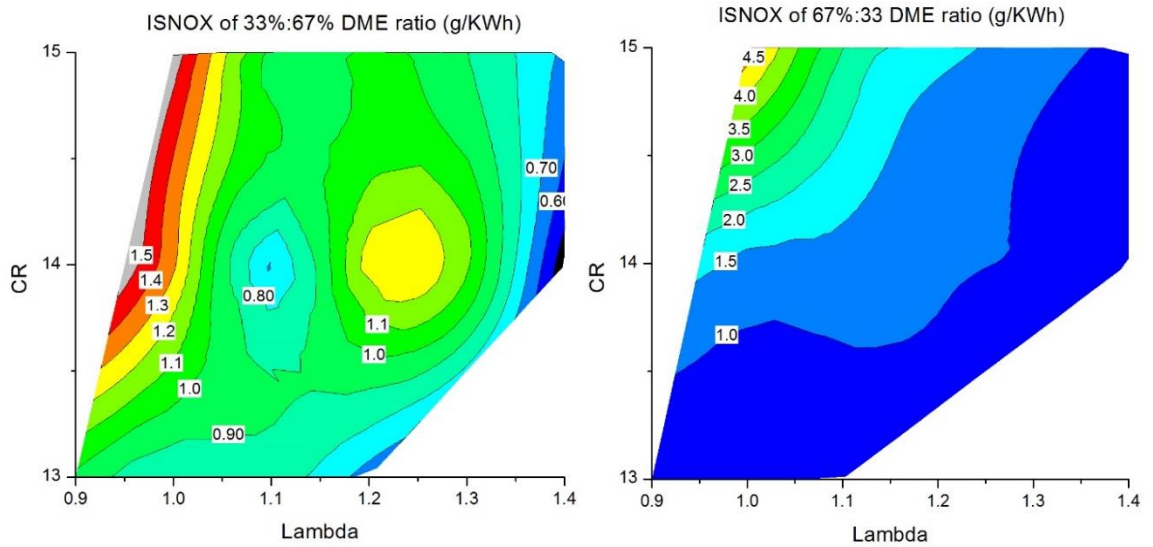

Figure 5-39: ISNOx of 33%:67% and 67%:33% split DME ratio

Figure 5-40 shows the exhaust temperature measurement result. It is noted that the exhaust temperature of the 33%:67% DME ratio depended on the air/fuel ratio while its 67%:33% was mainly affected by the compression ratio. This is thought to be the effect of combustion duration as the decreased combustion duration resulted in advanced combustion timing.
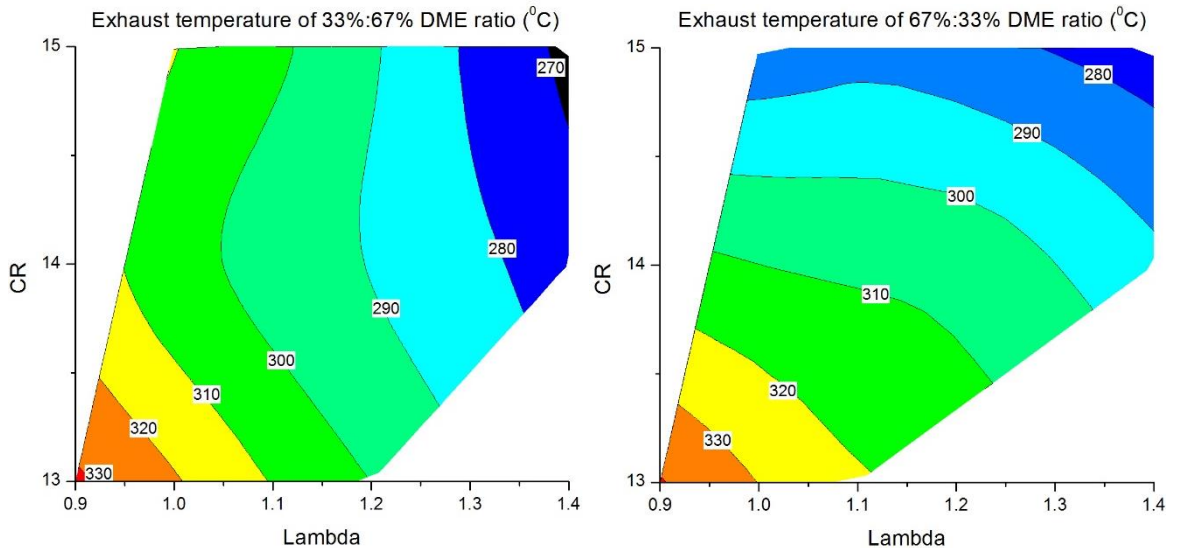

Figure 5-40: Exhaust temperature of 33%:67% and 67%:33% split DME ratio

Figure 5-41 shows the combustion efficiency. Combustion efficiency of the 33%:67% split DME ratio varied from 97% to 95%, and the maximum combustion efficiency was observed at CR 14 and lambda from 1.1 to 1.2, where the minimum

HC and CO emissions was observed. The combustion efficiency of the 67%:33% split DME injection ratio also depended on its HC and CO emissions. The minimum combustion efficiency of 93% was observed at CR14 and lambda 0.95, where the maximum CO and HC emission was observed, and the maximum combustion efficiency of 97% was achieved at CR 15 and between lambda 1.2 and 1.3, where the minimum CO and HC emissions were obtained.
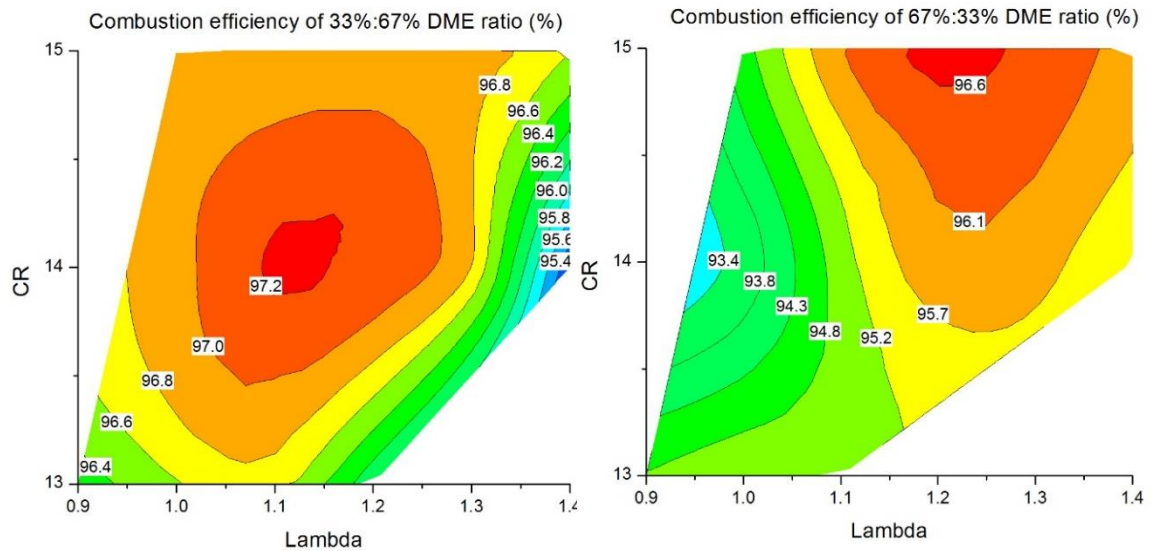

Figure 5-41: Combustion efficiency of 33%:67% and 67%:33% split DME ratio

Figure 5-42 shows the gas exchange efficiency of the two cases. As all tests were carried out at WOT, the result of gas exchange efficiency was over 98%. The gas exchange efficiency increased slightly with more fuel due to the charge cooling effect of gasoline.
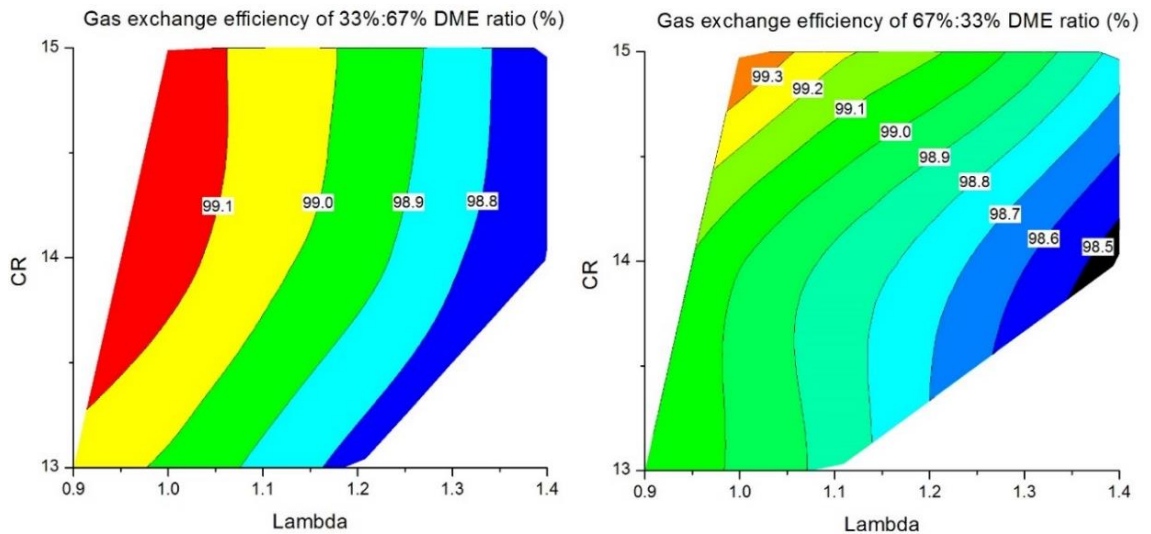

Figure 5-42: Gas exchange efficiency of 33%:67% and 67%:33% split DME ratio

Figure 5-43 and Figure 5-44 show thermal efficiency and the net indicated efficiency respectively. In the case of 33%:67% split DME injection ratio, higher efficiencies were produced with the highest compression ratio and leanest mixture as predicted by the ideal Otto cycle efficiency. However, 67%:33% split DME injection ratio produced the highest efficiency at the intermediate compression ratio of 14, when the combustion phasing was optimised.
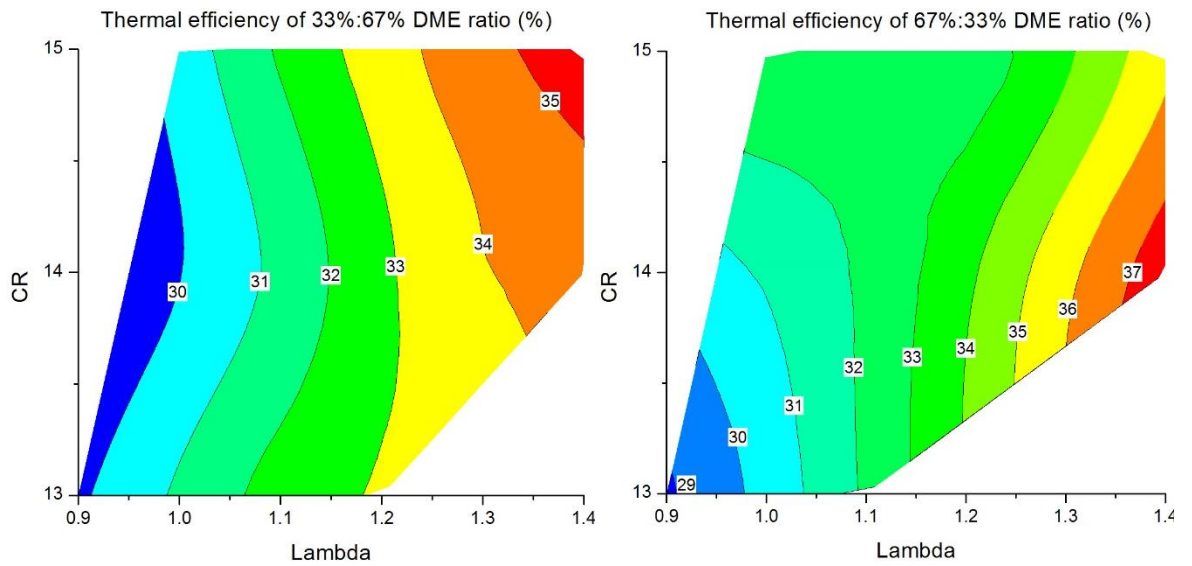

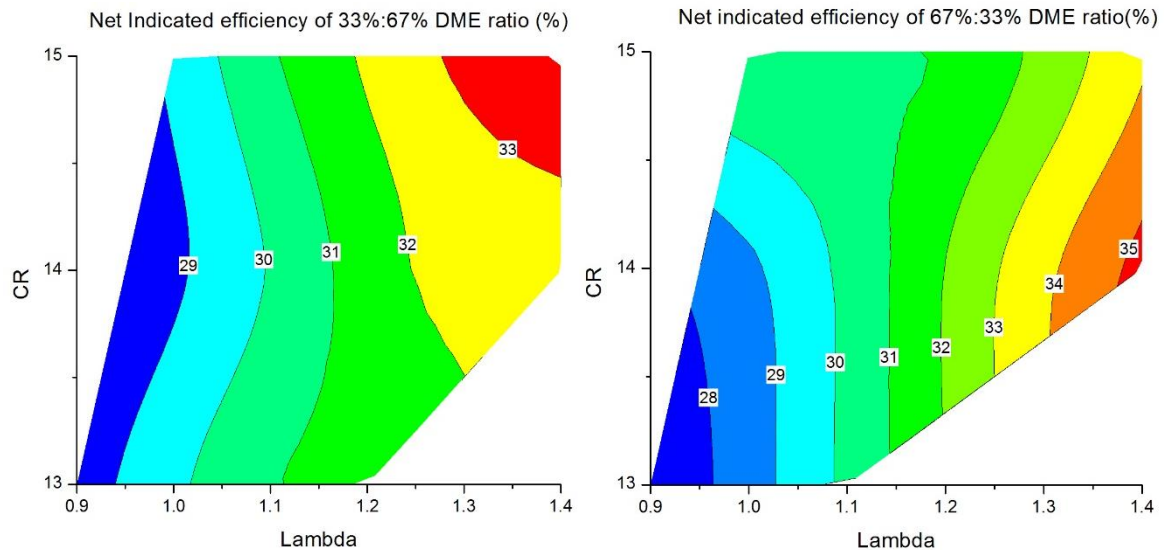*Figure 5-43: Thermal efficiency of 33%:67% and 67%:33% DME split ratio*

Figure 5-44: Net indicated efficiency of 33%:67% and 67%:33% split DME ratio

5.5 SUMMARY

This chapter has described the results of DME assisted gasoline CAI combustion with the intake re-breathing valve strategy. Effects of a number of variables were investigated, including the intake re-breathing timing, DME injection timing, split DME injection ratio, compression ratio and air/fuel ratio.

Retarded IVO timing increased the EGR rate from 25% to 27% and the volumetric efficiency from 51% to 55% due to the lower intake temperature. COV_{IMEP} was increased by decreased intake temperature and the higher concentration of EGR.

The effects of 2nd DME injection timing on net IMEP has similar effect to the spark discharge timing in a SI engine. Either too early or too late 2nd DME injection timing reduced engine output with increased CO and HC emission and decreased net indicated efficiency. In addition, too early 2nd DME injection led to knocking combustion while too late 2nd DME injection led to incomplete combustion with increased $COV_{IMEP.}$ Increasing 1st DME injection mass retarded the optimised 2nd DME injection timing due to knocking limit and increased combustion efficiency due to lower CO and HC emissions. However the higher mass of 1st DME injection ratio had little effect on the maximum IMEP or net indicated efficiency.

The compression ratio affected the operation range that could be achieved by varying the relative air/fuel ratio. Increasing the compression ratio allowed the engine to operate with leaner mixtures but its richer mixture operation limit was narrowed. Knocking combustion limited the high load while incomplete combustion limited low load. The maximum net indicated efficiency and maximum thermal efficiency were obtained with leaner mixtures. Increasing 1st DME injection ratio did not affect the operation range but render the auto-ignition timing less controllable by the 2nd DME injection timing, especially at higher compression ratios and near stoichiometric mixtures. Higher 1st DME injection ratio showed slightly improved net indicated efficiency at lower load operation while slightly higher net indicated efficiency was obtained at higher load by 2nd DME injection.

Chapter 6   EXPERIMENTAL INVESTIGATION OF DME ASSISTED GASOLINE CAI COMBUSTION WITH EXHAUST RE-BREATHING

6.1 INTRODUCTION

In this chapter, DME assisted gasoline CAI combustion with the exhaust re-breathing has been systematically researched to determine effects of air/fuel ratio, compression ratio, and split DME injection ratio. The exhaust re-breathing operation was achieved by swapping the intake re-breathing and exhaust ordinary cam lobes. Thus, the exhaust valve was opened during the normal exhaust stroke by the main cam lobe and during the intake stroke by the small secondary lobe which results in the burned gas being sucked back into the cylinder.

Results in Chapter 5 showed that the wider operation range could be achieved with stable combustion at a compression ratio of 14 during the intake re-breathing experiment. Therefore, a series of experiments were carried out to determine the operation range at the compression ratio of 14 by varying the air/fuel ratio with split DME injection ratios of 33%:67%, 56%:44% and 67%:33% at CR14. Then, the compression ratio was varied from 12 to 16 to produce contour maps for three split DME injections as a function of the relative air/fuel ratio and the compression ratio. Finally the results of intake re-breathing and exhaust re-breathing were compared to the SI baseline.

6.2 EXHAUST RE-BREATHING OPERATION RANGE

6.2.1 Experiment condition

Intake and exhaust valve timings were set to the optimised valve timings determined in Chapter 5. Figure 6-1 shows the valve opening profiles of intake re-breathing and exhaust re-breathing. The exhaust valve opened at 145 ^{0}CA and closed at 345 ^{0}CA, which was 20 ^{0}CA more advanced than the exhaust valve closing timing of 365 ^{0}CA in the intake re-breathing experiment. The secondary exhaust valve opening was at 440 ^{0}CA and its closing timing at 535 ^{0}CA. The intake valve open and close timings were kept constant. The exhaust valve open timing could be set to the main exhaust valve timing that used in the intake re-

breathing by retarding the exhaust valve opening timing. However the retarded exhaust valve opening would result in retarded post exhaust valve closing timing. The retarded exhaust valve timing would reduce the effective compression ratio as well as increasing the expansion stroke duration due to fixed dwell duration of main and post. Thereby in order to compare the intake re-breathing and exhaust re-breathing, the exhaust valve open timing was set to the pilot valve open timing in the intake re-breathing experiment.
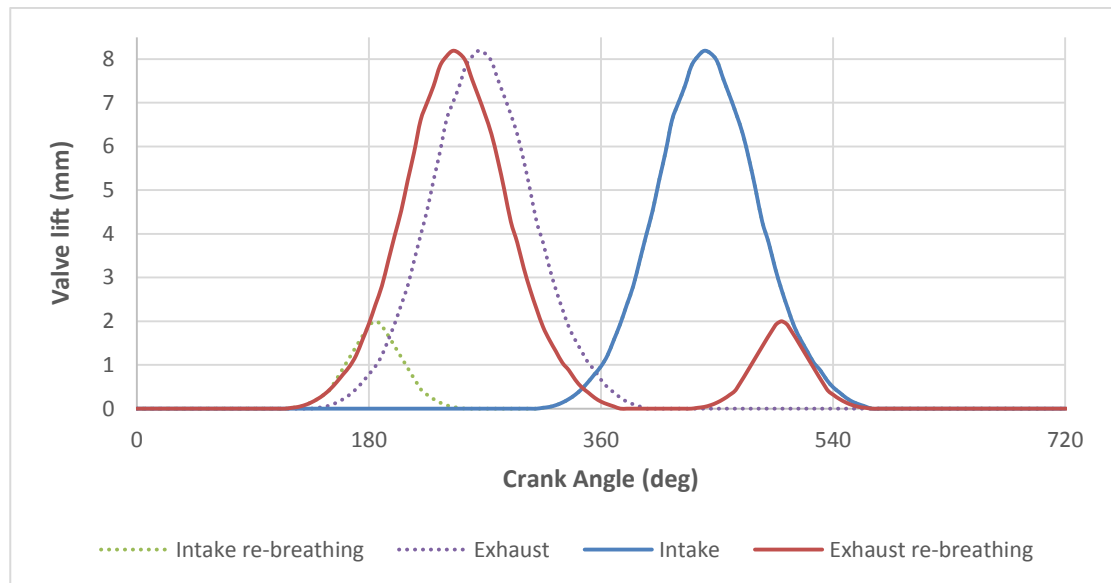

Figure 6-1: Valves profile comparison of intake re-breathing and exhaust re-breathing (dot line: intake re-breathing and solid line: exhaust re-breathing)

During the secondary exhaust valve opening period in the intake stroke, some of the exhaust gas was sucked back into the cylinder. In Chapter 5, in-cylinder gas sampling method was successfully used to measure the internal EGR rate through the intake rebreathing method. Figure 6-2 shows the measured EGR rate as a function of the in-cylinder gas sampling timing at three compression ratios of 12, 14 and 16. Unlike the constant EGR rate measured at different sampling timings, it can be seen that the EGR rate varied with the sampling timing during the exhaust re-breathing operation. This can be attributed to the strong stratification of exhaust gas and their temporal variation in the cylinder because of the shorter mixing time available between the end of exhaust rebreathing period and the sampling measurement. As exhaust gas re-breathed from the exhaust port during the intake stroke, the compression ratio had a direct impact on the EGR rate. Increased compression ratio from CR 12 to CR 14 slightly increased EGR rate, but further

increased compression ratio dramatically reduced the EGR rate, because of the elevated in-cylinder pressure during the rebreathing period at the highest compression ratio.
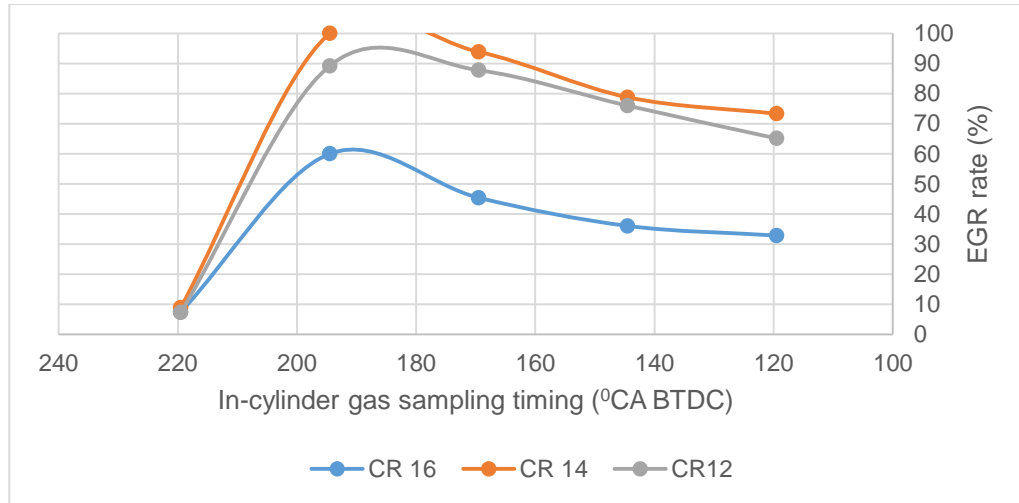

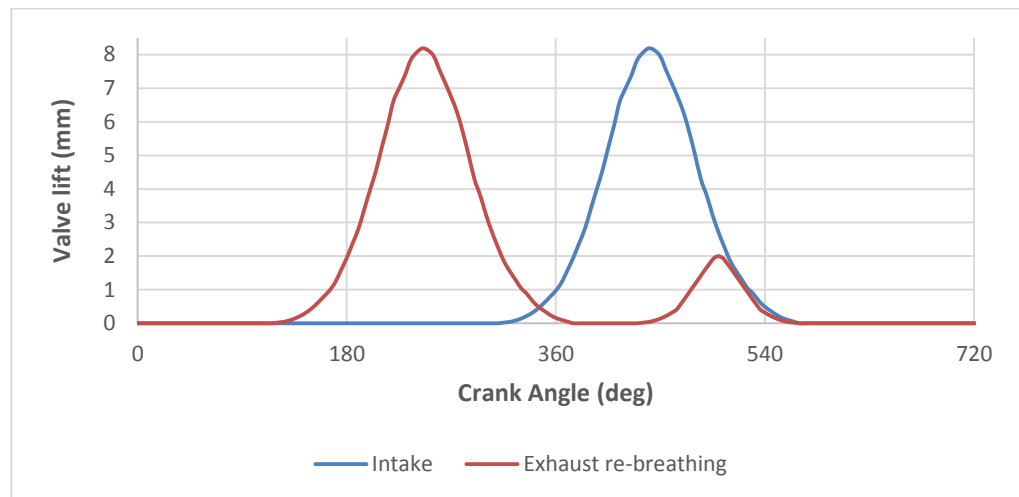Figure 6-2: Exhaust re-breathing EGR rate measured by the in-cylinder gas sampling method

Figure 6-3: Valve profiles for the Exhaust re-breathing experiments

Figure 6-3 shows the valve profiles that used for exhaust re-breathing experiment. Both intake and exhaust valve opening/closing timings were defined by 0.5mm valve lift.

Exhaust re-breathing experiments employed split DME injection ratios of 67%:33%, 56%:44% and 33%:67%. As the single DME injection (0%:100%) showed lower net indicated efficiency than split DME injection ratios, the single DME injection was not tested with the exhaust re-breathing. 1st DME injection timing was fixed at 130 ^{0}CA BTDC for all split DME injection ratio, while 2nd DME

injection timing was optimised for each case. The 1st DME injection timing was more advanced than its intake re-breathing experiment (56 ^{0}CA BTDC). This allowed more advanced 2nd DME injection timing for exhaust re-breathing experiments.

The minimum quantity of DME injection is limited by the minimum pulse width of 0.4ms to operate the DI injector, and the maximum pulse width was 0.8ms to satisfy the split DME injection ratio. Figure 6-4 shows the in-cylinder pressure, 1st DME injection and 2nd DME injection timings and their pulse width. The test was carried out at a fixed engine speed of 1,500 rpm, lambda 1.9, and CR 14. At the engine speed of 1,500 rpm, the crankshaft spun at 9 CA/ms, thus, the minimum injection duration is 3.6 CA (0.4ms) and the maximum injection duration is 7.2 CA (0.8ms). 2nd DME injection timing highly depends on the split DME injection ratio. In the case of the 63%:33% split DME injection ratio, the latest 2nd DME injection timing was 22 ^{0}CA BTDC. In the case of 33%:67% split DME injection ratio, 2nd DME injection timing was advanced to 47.5 ^{0}CA BTDC and followed by 56%:44% of 2nd DME injection timing of 57.5 ^{0}CA BTDC. In-cylinder pressure was gradually increased by the increased 1st DME injection ratio due to the improved reactivity of the premixed gasoline/air mixture at the fixed relative air/fuel ratio and DME/gasoline ratio.

The relative air/fuel ratio was controlled by gasoline injection pulse width at a fixed DME injection pulse width. Thus, the DME/gasoline ratio was changed with the relative air/fuel ratio.
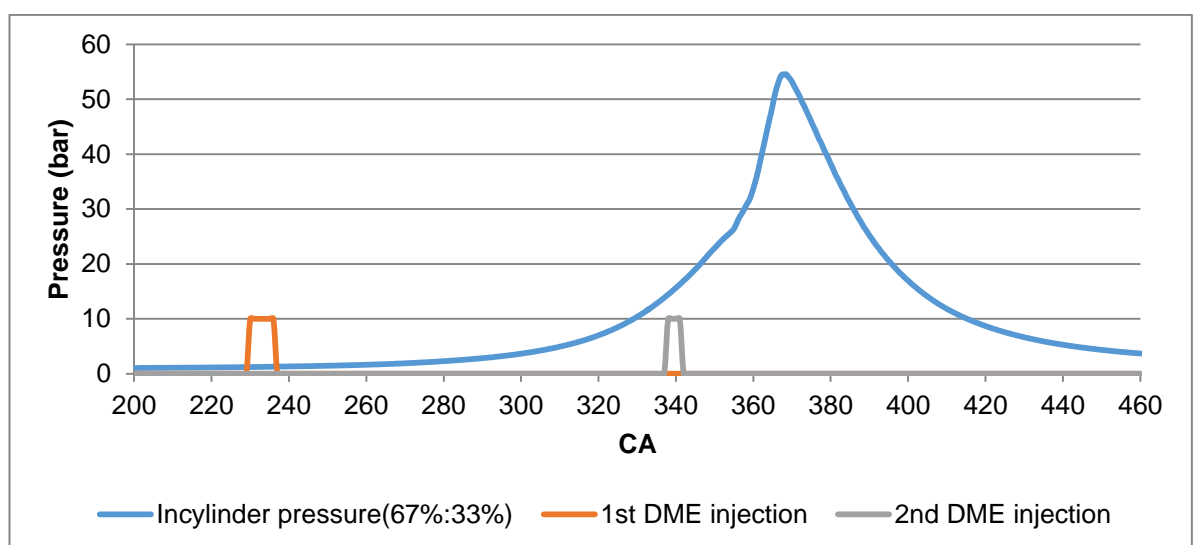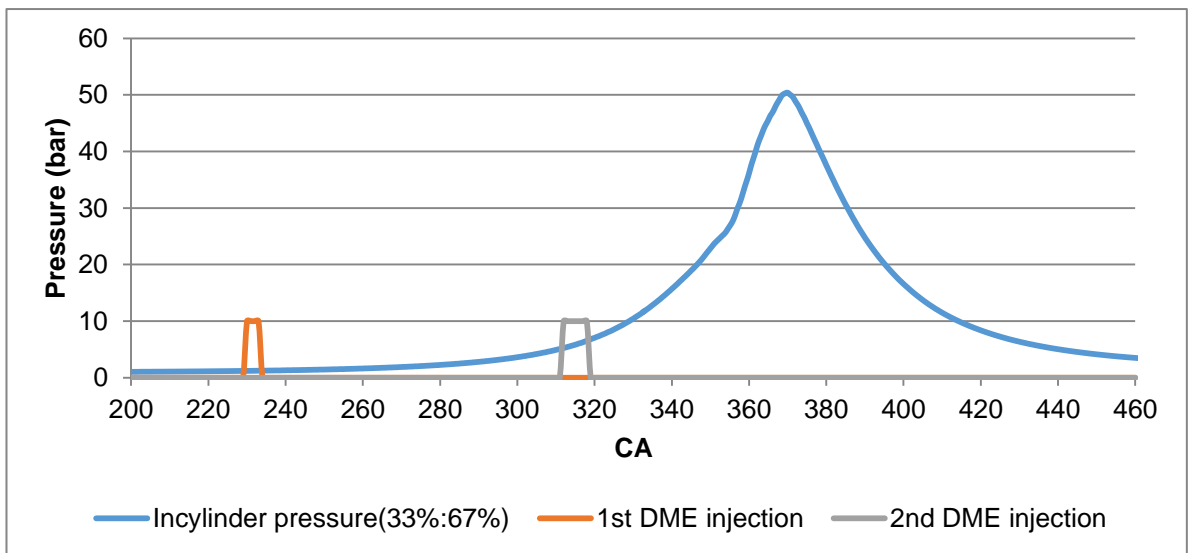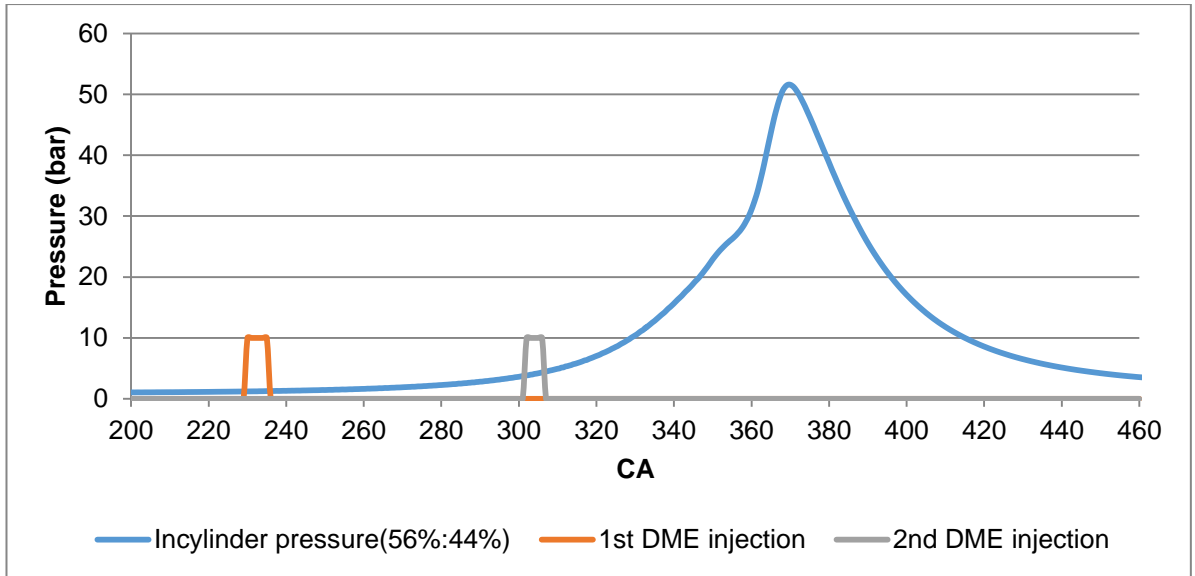
Figure 6-4: Split DME injection timings and durations

Table 6-1 shows the test condition for all exhaust re-breathing experiments. It is noticed that DME mass was varied with the injection timing although DME injection pulse width was fixed for all the test point. As the DME injector needle was lifted for between 3.6 ^{0}CA and 7.2 ^{0}CA, DME injection quantity was affected by its 2nd DME injection timing due to the in-cylinder back pressure. 67%:33% split DME injection ratio showed minimum reduction as its 2nd DME injection timing was the most advanced and followed by 33%:67% and 56%:44%.

Table 6-1: Test conditions for exhaust re-breathing experiments

Parameters	Split DME injection ratio		
	67%:33%	56%:44%	33%:67%
Gasoline SOI timing	16 ^{0}CA BTDC		
Mass of gasoline	17 to 34 mg/cycle	14 to 29.25 mg/cycle	13.65 to 28mg/cycle
Gasoline injection pressure	2.5 bar		
1st DME SOI timing	130 ^{0}CA BTDC		
2nd DME SOI timing	24 to 7.5 ^{0}CA BTDC	38 to 10 ^{0}CA BTDC	45 to 17 ^{0}CA BTDC
Total mass of DME	5.3 to 2.6 mg/cycle	5.1 to 1.9 mg/cycle	4.1 to 2.1 mg/cycle
DME/gasoline ratio	23:77 to 7:93	26:74 to 6:94	23:77 to 7:93
DME injection pressure	100 bar		
Compression ratio	12, 14, 16 (geometric)		
Engine speed	1,500 rev/min		
Coolant temperature	80 ^{0}C		
Intake pressure	Naturally Aspirated (1bar)		

6.2.2 Effects of CR, air/fuel ratio and split DME injection ratio on performance

Figure 6-5 shows net IMEP contour maps for the three split DME injection ratios, as a function of the relative air/fuel ratio and compression ratio. The high load boundary was limited by the knocking combustion (dp/dθ > 10bar/CA), whereas the low load boundary was limited by the unstable combustion (COVimep > 10%). Since the engine was operated at wide open throttle, the engine output was mainly controlled by the amount of fuel or the relative air/fuel ratio.

Compared to the intake re-breathing experiment, an extended operation range has been achieved by the exhaust re-breathing method. This is thought to be the combined effect of increased volumetric efficiencies and stratified hot EGR. In the case of exhaust re-breathing, exhaust gas was re-breathed during the intake stroke thus temperature at the intake port was not affected by the trapped residual gas. At CR14, the volumetric efficiency was increased from 45% to 85%, thereby fuel injection quantity could be increased and high load boundary was extended. Low load boundary seems to be extended by the stratified EGR. As the exhaust gas was re-breathed during the intake stroke, there was less time available for EGR to premix with fresh charge and no heat transferred to the cooler intake

ports. Thus some of part in the cylinder temperature would be result in higher temperature at the end of compression stroke.

The compression ratio and the split DME injection ratio had direct impact on the auto-ignition and combustion process. Increasing compression ratio extended low load boundary because more complete combustion was achieved by increased charge temperature and pressure, but reduced the high load boundary due to increased heat release rate. As more DME was injected in the first injection both the high load boundary and the low load boundary were reduced as shown in Figure 6-5. At CR14, increasing 1st DME injection mass from 33% to 67% (a) reduced the high load boundary from 6.6 bar to 3.3 bar and reduced the low load boundary from 2.2 bar to 3.8 due to the increased reactivity of the gasoline/air mixture and decreased heat release from 2nd DME injection.

(a) 67%:33% DME ratio (bar)   (b) 56%:44% DME ratio (bar)

(c) 33%:67% DME ratio (bar)   (d) volumetric efficiency (%)
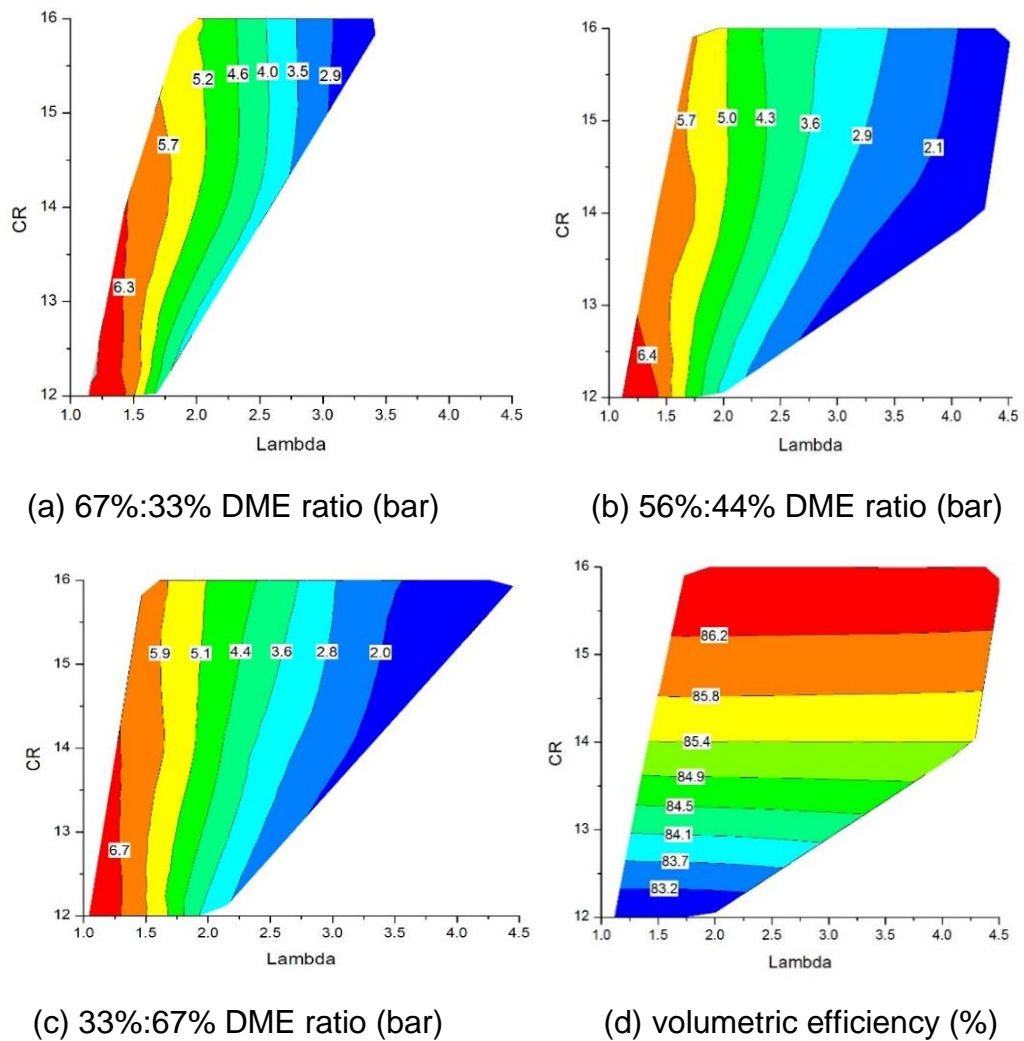
Figure 6-5: (a)-(c) Net IMEP contours as function of CR, air/fuel ratio and the split DME injection ratio variation (d) volumetric efficiency of 56%:44%
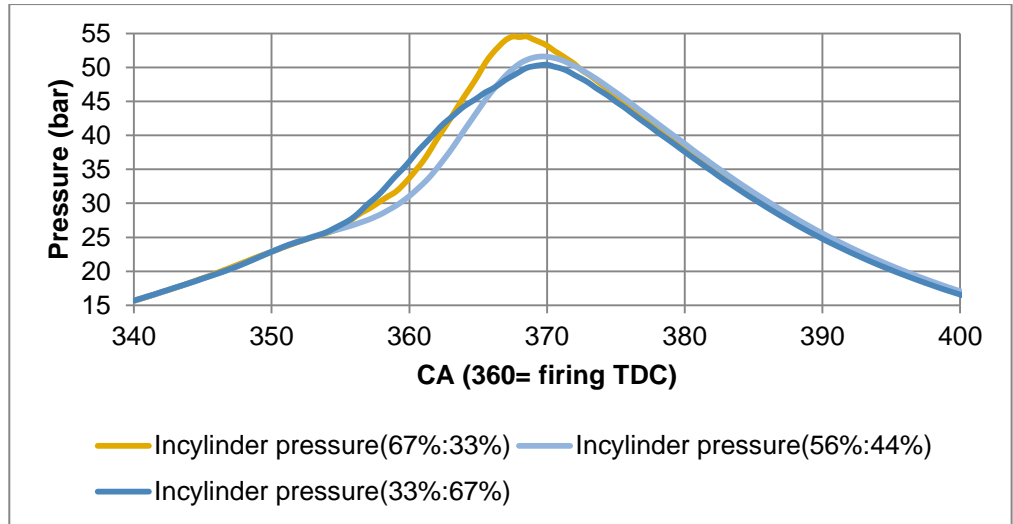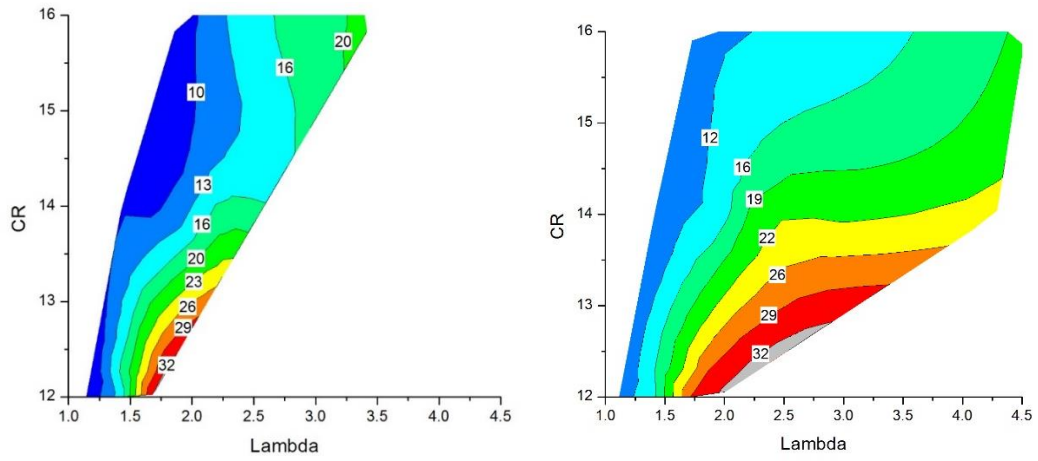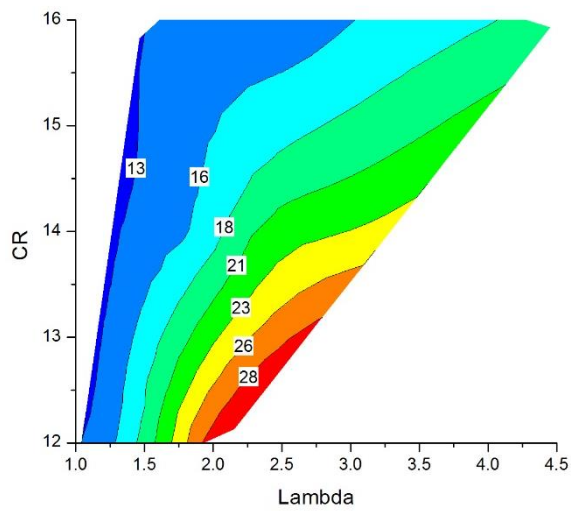
Figure 6-6: In-cylinder pressures of three split DME injection ratios at CR 14 and lambda 2.0 (injection timings are shown in Figure 6-4)

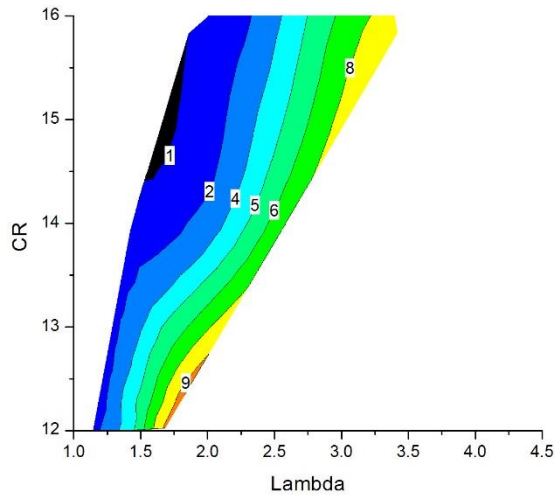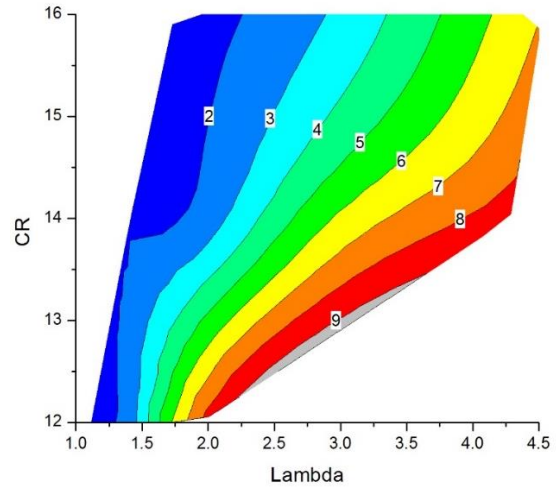(a) 67%:33% DME ratio (^{0}CA)

(b) 56%:44% DME ratio (^{0}CA)
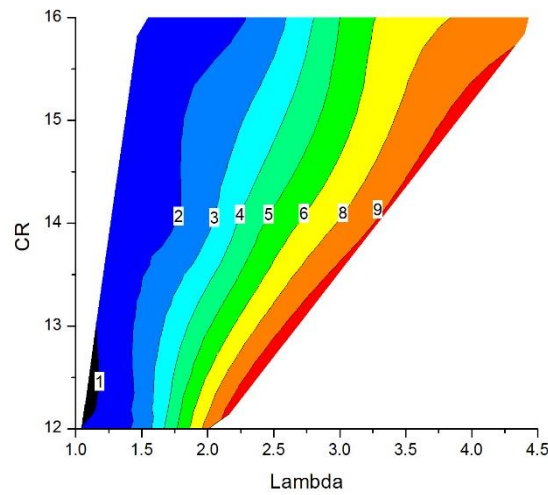

(c) 33%:67% DME ratio (^{0}CA)

Figure 6-7: Combustion duration variations with CR, air/fuel ratio and the split DME injection ratio

(b) 56%:44% DME ratio (%)   (a) 67%:33% DME ratio (%)

(c) 33%:67% DME ratio (%)

Figure 6-8: COVIMEP variations with CR, air/fuel ratio and the split DME injection ratio

The increased 1st DME injection ratio shortened the combustion duration and increased the maximum rate of pressure rise. Figure 6-6 shows the in-cylinder pressure trace of three split DME injections that discussed in Figure 6-4. The increased 1st DME injection ratio resulted in lower In-cylinder pressure at TDC due to the retarded CA10, but increased the maximum rate of pressure rise due to fast combustion speed. Figure 6-7 shows the combustion duration (from 10% MFB to 90% MFB). Although 67%:33% split DME injection ratio showed longer combustion duration than the other split DME injection ratio at CR12 with leaner condition due to leaner mixture with lower charge temperature, combustion duration became shorter as more heat was released as more DME was injected earlier.

The reduced low load boundary is thought to be the small heat release from 2nd DME injection combustion. Although the reactivity of premixed gasoline/air mixture was increased by the increased 1st DME injection, reduced heat release from the equally reduced 2nd DME injection quantity would not be able to initiate auto ignition of premixed DME/gasoline/air mixture. Thus the low load boundary was reduced by the decreased heat release from the 2nd DME injection.

Therefore, higher 2nd DME split injection ratio was more favourable for controlling the combustion phasing due to the moderated heat release rate and higher heat release from 2nd DME injection, and thus wider operation range could be achieved at both the high load and low load.
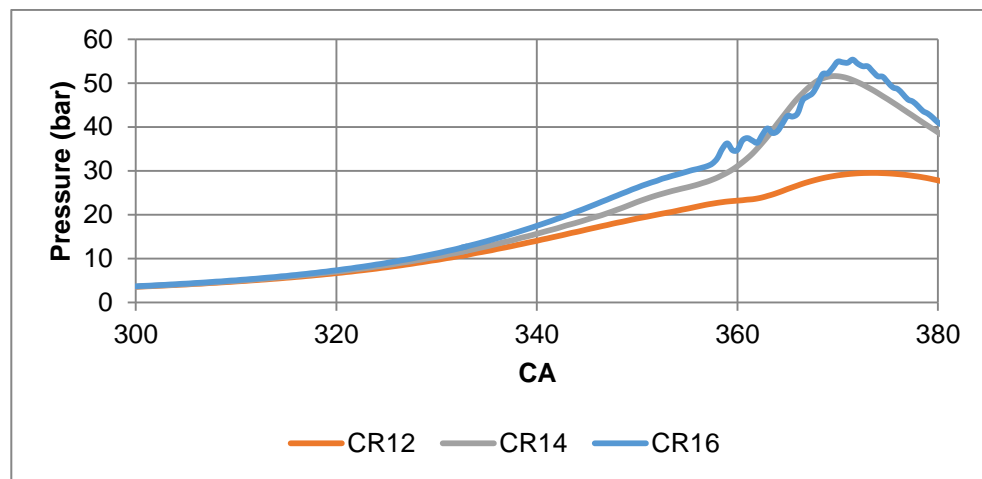

Figure 6-9: In-cylinder pressure at different compression ratios at fixed lambda

Figure 6-8 shows the results of COV_{IMEP} which defined the low load boundary. As the relative air/fuel ratio was reduced, more stable combustion was achieved with the reduced combustion duration. Figure 6-9 shows in-cylinder pressures of CR 12, CR14 and CR16 with 56%:44% split DME injection ratio at lambda 1.8. Increasing compression ratio reduced both COV_{IMEP} and combustion duration due to the increased charge temperature and pressure. High compression ratio also reduced the high load limit due to the knocking combustion. The knocking combustion of in-cylinder fluctuation can be seen from CR16 in Figure 6-9.

Figure 6-10 and Figure 6-11 show the knocking probability (% of $dp/d\theta >$ 10bar/CA) and the average maximum pressure rise rate (MPRR), respectively. The average MPRR was increased by increasing the compression ratio and reducing the relative air/fuel ratio. After MPRR 4 bar, the MPRR was rapidly

increased and knocking probability was also started to increase. This is because at the fuel leaner condition, the combustion phasing could be controlled by 2nd DME injection timing, however as the relative air/fuel ratio was reduced, 2nd DME injection timing could not control the combustion phasing due to the increased heat release rate. Since increasing 1st DME split injection ratio increased the reactivity of mixture, it has similar effect to increasing compression ratio. As 1st DME injection ratio was increased, 2nd DME injection timing did not controlled the start of combustion timing. In the case of 67%33% split DME injection ratio in Figure 6-10, at CR16 the combustion was initiated without 2nd DME injection when the relative air/fuel ratio was lower than lambda 2.5.

(a) 67%:33% DME ratio (%)   (b) 56%:44% DME ratio (%)
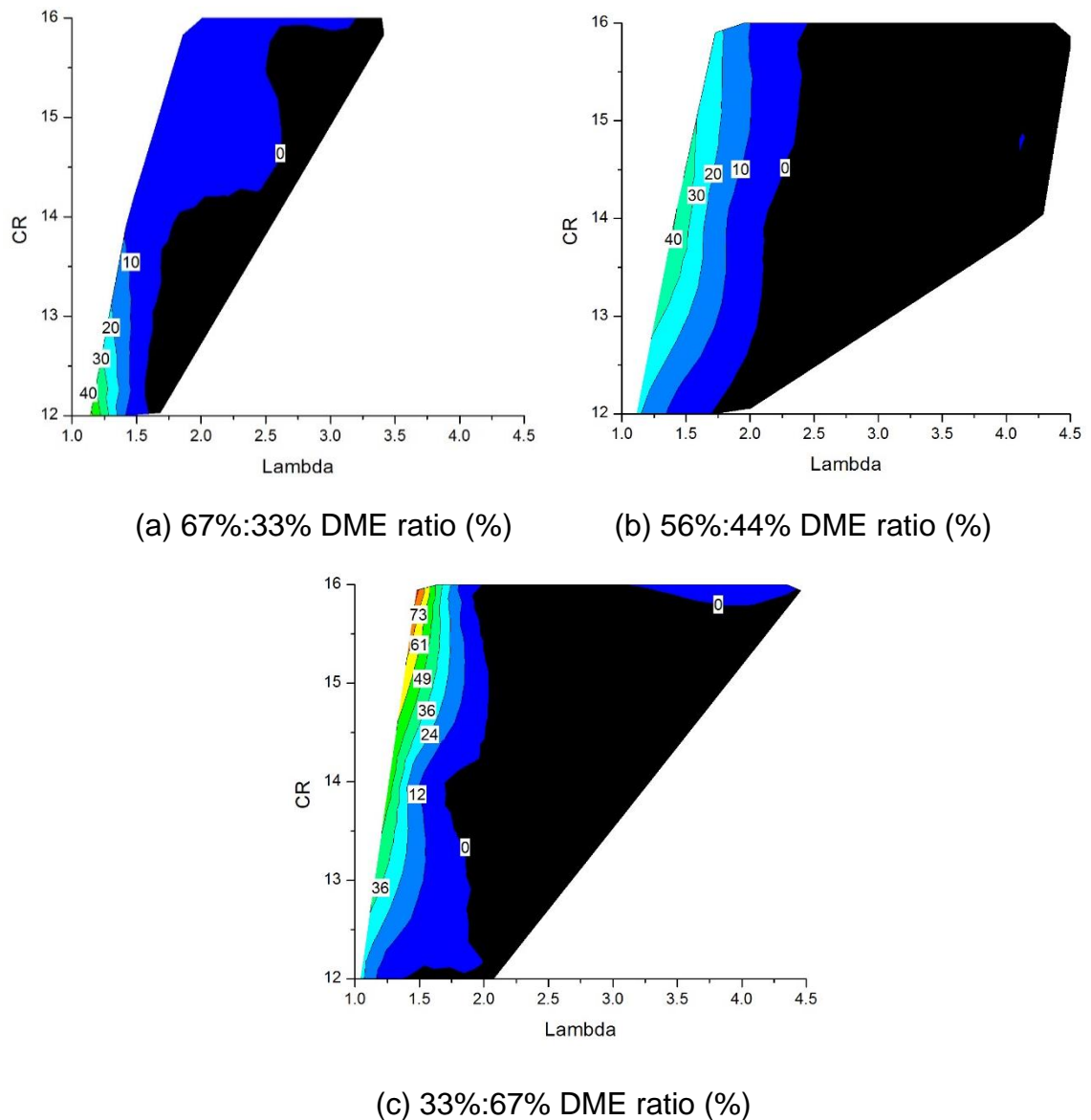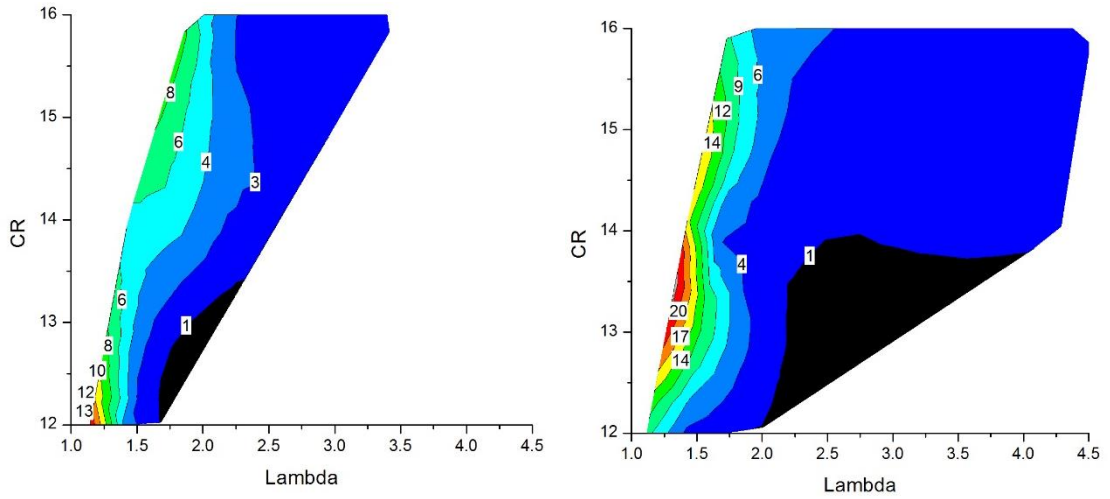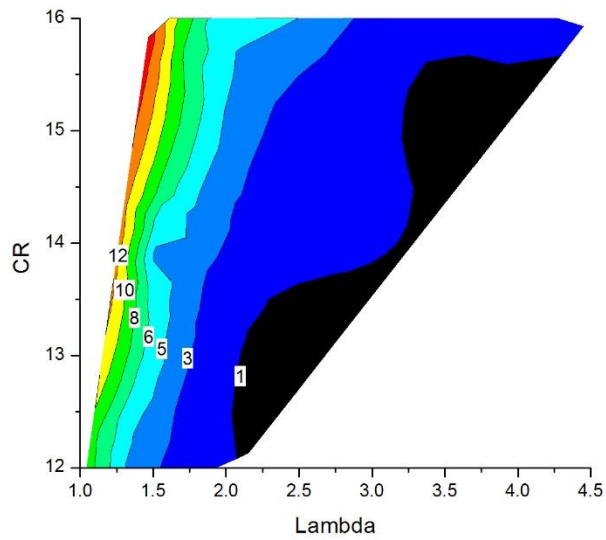
(c) 33%:67% DME ratio (%)

Figure 6-10: Knocking probability variations with CR, air/fuel ratio and the split DME injection ratio

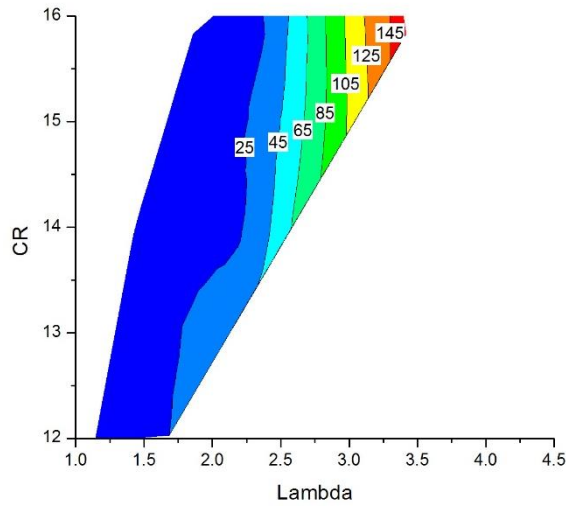(a) 67%:33% DME ratio (bar)   (b) 56%:44% DME ratio (bar)
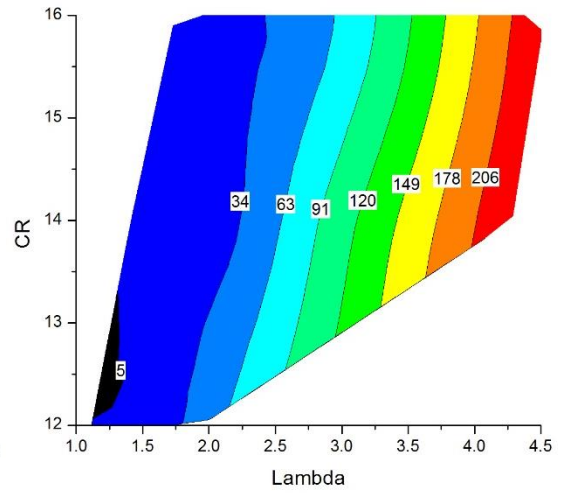

(c) 33%:67% DME ratio (%)

Figure 6-11: Average maximum pressure rise variations with CR, air/fuel ratio and the split DME injection ratio

6.2.3 Effects of CR, air/fuel ratio and split DME injection ratio on emission and efficiencies
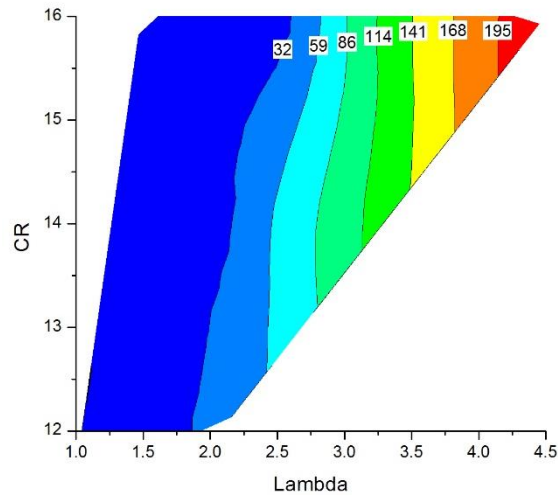
CO emission decreased with the reduced relative air/fuel ratio as combustion became more complete. As show in Figure 6-12. The split DME injection ratio had a direct impact on CO emission as the heat release was increased by increased the 1st DME injection ratio.
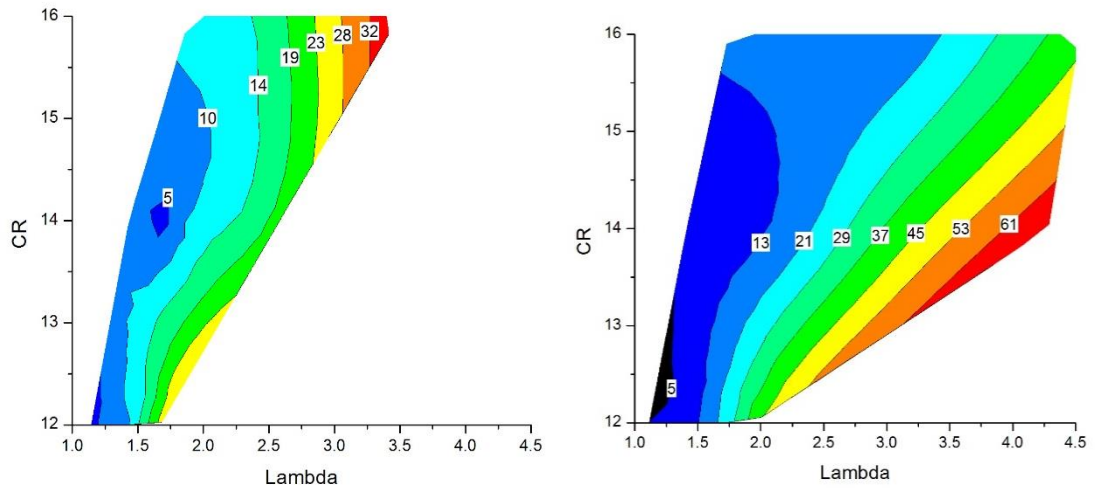
(a) 67%:33% DME ratio (g/KWh)   (b) 56%:44% DME ratio (g/KWh)

(c) 33%:67% DME ratio (g/KWh)

Figure 6-12: ISCO of 67%:33%, 56%:44% and 33%:67% split DME ratio

Figure 6-13 shows the ISHC emission of the split DME injection ratios. As expected, HC emission was reduced with lower relative air/fuel ratio and increased compression ratio due to the increased mixture reactivity and higher charge temperature. As 1st DME injection quantity was increased, specific HC emission was decreased due to the increased heat release rate and more complete combustion.

(a) 67%:33% DME ratio (g/KWh)

(b) 56%:44% DME ratio (g/KWh)

(c) 33%:67% DME ratio (g/KWh)

Figure 6-13: ISHC of 67%:33%, 56%:44% and 33%:67% split DME ratio

As shown in Figure 6-14, the maximum ISNOx occurred at the lower compression ratio with near stoichiometric mixture where the maximum IMEP was produced and hence the highest peak combustion temperature. Smaller 1st DME injection produced less NOx emission by moderating the heat release rate. Interestingly 33%:67% split DME injection ratio produced the maximum ISNOx emission at the lowest compression near the low load boundary, where SI combustion was dominate as the mixture was too lean to auto ignite by 2nd DME injection at CR 12 with lower 1st DME injection ratio.

(a) 67%:33% DME ratio (g/KWh)   (b) 56%:44% DME ratio (g/KWh)
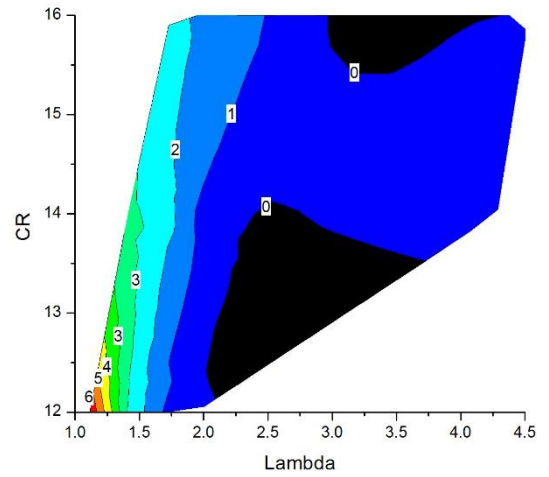
(c) 33%:67% DME ratio (g/KWh)
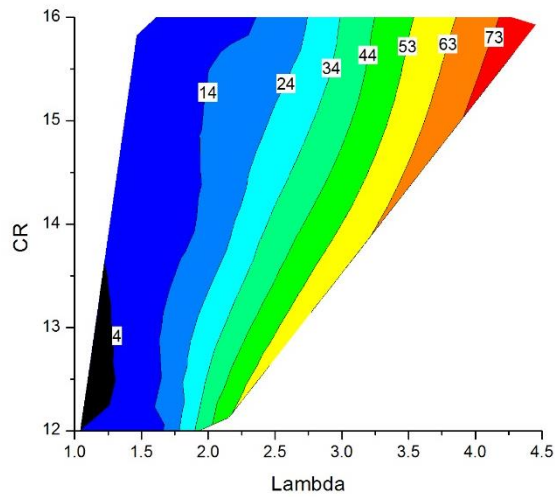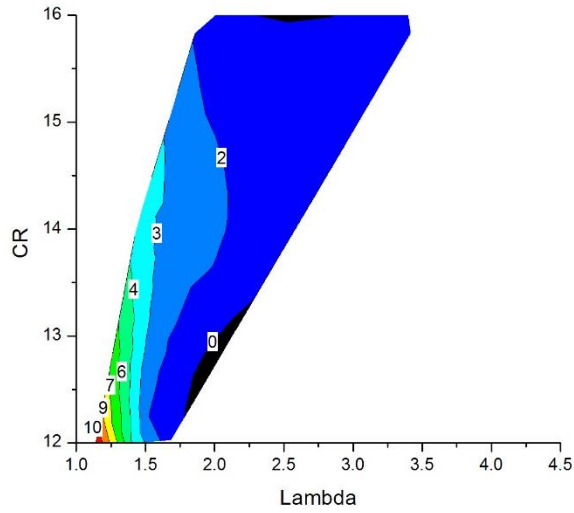
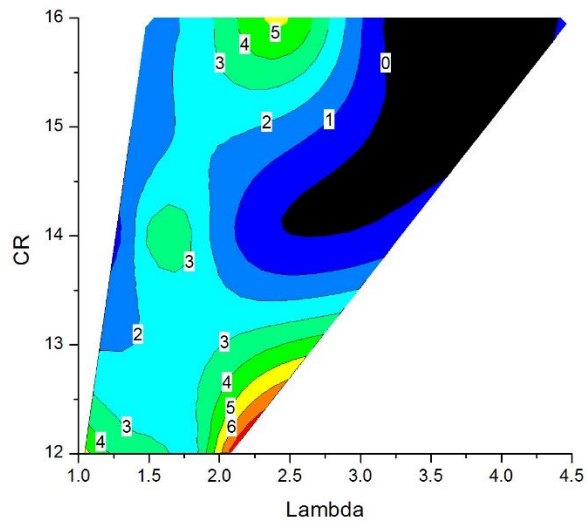*Figure 6-14: ISNOx of 67%:33%, 56%:44% and 33%:67% split DME ratio*

As Figure 6-15 shows, the exhaust temperature increased with decreasing relative air fuel ratio and increased 1st DME injection ratio as the heat release process finished earlier.
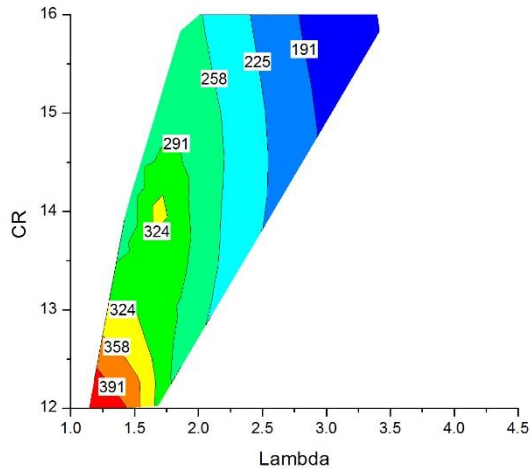
(a) 67%:33% DME ratio (^{0}C)   (b) 56%:44% DME ratio (^{0}C)
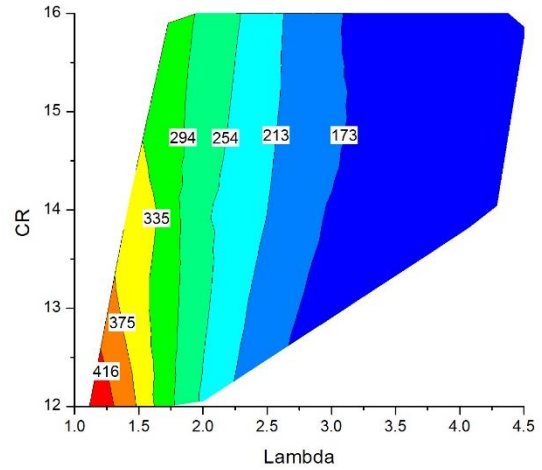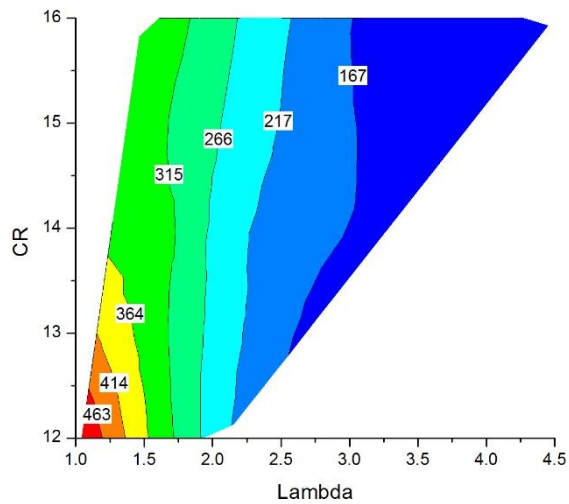
(c) 33%:67% DME ratio (^{0}C)

Figure 6-15: Exhaust temperature of 67%:33%, 56%:44% and 33%:67% split DME ratio

Figure 6-16 shows the combustion efficiency results. In the case of 33%:67% split DME injection ratio, the maximum combustion efficiency of over 98% was achieved at CR 12 with the near stoichiometric mixture, whereas the minimum combustion efficiency less than 77% was found at CR 16 with lambda 4.3. As CO and HC emissions were dominant factors for the combustion efficiency, the combustion efficiency was increased by decreased relative air/fuel ratio and increased 1st DME injection ratio.
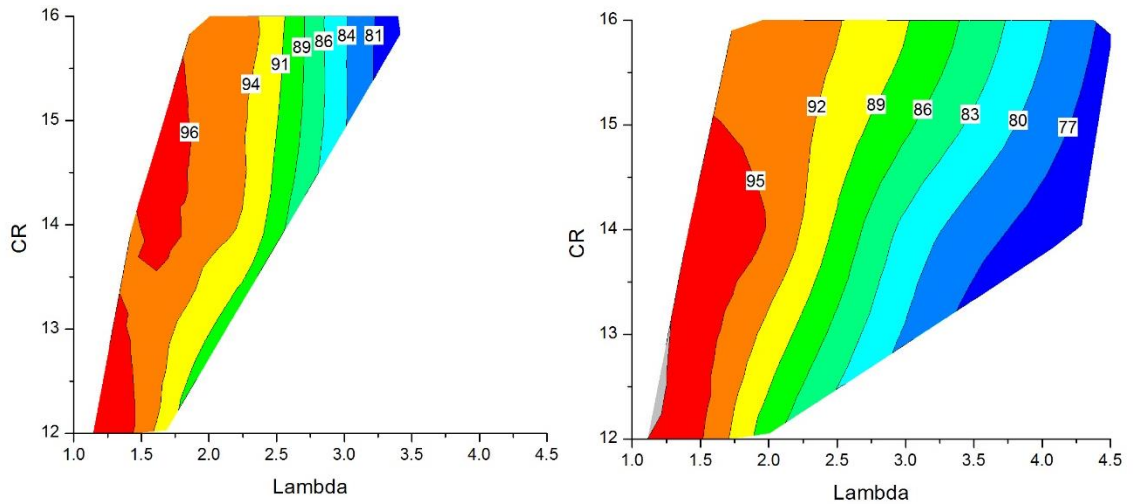
(a) 67%:33% DME ratio (%)   (b) 56%:44% DME ratio (%)
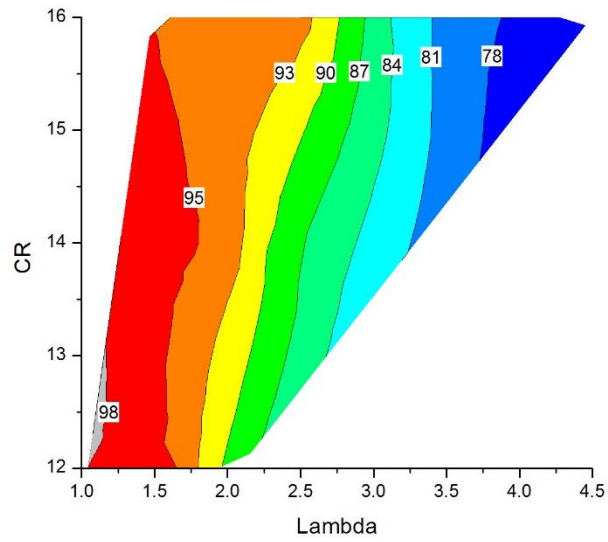
(c) 33%:67% DME ratio (%)

Figure 6-16: Combustion efficiency results of 67%:33%, 56%:44% and 33%:67% split DME ratio

Figure 6-17 shows the thermal efficiency results. Thermal efficiency was increased by increased compression ratio due to more complete combustion by higher charge temperature and pressure. Over 57% of the maximum thermal efficiency was achieved by 56%:44% split DME ratio at CR 16 with lambda 4, whereas around 31% of the minimum thermal efficiency was achieved by 33%:67% split DME ratio at CR 12 with lambda 1.1.

(a) 67%:33% DME ratio (%)　　　　(b) 56%:44% DME ratio (%)
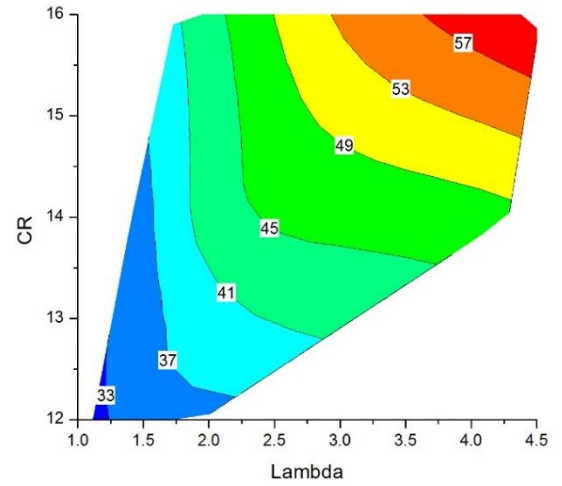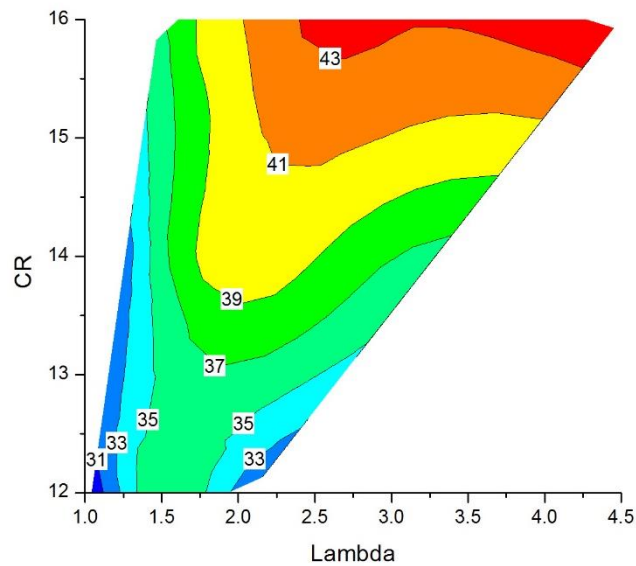
(c) 33%:67% DME ratio (%)

Figure 6-17: Thermal efficiency results of 67%:33%, 56%:44% and 33%:67% split DME ratio

Figure 6-18 shows the results of net indicated efficiency. As the ideal Otto cycle efficiency predicted higher engine efficiency at a higher compression ratio with a leaner mixture, the net indicated efficiency was increased by the increased compression ratio and the relative air/fuel ratio. Since the split DME injection ratio had direct impact on the start of combustion timing and combustion phasing, increasing the 1st DME injection ratio improved the engine efficacy until the knocking combustion occurred.
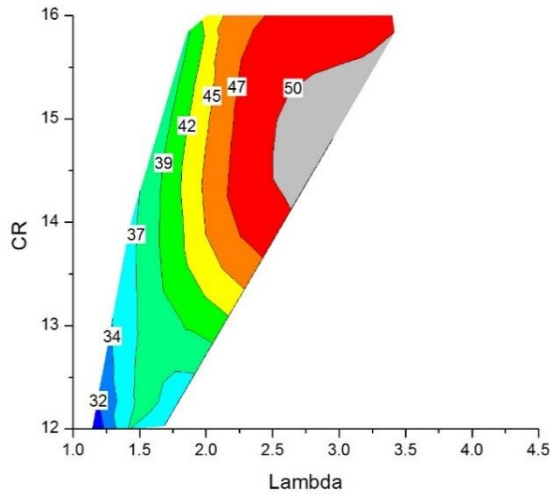
(a) 67%:33% DME ratio (%)

(b) 56%:44% DME ratio (%)

(c) 33%:67% DME ratio (g/KWh)
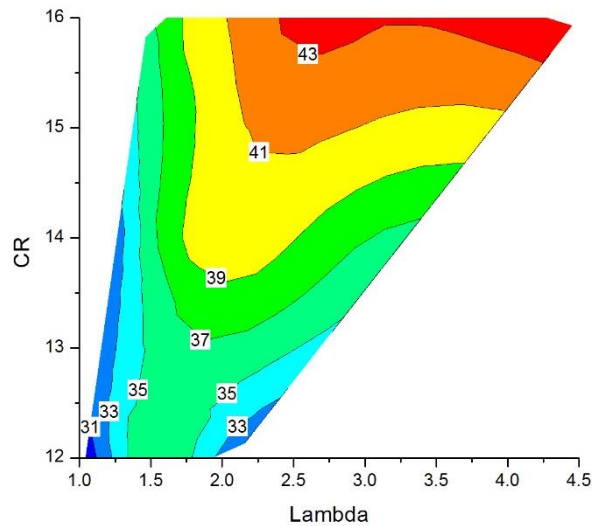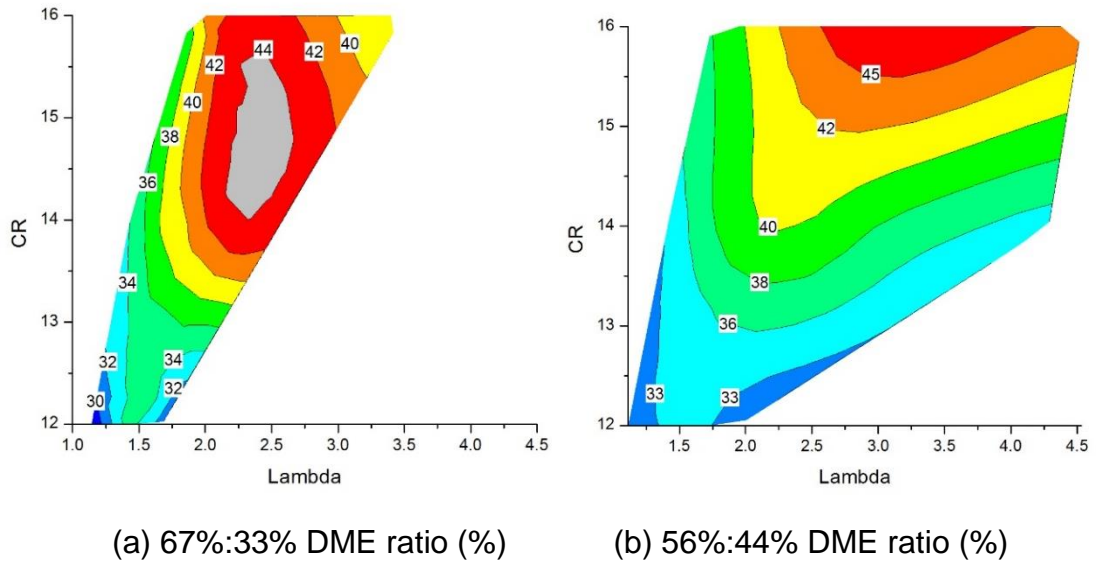
Figure 6-18: Net indicated efficiency of 67%:33%, 56%:44% and 33%:67% split DME ratio

6.3 COMPARISON OF DME ASSISTED GASOLINE CAI COMBUSTION WITH SI COMBUSTION

In this section, conventional SI combustion was compared to DME assisted gasoline CAI combustion with the intake and exhaust re-breathing methods. As the gasoline combustion engine has to operate at lambda 1 due to the three-way catalyst, the engine load was controlled by throttle at fixed lambda. In order to compare results of both the intake and the exhaust re-breathing operations, only compression ratio 14 was used for the comparison with varied split DME injection ratios.

6.3.1 Experiment condition

Table 6-2 shows SI test condition. In order to control the engine load, throttle position was varied from 4% to 20% while fixing the compression ratio at 13. SI test was carried out with positive valve overlap as shown in Figure 6-19.

Table 6-2: SI test condition

Parameters	Value
Compression ratio	13:1 (geometric)
Engine speed	1,500 rev/min
Coolant temperature	80 ^{0}C
Intake pressure	Naturally Aspirated (1bar)
Gasoline Injection pressure	2.5 bar
lambda	1.0
Spark timing	MBT
Throttle position	4% to 20%
Gasoline SOI timing	16 ^{0}CA BTDC

Figure 6-19: Valve profiles for SI test

33%:67% and 67%:33% of the split DME injection ratios were chosen for their superior efficient operations. Both intake and exhaust re-breathing valve strategies employed 67%:33% split DME injection ratio for low load and 33%:67% split DME injection ratio was employed for high load.

Table 6-3: Split DME injection ratio for the re-breathing strategies

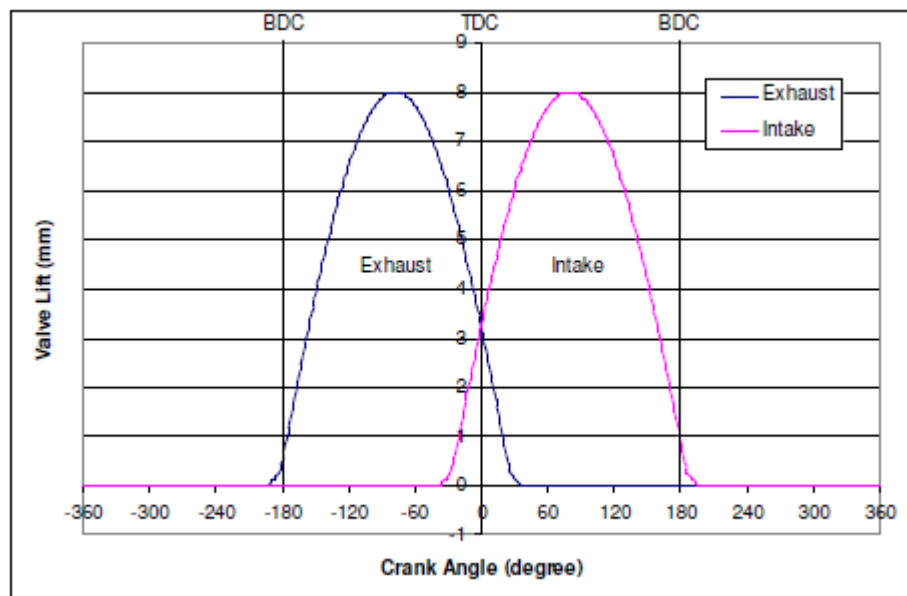| Parameters	Value
Compression ratio	13:1 (geometric)
Engine speed	1,500 rev/min
Coolant temperature	80 ^{0}C
Intake pressure	Naturally Aspirated (1bar)
Intake re-breathing	**Split DME injection ratio**
Net IMEP from 3.7 bar to 4.0bar	67%:33%
Net IMEP from 4.0 bar to 4.4bar	33%:67%
Exhaust re-breathing	**Split DME injection ratio**
Net IMEP from 3.7 bar to 5.8bar	67%:33%
Net IMEP from 5.8 bar to 6.6bar	33%:67%

6.3.2   Performance comparison

Figure 6-20 shows operation range of the intake and the exhaust re-breathing and the SI base line. As expected, the low load boundary of CAI combustion and SI combustion were limited by the unstable combustion (COVimep > 10%), whereas the high load boundary was limited by the knocking combustion (dp/dθ > 10bar/CA for CAI and dp/dθ > 10bar/CA for SI). The maximum operation range was achieved by SI combustion and follow by CAI combustion with exhaust re-breathing and CAI combustion with intake re-breathing, respectively. The high load boundary of SI was decreased by 43% with the intake re-breathing and 9.6% with the exhaust re-breathing, while the low load boundary was decreased by 36% for both CAI combustion.

Greatly improved CAI combustion with the exhaust re-breathing is thought to be the improved volumetric efficiency as shown in Figure 6-21. The higher volumetric efficiency of the exhaust re-breathing was achieved by high charge density of low intake charge temperature as the exhaust gas was directly introduced to in-cylinder. Because the volumetric efficiency would be over 100% by combining the 86% volumetric efficiency and measured EGR rate (Figure 6-2), it is probable that the EGR in the exhaust re-breathing could be an additional charge to pre-mixed charge from the intake port. The low load range of the exhaust re-breathing could be extended to a lower load if other split ratio operations can be employed, e.g.

the 56%:44% split DME injection ratio had a low load limit of 1.4 bar net IMEP (COV_{IMEP}=8%)
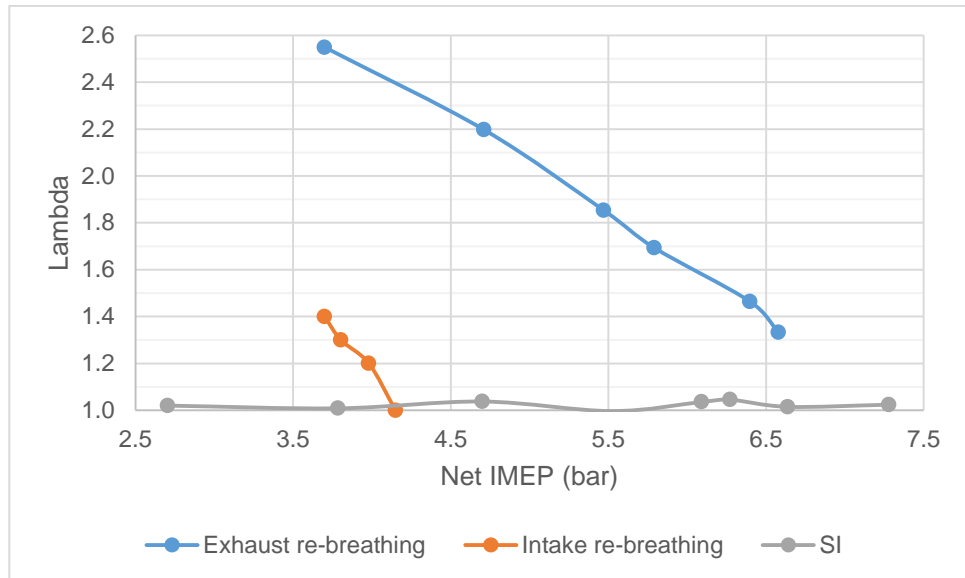
Figure 6-20: Comparison of operation ranges
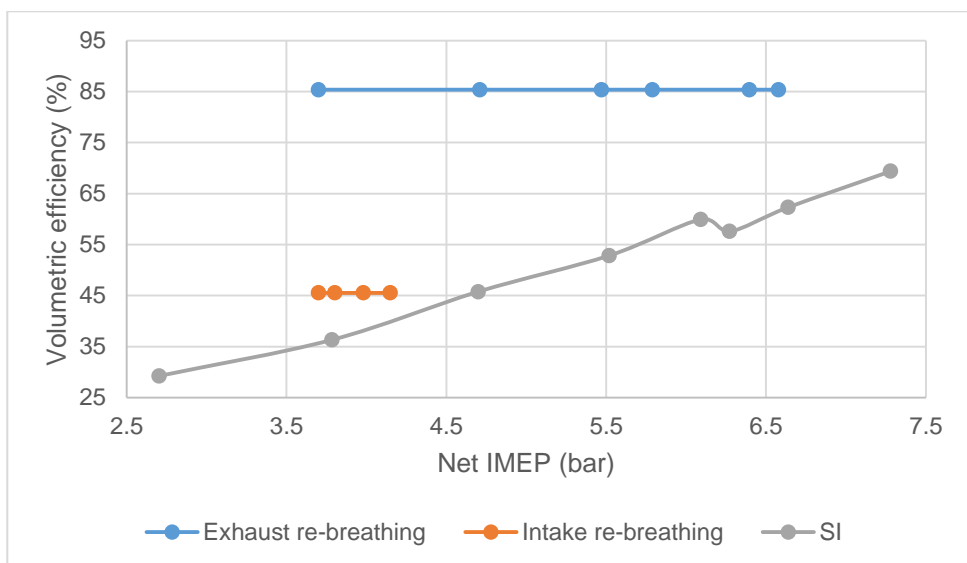
Figure 6-21: Comparison of Volumetric efficiencies
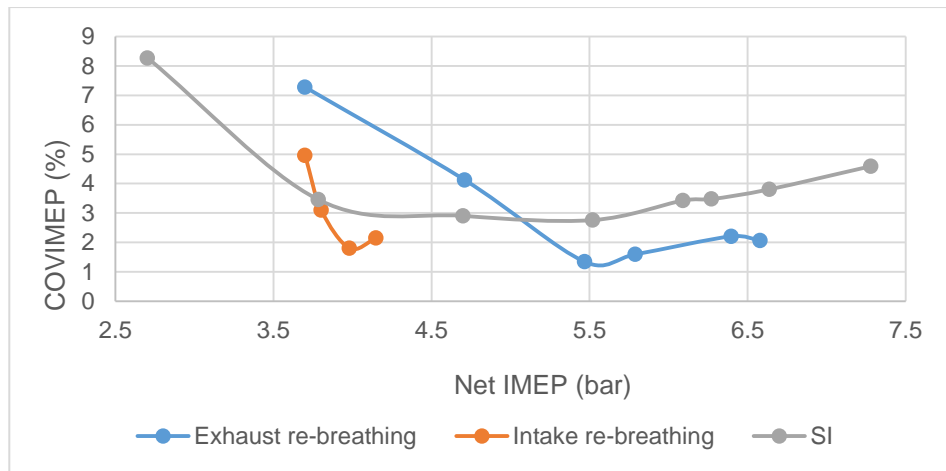
Figure 6-22: Comparison of combustion stability

Figure 6-22 and Figure 6-23 show the combustion stability result and combustion duration result. COV_{IMEP} was increased by increased combustion duration as slower combustion can cause incomplete combustion for CAI combustion with intake re-breathing and SI baseline. However combustion duration during the exhaust re-breathing operation remained relatively constant although COV_{IMEP} was increased as the split DME injection ratio was changed from 33%:67% to 67%:33%. At the same low load, CAI combustion with intake re-breathing shows more stable combustion than the exhaust re-breathing due to more homogenous EGR and in-cylinder temperature.
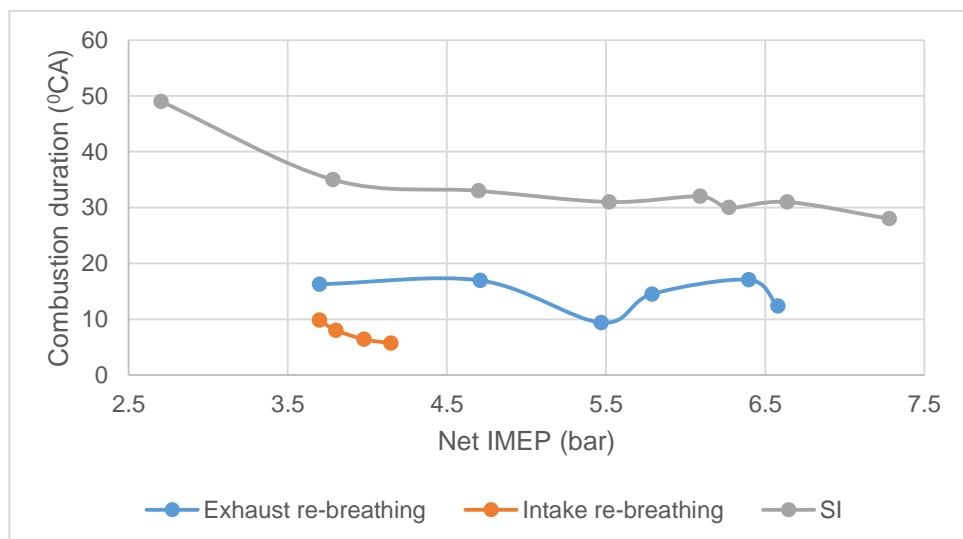
Figure 6-23: Comparison of combustion duration

As combustion duration was reduced, the knocking cycle occurred due to the increased combustion speed as shown in Figure 6-24.
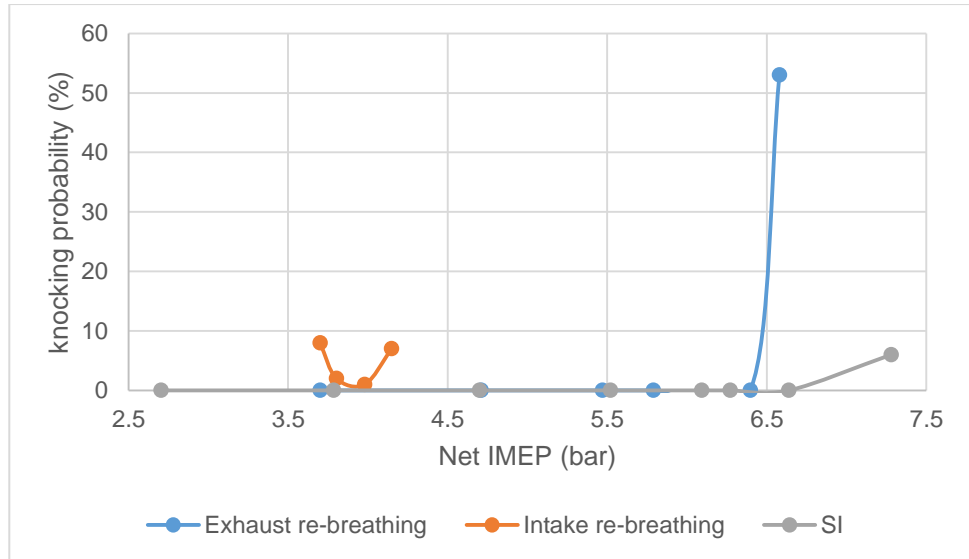
Figure 6-24: Comparison of knocking probability

6.3.3 Emission and efficiencies comparison

Figure 6-25 and Figure 6-26 show the indicated specific CO and NOx emission respectively. As expected, higher CO and HC emission were measured by CAI combustion than SI combustion. However as the engine load reached near to the high boundary, the level of CO emission became similar to SI combustion. CAI combustion of HC emission was also reduced with the engine load, because more complete combustion was achieved by richer mixture.
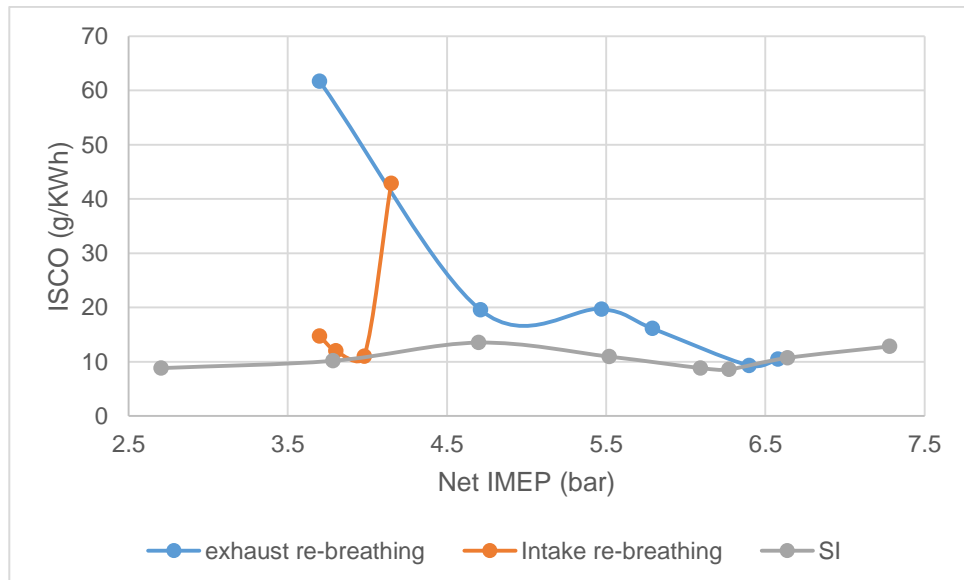
Figure 6-25: Comparison of ISCO emission
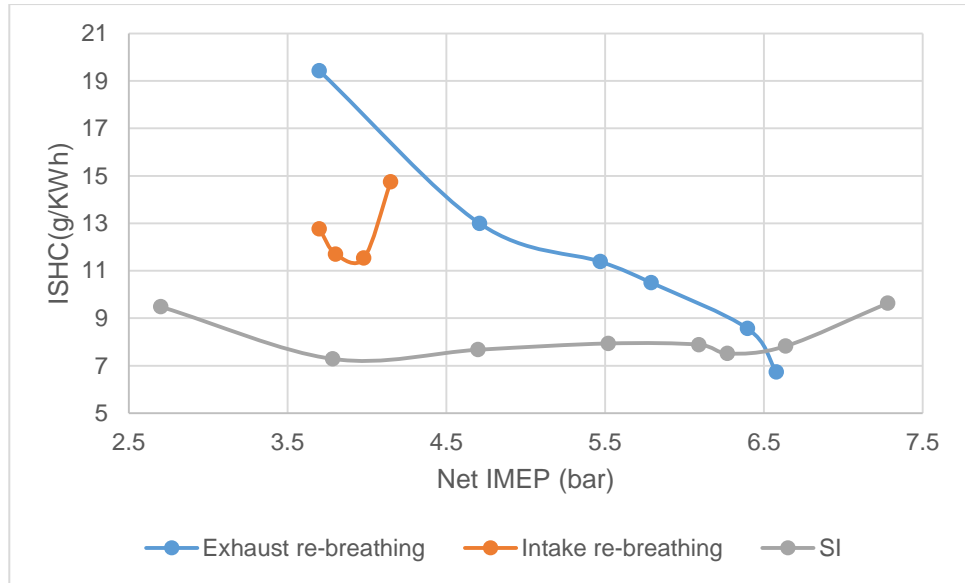
Figure 6-26: Comparison of ISHC emission

Figure 6-27 shows the indicated specific NOx emission result. Extremely low NOx emission was achieved by CAI with both the intake and exhaust re-breathing methods due to the low temperature combustion. Figure 6-28 shows the exhaust temperature results. The exhaust temperature of CAI combustion was lower than its SI baseline, due to the EGR, short combustion duration, and lean burn operation,
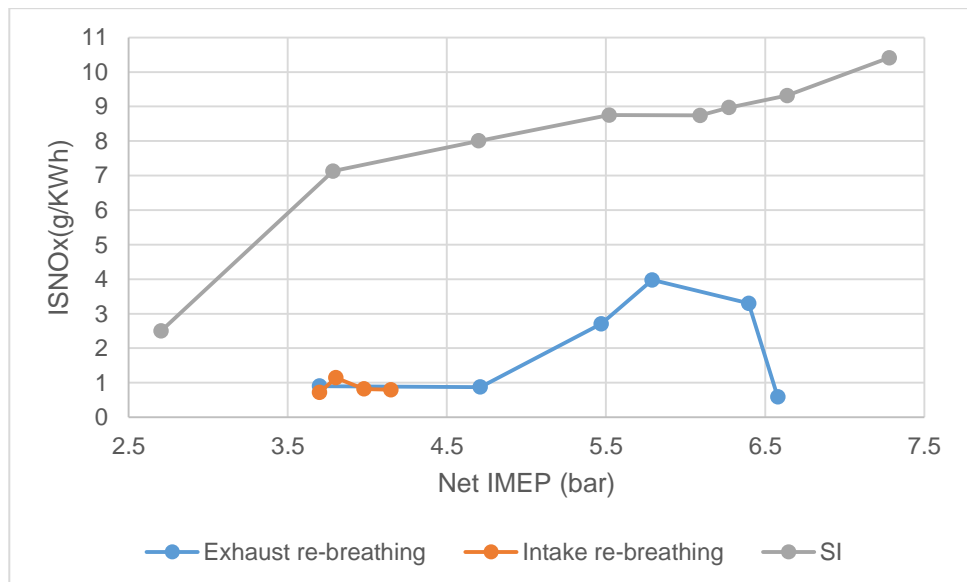
Figure 6-27: Comparison of ISNOx emission
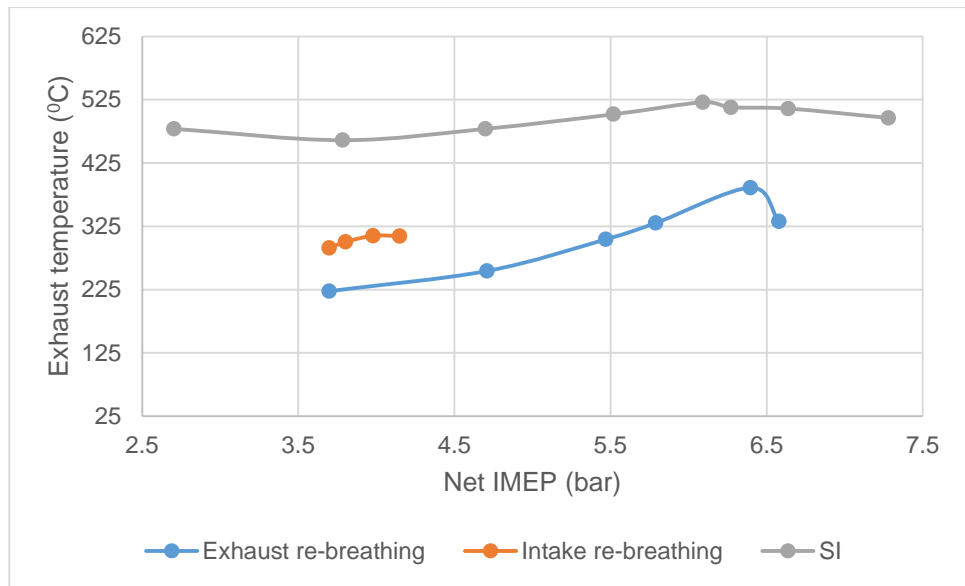
Figure 6-28: Comparison of Exhaust temperature

As higher HC and CO emissions were produced during CAI combustion, the combustion efficiency of CAI combustion was lower than its SI baseline as shown in Figure 6-29. Compared to the exhaust re-breathing operation, the intake re-breathing produced higher combustion efficiency due to the richer mixture operation. The stoichiometric SI combustion could produce the best combustion efficiency.
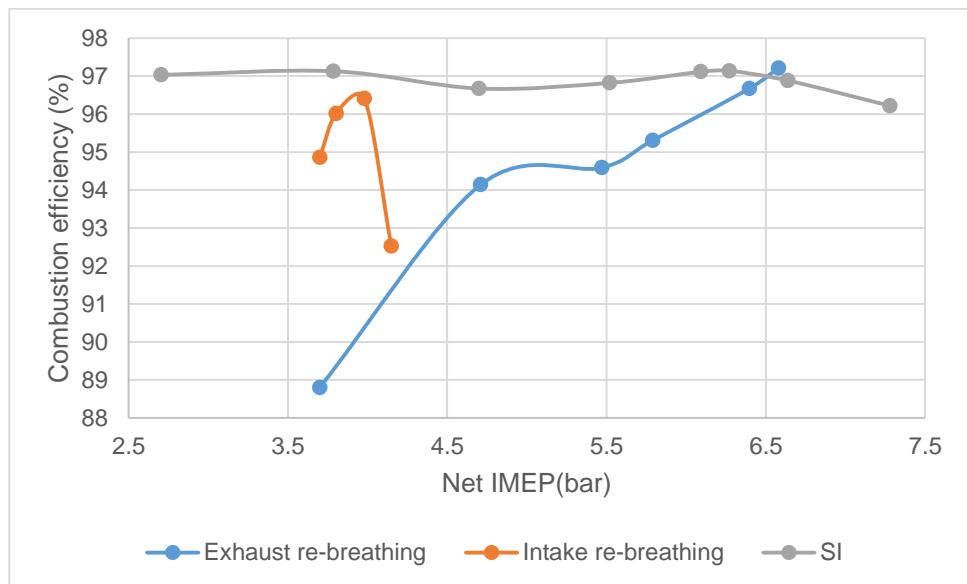
Figure 6-29: Comparison of Combustion efficiency

Figure 6-30 and Figure 6-31 show comparison of thermal efficiency and the net indicated efficiency. CAI combustion operations produced higher net indicated efficiency than its SI baseline. 43% of the maximum net indicated efficiency and

31% of the minimum net indicated efficiency was achieved by CAI combustion with exhaust re-breathing, while 28% of maximum and 24% of minimum net indicated efficiency was achieved by SI baseline. The change in net efficiencies of SI and CAI operations exhibited opposite trend with load. As the engine load was increased, the CAI combustion had a lower net indicated efficiency due to the decreased thermal efficiency, while the SI combustion increased net indicated efficiency due to the decreased pumping loss. CAI combustion with the exhaust re-breathing produced higher net indicated efficiency than with the intake re-breathing because the increased volumetric efficiency allowed the engine to operate at leaner condition.
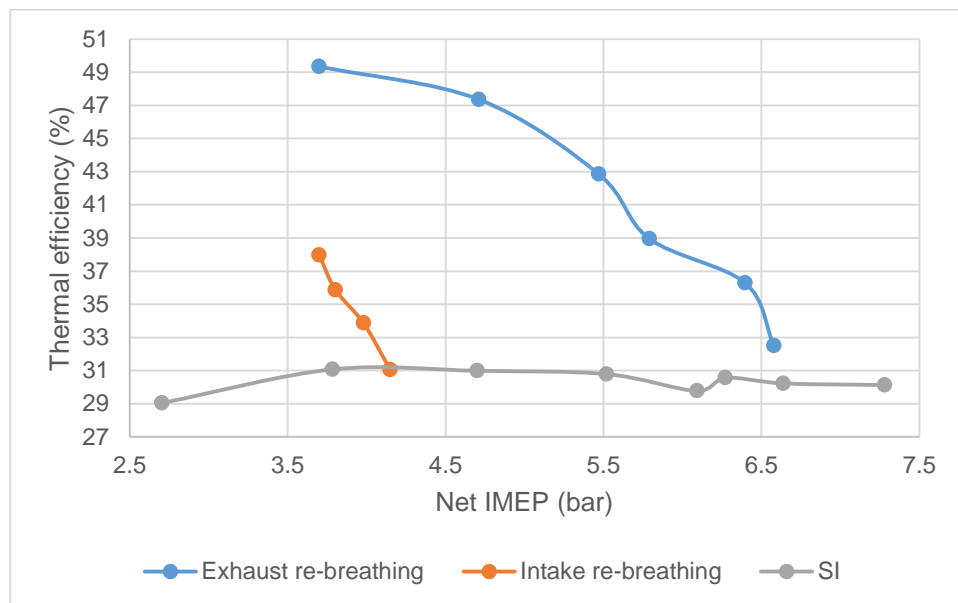
Figure 6-30: Comparison of thermal efficiency
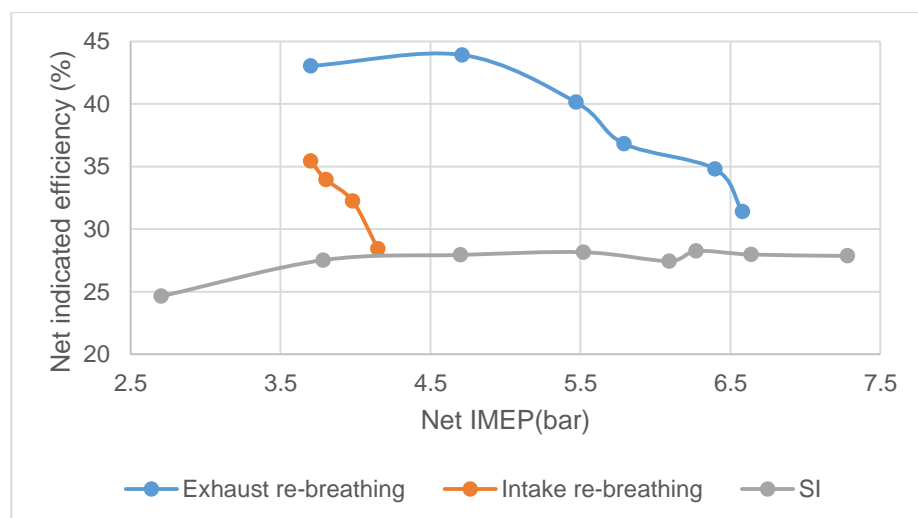
Figure 6-31: Comparison of net indicated efficiency

125

6.4 SUMMARY

This chapter has described the result of DME assisted gasoline CAI combustion with the exhaust re-breathing strategy. Effects of the compression ratio, the relative air/fuel ratio and split DME injection ratio have been investigated. The experimental results of CAI combustion with the exhaust re-breathing was compared to the results of CAI combustion with the intake re-breathing and SI baseline.

The results have demonstrated that the exhaust re-breathing operation provided enough heat to initiate DME assisted gasoline CAI combustion. The exhaust re-breathing strategy provided stratified and hotter internal EGR that does not impact negatively on the volumetric efficiency as exhaust gas was re-breathed from the exhaust port during the intake stroke. In-cylinder gas sampling method showed temporal variation of internal EGR and its results should be interpreted with caution.

The exhaust rebreathing method greatly extended both the high load and the low load boundary of the stable combustion operation. The extended high load was the result of the increased volumetric efficiency as it allows more fuel could be burn in the cylinder. The stratified and hot internal EGR was the dominant factor for the extended low load boundary as higher spot than its average in-cylinder temperature was presented due to less time available to mix with charge during the compression stroke.

Split DME injection ratio affected the operation range that could be achieved by varying the relative air/fuel ratio. As more DME was injected in 1st DME injection, both the high and low load limits were reduced due to the increased heat release and the reduced heat release from 2nd DME injection energy, respectively. On the other hand, increasing 1st DME injection ratio improved HC and CO emission due to the increased reactivity, and improved the net indicated efficiency as the combustion process was closed to constant volume combustion.

Comparison of DME assisted gasoline CAI combustion with the SI baseline, CAI combustion with the exhaust re-breathing provided only 9.6% decreased high load and 36% decreased low load boundary from SI baseline. Combustion duration of the both CAI and SI baseline was increased by reduced engine load, and

eventually increased COV_{IMEP} due to incomplete combustion. High load was limited by knocking combustion that caused exceed pressure rise between a crank angle. Compared to SI baseline, CAI combustion exhausted higher CO and HC emission, and these were resulted in the decreased combustion efficiency. Very low NOx emissions were obtained by DME/gasoline CAI operations. Most importantly, the exhaust rebreathing method produced dramatically improved overall efficiency of 43% compared to 28% of SI operation at a typical part-load operation of 4.0-5.0bar IMEP.

Chapter 7   SUMMARY AND CONCLUSIONS

7.1   INTRODUCTION

Comprehensive studies have been carried out on DME assisted gasoline CAI combustion with intake and exhaust re-breathing strategies. The first injection of split DME injections was used to increase the ignitability of premixed charge and 2nd DME injection was used to control the start of auto ignition combustion timing. The re-breathing valve strategy was used to provide hot internal EGR to slow down the combustion speed as well as the heat to initiate CAI combustion.

The one-dimensional engine simulation was used to design the re-breathing cam lobe in order to predict the EGR rate that could be achieved by the secondary valve opening. Both the intake and the exhaust re-breathing operations were tested on the E6 single cylinder engine. In a series of experiments, intake re-breathing valve timings were optimised and the effect of 2nd DME injection timing and split DME injection ratio were determined. Since the tests were carried out at WOT, the engine load was controlled by the amount of fuel in the cylinder. The operation range map was produced as a function of the relative air/fuel ratio and compression ratio.

Following the DME assisted CAI combustion with intake re-breathing, the CAI combustion with exhaust re-breathing test was carried out. Intake and exhaust re-breathing valve timing, split DME injection ratio and 2nd DME injection timing were set to the results of the CAI with intake re-breathing. The operation range map was then produced by variation of the relative air/fuel ratio and the compression ratio. The results of DME assisted gasoline CAI combustion with the intake and the exhaust re-breathing were compared to SI baseline results.

7.2   CONCLUSIONS

7.2.1   DME injection on DME/gasoline CAI operation

Extremely small amount of direct DME injection (0.004g/cycle) enabled gasoline CAI combustion without intake heating and could alter the start of combustion and combustion phasing.

In the split DME injection, 1st DME injection and 2nd DME injection showed opposite effects on the start of combustion and combustion phasing. The quantity of the first DME injection showed greater effect than its timing, whereas the injection timing of 2nd DME injection had a more dominant effect than its quantity. Increasing 1st DME injection mass retarded the optimum 2nd DME injection timing which was set to avoid knocking combustion and lower CO and HC emissions. The effects of 2nd DME injection timing on net IMEP has similar effect to the spark discharge timing in a SI engine. Either too early or too late 2nd DME injection timing reduced engine output due to knocking and incomplete combustion. Although it was possible to achieve CAI combustion with a single DME injection, the engine efficiency was lower than the split DME injection due to slower combustion.

The split DME injection ratio affected the operation range. As more DME was injected in 1st DME injection, both the high and low load limits were reduced due to either excess heat release rate or too slow combustion from 2nd DME injection, respectively. Higher 1st DME injection ratio showed slightly improved net indicated efficiency at lower load operation while slightly higher net indicated efficiency was obtained at higher load by increased 2nd DME injection. This effect was more pronounced during the exhaust re-breathing operation than the intake re-breathing.

7.2.2 Re-breathing valve strategy on DME/gasoline CAI operation

Both the intake and the exhaust re-breathing strategies provided enough heat and EGR for CAI combustion without controlling the exhaust back pressure. The mixture condition of hot internal EGR with fresh charge was found to be another dominant factor in CAI combustion operation range.

The exhaust re-breathing strategy provided stratified and hotter internal EGR that did not impact negatively on the volumetric efficiency, whereas the intake re-breathing strategy provided homogeneous internal EGR and hotter intake charge which had a negative impact on the volumetric efficiency. The in-cylinder gas sampling method was used to measure the EGR rate for the intake re-breathing, but could not be used for the exhaust re-breathing due to the EGR stratification.

The exhaust re-breathing strategy greatly extended both the high load and the low load boundaries of the stable combustion operation due to the increased volumetric efficiency and the stratified hot internal EGR.

Comparison of DME assisted gasoline CAI combustion with the SI baseline, CAI combustion with the exhaust re-breathing provided only 9.6% decreased high load and 36% decreased low load boundary from SI baseline. CAI combustion produced higher CO and HC emission, which resulted in the decreased combustion efficiency. Very low NOx emissions were obtained by DME/gasoline CAI operations. Most importantly, the exhaust rebreathing method produced dramatically improved overall efficiency of 43% compared to 28% of SI operation at a typical part-load operation of 4.0-5.0 bar IMEP

7.2.3 Other parameters on DME/gasoline CAI operation

The engine load was controlled by varying the relative air/fuel ratio. Knocking combustion limited the high load while incomplete combustion limited low load. The maximum net indicated efficiency and maximum thermal efficiency were obtained with leaner mixtures and higher compression ratio as predicted by the ideal Otto cycle.

The compression ratio affected the operation range. Increasing the compression ratio allowed the engine to operate with leaner mixtures but its richer mixture operation limit was narrowed due to more rapid heat release by the increased charge temperature. Increasing 1st DME injection ratio rendered the auto-ignition timing less controllable by the 2nd DME injection timing, especially at higher compression ratios and near stoichiometric mixtures.

7.3 RECOMMENDATIONS FOR FURTHER WORKS

7.3.1 Exhaust re-breathing strategy

The results presented in this research demonstrated that the exhaust re-breathing valve strategy has a great potential to overcome the limited operation range of CAI combustion without intake heating or controlling the exhaust back pressure. It is recommended that further study on exhaust re-breathing valve strategy with different pilot valve events and hence internal EGR rate. The simulation works can be used to optimise exhaust re-breathing valve profile, such as dwell duration

between the main and the late exhaust valve open, duration and the valve lift. In addition to the optimisation, it would be beneficial if the EGR rate is controlled by the late exhaust valve lift rather than duration as more stratified EGR can be obtained by reduced time available.

For experimental work, it is recommended to use a twin cam engine to test effects of late exhaust valve timing at fixed main exhaust valve. In this study, a single poppet valve engine was used to carry out the experiment, thus the main exhaust valve timing variation was unavoidable unless the cam lobe is changed. In order to understand the flow motion of exhaust gas during the late exhaust valve and its effect on mixing, it is recommended to use optical diagnostic such as PIV and LIEF.

7.3.2 DME injection strategy

DME injection was one of key parameters in this study as it was used control the start of combustion timing and combustion phasing. In order to understand the interactions of the DME ignition and premixed gasoline combustion, it is recommended to carry out the DME assisted gasoline combustion in an optical engine. The visualisation study will unveils the initiation combustion mode of direct DME injection and how that initiate auto-ignition of premixed charge.

The DME assisted CAI combustion of natural gas should be investigated as more natural gas becomes available for automotive applications.

References

[1] D. Hilling, Transport and developing conuntries, London and New York: Routledge, 1996.

[2] K. Michal, K.-D. Birgit and S. Jürgen, "Health effects of transport-related air pollution," The World Health Organization, Denmark, 2005.

[3] A. C. Waltner, ""Paradise delayed - the continuing sage of the Los Angeles Basin Federal Clean Air Implementation Plan," *UCLA Journal of Environmental Law & Policy,* pp. 247-283, 1996.

[4] "Carbon Monoxide poisoning," Headway - the brain injury association, [Online]. Available: https://www.headway.org.uk/carbon-monoxide-poisoning.aspx. [Accessed 14 06 2015].

[5] "Particulate Matter (PM) - health," United states Enviromental protection agency, 2009. [Online]. Available: http://www.epa.gov/airquality/particlepollution/health.html. [Accessed 13 06 2015].

[6] K. Michal, K.-D. Birgit and S. Jurgen, Health effects of transport-related air pollution, Copenhagen, Denmark: World Health Organization, 2005.

[7] "Car and light duty trucks - tier 1," ECOpoint Inc., 04 2007. [Online]. Available: https://www.dieselnet.com/standards/us/ld.php. [Accessed 03 06 2015].

[8] "Car and light duty truck - Tier 2," ECOpoint Inc., 12 2006. [Online]. Available: https://www.dieselnet.com/standards/us/ld_t2.php. [Accessed 03 06 2015].

[9] "Car and light duty Trucks - Tier 3," ECOpoint Inc., 03 2014. [Online]. Available: https://www.dieselnet.com/standards/us/ld_t3.php. [Accessed 3 06 2015].

[10] "Cars and light duty truck - California," 2015 ECOpoint Inc., 03 2014. [Online]. Available: https://www.dieselnet.com/standards/us/ld_t3.php. [Accessed 03 06 2015].

[11] "Car and light trucks for european union emission regulations," ECOpoint Inc., 01 2015. [Online]. Available: https://www.dieselnet.com/standards/eu/ld.php#stds. [Accessed 03 06 2015].

[12] I. c. o. c. transportation, "EU CO2 emission standards for passenger cars and light-commercial veicles," 01 2014. [Online]. Available: http://www.theicct.org/sites/default/files/publications/ICCTupdate_EU-95gram_jan2014.pdf. [Accessed 03 06 2015].

[13] U. s. e. p. agency, "EPA and NHTSA set standards to reduce greenhouse gases and improve fuel economy for model years 2017-2025 cars and light trucks," 08 2012. [Online]. Available: http://www.epa.gov/oms/climate/documents/420f12051.pdf. [Accessed 03 06 2015].

[14] J. A. Harrington and R. C. Shishu, "A Single Cylinder Study of the Effects of Fuel Type, Fuel Stoichiometry, and Hydrogen to Carbon Ratio and CO, NO and HC Exhaust Emissions," *SAE Paper,* no. 730476, 1973.

[15] H. John B., Internal combustion engine fundamentals, Singapore: McGraw-Hill, 1988.

[16] S. Richard, Introduction to internal combustion engine, Houndmills, Basingstoke, Hampshire RG21 6XS and London: Macmillan press LTD, 1999.

[17] F. Zhao, M. C. Lai and D. L. Harrington, "The Spray Characteristics of Automotive Port Fuel Injection," *SAE Paper ,* no. 950506, 1955.

[18] W. A. Daniel, "Flame Quenching at the Walls of an Internal Combustion Engine," in *Proceedings of the Sixth International Symposium on Combustion*, 1957.

[19] J. T. Wentworth, "The Piston Crevice Volume Effect on Exhaust Hydrocarbon Emission," *Combustion Science and Technology,* vol. Vol. 4, pp. pp 97-100,, 1971.

[20] P. Ralph H., H. William S, H. Geoff E and M. Jeff, General Chemistry: Principles and Modern Application, 9th Edition, Prentice Hall, 2006.

[21] F. Zhao, M.-C. Lai and D. Harrington, "Automotive spark-ignited direct-injection gasoline engines," *Energy and Combustion Science,* vol. 25, p. 437–562, 1999.

[22] K. T., I. Y, I. K., M. M, A. K and A. H, "Combustion Control Technologies for Direct Injection SI Engine," *SAE International,,* no. 960600.

[23] D. Boggs, H. Hilbert and M. and Schechter, "The Otto-Atkinson Cycle Engine-Fuel Economy and Emissions Results and Hardware Design," *SAE Technical Paper,* no. 950089, 1995.

[24] L. Miklanek, O. Vitek, O. Gotfryd and V. and Klir, "Study of Unconventional Cycles (Atkinson and Miller) with Mixture Heating as a Means for the Fuel Economy Improvement of a Throttled SI Engine at Part Load," *SAE International,* no. 2012-01-1678, 2012.

[25] M. S. S. and B. Karl-Heinz, "Parametric Studies of the Impact of Turbocharging," *SAE International,* no. 2009-01-1472, 2009.

[26] N. Fraser and M. Bassett, "Extreme Engine Downsizing with a Single Turbocharger – 100kW/l and 30 bar BMEP," in *Engine Downsizing Conference, Institute of Mechanical Engineers*, 2011.

[27] K. Norbert, Z. Christoph, S. Christian and S. Erik, "The New BMW Turbocharged SULEV 2.0-L Four-Cylinder Gasoline Engine," *MTZ worldwide,* vol. 73, no. 5, pp. 20-26, 2012.

[28] R. Friedfeldt, T. Zenner, R. Ernst and A. Fraser, "Three-cylinder Gasoline Engine with Direct Injection," *ATZ Autotechnology,* vol. Vol. 12, no. No. 2, 2012.

[29] J. Turner, A. Popplewell, R. Patel, T. Johnson, N. Darnton, S. Richardson, S. Bredda, R. Tudor, C. Bithell, R. Jackson, S. Remmert, R. Cracknell, J. Fernandes, A. Lewis, S. Akehurst, C. Brace, C. Copeland and Martin, "Ultra Boost for Economy: Extending the Limits of Extreme Engine," *SAE Internationa,* no. 2014-01-1185, 2014.

[30] F. Neil, B. Hugh, L. Grant and B. Mike, "Challenges for Increased Efficiency through Gasoline Engine Downsizing," *SAE International,* no. 2009-01-1053 , 2009.

[31] D. G. f. t. E. E. C. Brussels, "A technical study on fuels technology related to the Auto-Oil II programme – Volume II. Alternative fuels," 2000. [Online]. Available: http://ec.europa.eu/environment/archives/autooil/pdf/auto-oil_en.pdf. [Accessed 04 07 2015].

[32] R. Verbeek and D. W. J. Van, "Global assessment of dimethyl-ether: comparison," *SAE,* no. SAE paper no. 971607, 1997.

[33] Z. Hua, HCCI and CAI engines for the automotive industry, Cambridge: Woodhead Publishing limited, 2007.

[34] S. Onishi, J. Soukhong, K. Shoda, D. J. Pan and S. Kato, "Active Thermo Atmosphere Combustion (ATAC)- A New Combustion Process for Internal Combustion Engines," *SAE,* no. 790501, 1979.

[35] M. Sjöberg, J. Dec, A. Babajimopoulos and D. and Assanis, "Comparing Enhanced Natural Thermal Stratification Against Retarded Combustion Phasing for Smoothing of HCCI Heat-Release Rates," *SAE Technical Paper,* no. 2004-01-2994, 2004.

[36] C. Wildman, High Load Limits of the Controlled Autoignition Engine, Ph.D. Thesis, Dept. of Mech. Eng., MIT, 2009, 2009.

[37] R. Scaringe, Extension of the High Load Limit in the Homogenous Charge Compression Ignition Engine, Ph.D. Thesis, Dept. of Mech. Eng., MIT, 2009.

[38] Y. Changho, Z. Hua and M. Thanos, "Investigation of CAI Combustion with

Positive Valve Overlap," *SAE International,* no. 2009-01-1104, 2009.

[39] J. Dec and Y. Yang, "Boosted HCCI for High Power without Engine Knock and with Ultra-Low NOx Emissions - using Conventional Gasoline," *SAE international,* no. 2010-01-1086, 2010.

[40] C. Alasdair and H. Blaxill, "The Effects of Combined Internal and External Exhaust Gas Recirculation on Gasoline Controlled Auto-Ignition," *SAE International,* no. 2005-01-0133, 2004.

[41] L. Yufeng, Z. Hua, B. Nikolaos and M. Tom, "Effect of Injection Timing on Mixture and CAI Combustion in a GDI Engine with an Air-Assisted Injector," *SAE International,* no. 2006-01-0206, 2006.

[42] X. Hui, Y. Lin, Q. Jing, G. Rui, Z. Hong-Guo, H. Bang-Quan and Z. Hua, "The Effect of Spark Ignition on the CAI Combustion Operation," *SAE International,* no. 2005-01-3738, 2005.

[43] M. Nebojsa, B. Dave, P. Richard and T. Jamie, "Enlarging the Operational Range of a Gasoline HCCI Engine By Controlling the Coolant Temperature," *SAE TECHNICAL PAPER,* no. 2005-01-0157, 2005.

[44] Z. Hua, L. Jian, M. Tom and L. Nicos, "Performance and Analysis of a 4-Stroke Multi-Cylinder Gasoline Engine with CAI Combustion," *SAE International,* no. 2002-01-0420, 2002.

[45] O. Aaron, Z. Hua and L. Nicos, "Experimental Studies on Controlled Auto-ignition (CAI) Combustion of Gasoline in a 4-Stroke Engine," *SAE International ,* no. 2001-01-1030, 2001.

[46] M. Christensen, A. Hultqvist and B. Johansson, "Demonstrating the multi fuel capability of a homogeneous charge compression ignition engine with variable compression ratio," *SAE paper,* no. 1999-01-3679, 1999.

[47] S. Onishi, S. Hong Jo, K. Shoda, P. Do Jo and S. Kato, "Active Thermo-Atmosphere Combustion (ATAC) – A new Combustion Process for Internal Combustion Engines," *SAE paper ,* no. 790501, 1979.

[48] B. Patrick, T. Per and J. Bengt, "Investigation and Comparison of Residual Gas Enhanced HCCI using Trapping (NVO HCCI) or Rebreathing of Residual Gases," *SAE International,* no. 2011-01-1772, 2011.

[49] H. Jari, W. Carl and J. Bengt, "The Effect of Displacement on Air-Diluted Multi-Cylinder HCCI Engine Performance," *2006 SAE World Congress Detroit, Michigan,* no. 2006-01-0205, 2006.

[50] D. John E., Y. Yi and D. Nicolas, "Improving Efficiency and Using E10 for Higher Loads in Boosted HCCI Engines," *SAE International,* no. 2012-01-1107, 2012.

[51] Z. H., P. Z., W. J. and L. N., "Understanding the Effects of Recycled Burnt Gases on the Controlled Autoignition (CAI) Combustion in Four-Stroke Gasoline Engines," *SAE International ,* no. 2001-01-3607, 2001.

[52] J. Dec, M. Sjöberg and W. Hwang, "Isolating the Effects of EGR on HCCI Heat-Release Rates and NOX Emissions," *SAE international,* no. 2009-11-02, 2009.

[53] L. Don, K. Dan, A. Jeff, K. Gary and C. Ted, "Controlled Combustion in an IC-Engine with a Fully Variable Valve Train," *SAE Internationa,* no. 2001-01-0251 , 2001.

[54] P. Håkan, A. Mats, O. Jan-Ola and J. Bengt, "The Effect of Intake Temperature on HCCI Operation Using Negative Valve Overlap," *SAE International,* no. 2004-01-0944, 2004.

[55] H. Göran, T. Per and J. Bengt, "HCCI Combustion Phasing in a Multi Cylinder Engine Using Variable Compression Ratio," *m SAE International,* no. 2002-01-2858, 2002.

[56] A. H. a. B. J. Magnus Christensen, "Demonstrating the Multi Fuel Capability of a Homogeneous Charge Compression Ignition Engine with Variable Compression Ratio," *SAE International,* no. 1999-01-3679, 1999.

[57] A. Tanet, F. David, M. Takeshi and I. Minoru, "Comparison of HCCI Operating Ranges for Combinations of Intake Temperature, Engine Speed and Fuel Composition," *SAE International,* no. 2002-01-1924, 2002.

[58] B. Paul W., S. Charles H., D. Kevin P., H. William L. and L. Michael P., "Effects of Fuel Property Changes on Heavy-Duty HCCI Combustion," *SAE International,* no. 2007-01-0191, 2007.

[59] J. M. a. N. Jeuland, "Which Fuel Properties for Improved CAI Combustion ? Study of Fuel Impacts on the Operating Range of a CAI PFI Engine," *SAE International,* no. 2009-01-1100 , 2009.

[60] L. Guntram A., J. Timothy J., C. Christos A., A. Dennis N. and S. Robert M., "Evaluation of a Narrow Spray Cone Angle, Advanced Injection Timing Strategy to Achieve Partially Premixed Compression Ignition Combustion in a Diesel Engine," *SAE International,* no. 2005-01-0167, 2005.

[61] Z. Fan, X. Hongming, R. Soheil Zeraati, K. Gautam and S. Shi-Jin, "Combustion and Emission Characteristics of a PPCI Engine Fuelled with Dieseline," *SAE International,* no. 2012-01-1138, 2012.

[62] S. Derek, H. Reed, K. Sage and R. Rolf, "Reactivity Controlled Compression Ignition (RCCI) Heavy-Duty Engine Operation at Mid-and High Loads with Conventional and Alternative Fuels," *SAE International,* no. 2011-01-0363, 2011.

[63] Kihyun, C. Kim and Bae, "Operating Characteristics of DME-Gasoline Dual fuel in a Compression Ignition Engine at the Low Load Condition," *SAE International,* no. 2013-01-0049, 2013.

[64] Z. H.F., S. K. and H. Z. , "Combustion and emission analysis of the direct DME injection enabled and controlled auto-ignition gasoline combustion engine operation," *Fuel,* vol. 107, p. 800–814, 2013.

[65] Z. Yan, Z. Hua, P. Mark and B. Campbell, "Direct In-cylinder CO2 Measurements of Residual Gas in a GDI Engine for Model Validation and HCCI Combustion Development," *SAE International,* no. 2013-01-1654, 2013.

[66] D. Florence, V. Franck, K. Vincent and F. Loïc de, "Influence of the Valve-lift Strategy in a CAI™ Engine using Exhaust Gas Re-Breathing – Part 1: Experimental Results and 0D Analysis," *SAE International ,* no. 2009-01-0299, 2009.

[67] K. Kiyoshi, H. Kazuki, N. Shingo, Y. Koji, O. Hiroyuki and N. Toru, "Improvement of Natural-gas HCCI Combustion by Internal EGR by Means of Exhaust Valve Re-opening," *SAE International,* no. 2009-32-0079, 2009.

[68] Z. Hua, G. Lowry and N. Ladommatos, "Time-Resolved Measurements and Analysis of In-Cylinder Gases and Particulates in Compression-Ignition Engines," *SAE international,* p. 961168, 1996.

[69] World Oil Outlook 2011, Organization of the Petroleum Exporting Countries (OPEC), 2011.

[70] "The Great Smog of 1952," metoffice.gov.uk, Last updated 20 April 2015.

[71] T. Kume, Y. Iwamoto, K. Iida, M. Murakami, K. Akishino and H. Ando, "Combustion Control Technologies for Direct Injection SI Engine," *SAE International,* 960600.

[72] J. Harada, T. Tomita, H. Mizuno, Z. Mashiki and Y. Ito, "Development of Direct Injection Gasoline Engine," *SAE International,* 970540.

[73] M. Kano, K. Saito, M. Basaki, S. Matsushita and T. Gohno, "Analysis of Mixture Formation of Direct Injection Gasoline Engine," *SAE Technical Paper,* 980157.

[74] K. M., S. K., a. M., M. S. and G. T., "Analysis of Mixture Formation of Direct Injection Gasoline Engine," *SAE Technical Paper,* no. 980157.

[75] N. Unger, T. S. D. and S. W. J, " Climate forcing by the on-road transportation and power generation sectors," *Atmos. Environ,* vol. 43, pp. 3077-3085, 2009.

[76] M. Christensen, A. Hultqvist and B. Johansson, "Demonstrating the Multi Fuel Capability of a Homogeneous Charge Compression Ignition Engine with Variable Compression Ratio," *SAE Technical Paper,* Vols. 1999-01-3679,

1999.

[77] T. Aroonsrisopon, D. E. Foster, T. Morikawa and M. Iida, "Comparison of HCCI Operating Ranges for Combinations of Intake Temperature, Engine Speed and Fuel Composition," *SAE Technical Paper,* Vols. 2002-01-1924, 2002.

[78] P. W. Bessonette, C. H. Schleyer, K. P. Duffy, W. L. Hardy and M. P. Liechty, "Effects of Fuel Property Changes on Heavy-Duty HCCI Combustion," *SAE Technical Paper,* Vols. 2007-01-0191, 2007.
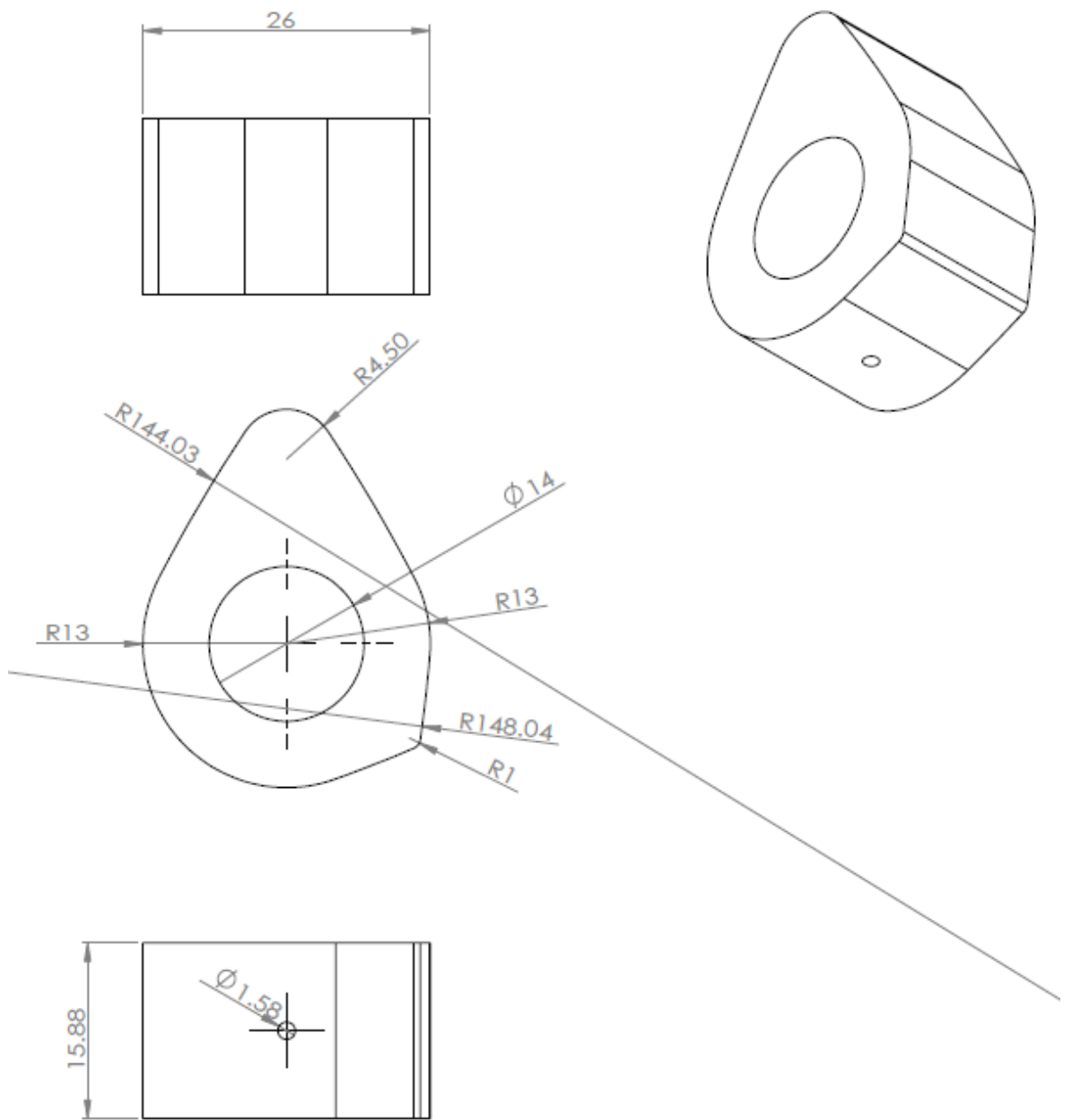
Appendix
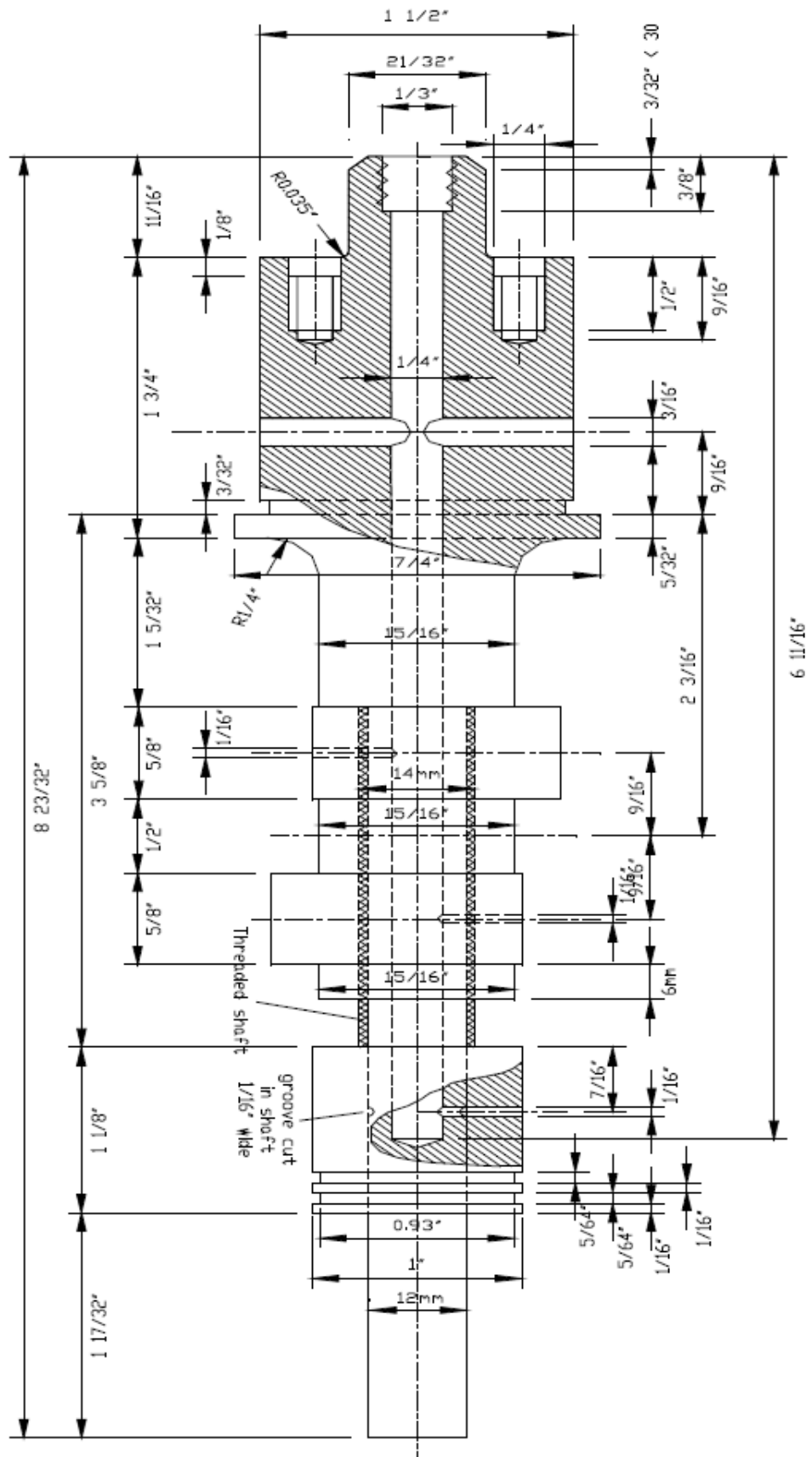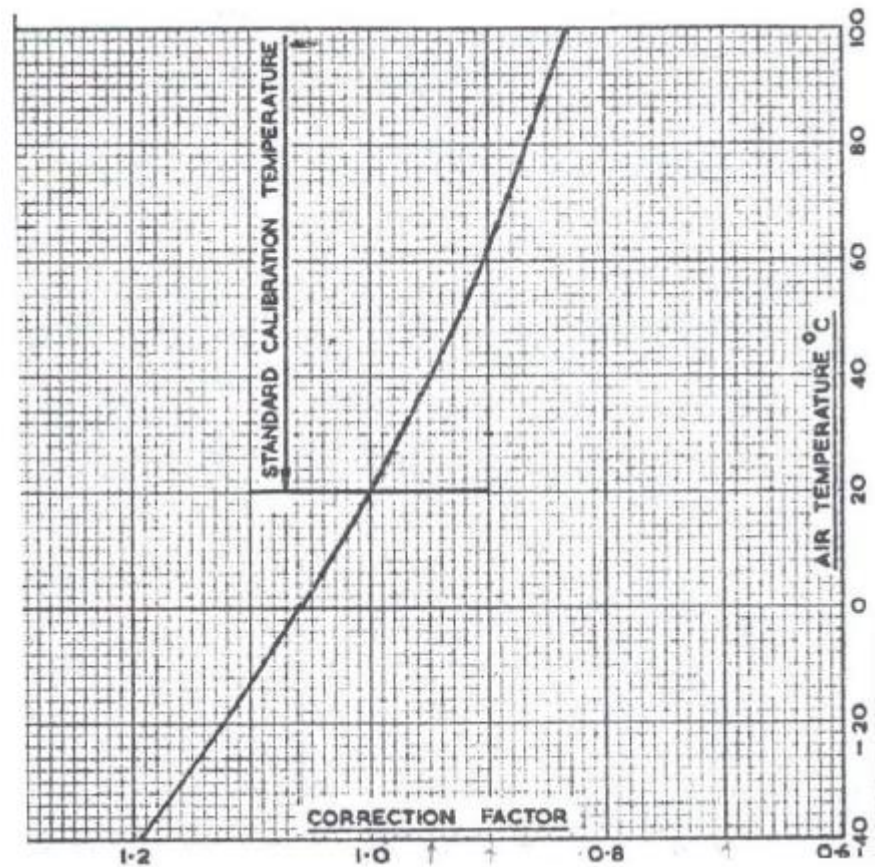

Figure A1: Re-breathing cam lobe drawing

Figure A2: Adjustable valve timing camshaft for Ricardo E6 engine

Manometer of Orifice measurement part and reading meter

Viscous flow air meter

Temperature correction for meters calibrated at 20 ^{0}C

Figure A3: Alcock viscous flow air meter